Solar models, neutrino experiments, and helioseismology

John N. Bahcall

Institute for Advanced Study, Princeton, New Jersey 08540

Roger K. Ulrich

University of California at Los Angeles, Los Angeles, California 90024

The event rates and their recognized uncertainties are calculated for eleven solar neutrino experiments using accurate solar models. The same solar models are used to evaluate the frequency spectrum of the p and g oscillation modes of the sun and to compare with existing observations. A numerical table of the characteristics of the standard solar model is presented. Improved values have been calculated for all of the neutrino absorption cross sections evaluating the uncertainties for each neutrino source and detector as well as the best estimates. The neutrino capture rate calculated from the standard solar model for the ^{37}Cl experiment is $7.9(1\pm0.33)$ SNU, which spans the total theoretical range; the rate observed by Davis and his associates is (2.0 ± 0.3) SNU. The ratio of the observed to the predicted flux at Earth of neutrinos from ^{8}B decay lies in the range $0\leq[\varphi(^{8}\mathrm{B})_{\mathrm{observed}}/\varphi(^{8}\mathrm{B})_{\mathrm{predicted}}]\leq0.5$. The recent results from the Kamiokande II electron scattering experiment confirm this conclusion. This discrepancy between calculation and observation is the solar neutrino problem. Measurements of the energy spectrum of solar neutrinos can discriminate between suggested solutions of the solar neutrino problem. Nonstandard solar models, many examples of which are also calculated in this paper, preserve the shape of the energy spectrum from individual neutrino sources, whereas most proposed weak-interaction explanations imply altered neutrino energy spectra. Detailed energy spectra of individual neutrino sources are presented as well as a composite solar neutrino spectrum. hep neutrinos from the ^{3}He$+p$ reaction, probe a different region of the solar interior than do ^{8}B neutrinos. Measurements of the very rare but highest-energy hep neutrinos are possible in proposed experiments using electron scattering, ^{2}H, and ^{40}Ar detectors. The standard solar model predicts p-mode oscillation frequencies that agree to within about 0.5% with the measured frequencies and reproduce well the overall dispersion relation of the modes. However, there are several small but significant discrepancies between the measured and observed frequencies. The complementarity of helioseismology and solar neutrino experiments is demonstrated by constructing a solar model with a drastically altered nuclear energy generation that eliminates entirely the important high-energy ^{8}B and ^{7}Be neutrinos, but which affects by less than 0.01% the calculated p-mode oscillation frequencies.

CONTENTS

Copyright ©1988 The American Physical Society

I. INTRODUCTION

A. Why?

Do we understand how the sun shines? Is the theory of stellar evolution seriously challenged by the results of the ^{37}Cl solar neutrino experiment? Or, on the other hand, is our understanding of solar energy generation sufficiently reliable that one can use the sun to study weak interactions with greater sensitivity than is possible with terrestrial sources? We have been trying to answer these questions for the past two decades. Why are we still at it? The reason is simple. There is not yet a definitive solution of the solar neutrino problem.

There are other reasons why we are still working on what seems like such a simple problem, perhaps the conceptually simplest problem of stellar evolution. The calculations are complicated and involve a number of different branches of physics and astronomy. Definitive comparisons with solar neutrino experiments require greater accuracy and detail than is necessary for studying energy generation in less accessible, more evolved stars. Each time that we have come back to this problem there have been new (to us), previously uninvestigated effects that we had to evaluate quantitatively. In addition, the *uncertainties* in the predicted fluxes must be calculated explicitly in order to decide if there is really a problem and, if there is, how accurately one can presume to know the neutrino production rates that are essential in using solar neutrinos for experiments on the nature of the weak interactions. The quantitative evaluation of uncertainties is not as crucial in other areas of stellar evolution for which a statistical comparison between observations and calculations is the more typical mode of testing the theory. Moreover, new solar neutrino experiments that are under way require for their interpretation specialized calculations that we have not previously performed.

Finally, confrontation with the abundant and precise measurements of p-mode solar oscillation frequencies also demands extensions of our previous analysis.

We continue to use the "best available physics" even when this leads to major complications in the computer codes. We believe that the origin of discrepancies between theory and observation will be most clearly revealed by comparison of the data with the most accurate possible theoretical calculations. Simplifications can blur discrepancies or conceal improvements inherent in better physics. Effort and precision are required to obtain theoretical results for solar neutrino and solar oscillation calculations that approach the accuracy being obtained experimentally. Most of the improvements we make in our analysis do not have a significant effect, but we never know for sure which are important until we implement the corrections. We therefore continuously refine our codes, incorporating improved physics and input data.

There are feasible experiments, some in progress, that can measure the energy spectrum of solar neutrinos. In this paper, we emphasize future measurements of the neutrino spectrum. We provide detailed figures and tables for the calculated energy spectra from different solar neutrino sources. We also present an overall spectrum that is obtained from the standard solar model. The most popular particle physics explanations of the solar neutrino problem predict that the neutrinos incident at Earth have an energy spectrum significantly different from what is presented in this paper (see especially Figs. 2–5), while speculations that the standard solar model is incorrect suggest only a change in the normalization of some (or all) of the individual fluxes, but not in their shape. Thus a measurement of the *shape* of the incident solar neutrino spectrum will discriminate between different possible explanations.

In the last 5 years, there has been an upsurge in the interest of particle physicists in solar neutrinos (see Haxton, 1986; Okun, 1986; Weinberg, 1987). This is partly due to a flowering of particle physics explanations of the solar neutrino problem (e.g., WIMP's, resonant neutrino oscillations, neutrino decay, neutrino electric or magnetic dipole moments) and partly to a growing conviction among the scientific community that the solution of the problem is probably not a trivial error. One final reason for reinvestigating standard solar models is that the explanation of the solar neutrino problem in terms of resonant neutrino oscillations [the Mikheyev-Smirnov-Wolfenstein (MSW) effect; Mikheyev and Smirnov, 1986; Wolfenstein, 1978] requires, for accurate calculations, detailed information about the distribution of neutrino production within the sun, the electron density profile, the shape of the neutrino energy spectra, and the neutrino absorption cross sections as a function of energy. We provide the required information in tabular form. Machine readable versions of these tables will be provided upon request.

B. Definition of uncertainties

Is there a solar neutrino problem? Yes, provided the difference for the ^{37}Cl experiment between the astrophys-

ical prediction and the measured capture rate exceeds the range of the uncertainties. No, if the uncertainties exceed the discrepancy between observation and theory. A quantitative statement of the uncertainties is at the heart of our subject.

We present the calculated uncertainties in terms of a "total theoretical range" (cf. Bahcall, Huebner, Lubow, Parker, and Ulrich, 1982, hereafter referred to as paper I, where the same quantity was referred to as an "effective 3σ level of confidence"). We would like to provide a *true* "3σ level of confidence," but we cannot do so because we do not know the probability distribution for parameters that must be calculated (e.g., radiative opacity or forbidden corrections to neutrino cross sections), not measured. In practice, our total theoretical range is equivalent to the requirement that if the true value lies outside the estimated range, someone has made a mistake. The reader will recognize that matters of judgment are important in this undertaking, especially when systematic errors are likely to exceed the measuring errors.

We use standard 3σ limits for measured quantities (e.g., nuclear reaction rates). Uncertainties in theoretical quantities are sometimes calculated explicitly by the original authors. However, more often, we have had to make our own assessments of possible errors. In practice, we have often taken uncertainties in quantities that are calculated, not measured, to be equal to the range in values in published state-of-the-art calculations. In cases where only one calculation is available, we have had to make a more delicate judgment. For example, we have chosen to multiply the value of forbidden corrections to neutrino capture cross sections by 3 and call this the total uncertainty. It is possible that we assign relatively larger errors for experimentally determined parameters (for which the errors are more easily quantifiable) than we do for the calculated parameters such as the opacity. However, the adopted procedure is as objective as any we can think of and has the advantage of simplicity.

In the final analysis, our method for estimating errors is defined by the examples we discuss (see also paper I). In all cases, the procedures and assumptions we use to obtain the final uncertainties are stated explicitly. If the reader has a better (or different) way of estimating the errors, then he can recalculate easily the uncertainties in all the predicted event rates using the results and prescriptions described in this paper.

We have had to combine theoretical uncertainties with statistical (and systematic) errors in measured quantities. In doing so, we have adopted three rules. (1) Errors from different sources are combined incoherently (the total uncertainty is the square root of the sum of the squares of the individual uncertainties). (2) The effects of individual parameter uncertainties are determined by calculating stellar models with different values of the parameters of interest. (3) Only data published prior to January 1987 are used.

We have verified by constructing 1000 accurate solar models (see Sec. VII) that this procedure correctly reproduces the theoretical probability distribution of neutrino fluxes provided that the input parameters are normally distributed.

Most of the predicted rates and uncertainties that we give in this paper are calculated for the standard solar model, assuming also that nothing happens to the neutrinos on the way to the Earth from the sun. However, there is convincing experimental evidence that this combined conservative hypothesis is incorrect.

How can we calculate the rates and uncertainties for the likely situation in which the incident neutrino energy spectrum is different from the standard spectrum? The procedure is relatively simple if the shape of the energy spectrum for each of the individual neutrino sources is unchanged and only the total number of neutrinos of a specified type is altered. This condition is satisfied for all of the so-called nonstandard solar models (including the WIMP hypothesis; see Faulkner and Gilliland, 1985; Spergal and Press, 1985), since for these models the relative numbers of neutrinos of different kinds are not the same as in the standard model but the normalized energy spectra are unchanged. In this case, we use the cross sections that are given below (see Tables VII and VIII), together with the appropriate neutrino fluxes and the uncertainties specified in Secs. II and IV. The situation is more complicated if the shape of the individual energy spectra are altered by physical processes such as the MSW effect. In this case, one must use the individual cross sections as a function of energy (given in Table IX) to calculate effective absorption cross sections for the specified spectrum shape. The uncertainties can be inferred in most cases from the information given in Sec. IV.B, since the fractional uncertainties in the cross section for a given source are, to a satisfactory approximation in most instances, independent of the precise shape of the spectrum.

C. What?

In this paper we have taken advantage of a number of advances that have occurred since our last extensive investigation, in 1982, of solar models and neutrino fluxes. The improvements considered here include a number of important new laboratory experiments on nuclear reaction cross sections, some fine-tuning of our model codes, (p,n) experiments on nuclei that will be used as neutrino detectors, as well as improved determinations of the surface abundances of the chemical elements in the sun and appropriately refined opacity calculations. We have also reevaluated the neutrino absorption cross sections taking account of recent theoretical and experimental developments.

In addition, we have responded to the blossoming of the field of helioseismology, there now being available about 10^3 accurately measured (precision between 0.01% and 0.04%) p-mode oscillation frequencies. Solar neutrinos and solar seismology are complementary and rein-

forcing tools for studying the solar interior. *We have therefore extended the subject of this series of papers by including a detailed discussion of the interrelation between the oscillation frequencies and the neutrino fluxes.*

This paper is not a review article. We concentrate on new results that are necessary for interpreting solar neutrino experiments and for understanding their relation to measurements of solar oscillation frequencies. The reader is referred to an extensive discussion in the Reviews of Modern Physics (paper I) for a description of the background, the techniques, and the literature references. We describe in this paper only improvements made on previous calculations and the new numerical results that are relevant for comparisons with observations.

Details are the most important but the least interesting aspect of this subject, except to the expert in each area. We must get the details right in order to calculate accurately the interesting quantities, which are neutrino fluxes, oscillation frequencies, and their associated uncertainties. The experts need to know how we have handled all of the details in order to appraise the final results. We therefore present an account of the calculations which is succinct but we believe complete (when considered together with paper I).

In order to help the reader find those parts of the paper that fit his particular interests, we provide here a brief summary of what is contained in each section. In Sec. II we describe the *input parameters* for the solar models. The nuclear parameters are discussed in Sec. II.A; our best estimates and associated uncertainties are given in Table I. Appendix A describes how we computed the *nuclear energy generation* and gives in Table XXI the effective Q values that include neutrino energy loss and the thermal motion of the reacting particles. The element abundance of the primordial composition is discussed in Sec. II.B and Eq. (1). The adopted *fractional abundances* of the heavy elements are given in Table II, where they are compared with the abundances that we used previously. The *radiative opacities* are discussed in Sec. II.C. We give in Table III a convenient numerical representation of the radiative opacity that is required to compute a standard solar model. This table is derived from a set of tapes supplied by the Los Alamos Opacity Library and can be used by different groups to compare results that are obtained for standard solar models with independent computer codes. Figure 1 illustrates an effect that we have included for the first time in this paper, the fractional increase of the opacity as a function of solar radius that is caused by the conversion of carbon and oxygen to nitrogen.

In Sec. III, we describe the most important *neutrino sources and their energy spectra.* We describe in Sec. III.A the individual sources: p-p, pep, hep, ^{7}Be, ^{8}B, ^{13}N, ^{15}O, and ^{17}F neutrinos.

We discuss the neutrino *energy spectra* in Sec. III.B. Figure 2 shows the combined energy spectrum that is obtained with the standard solar model. Figures 3–5 illustrate the shapes of the individual spectra from the p-p, ^{8}B, hep, and ^{13}N neutrinos. We also present tables of the calculated energy spectra from the fundamental p-p reaction (Table IV), the ^{8}B neutrinos (Table V), and the hep (highest energy, Table VI) neutrinos.

We have recalculated *neutrino absorption cross sections* for detectors for which experiments are under way or are being developed. The new values of the absorption cross sections are discussed in Sec. IV. The best estimates are given in Sec. IV.A and the uncertainties in Sec. IV.B. Table VII gives the cross sections for each of the neutrino sources incident on the following detectors: ^{7}Li, ^{37}Cl, ^{71}Ga, ^{81}Br, ^{98}Mo, and ^{115}In. These results were computed assuming that electron neutrinos are not affected by interactions within the sun or by the journey from the sun to the detector on Earth. For detectors of ^{2}H and ^{40}Ar, which record individual electrons produced by the capture process, the cross sections are given in Table VIII as a function of the minimum electron kinetic energy that is accepted. In order to facilitate the calculations of how the MSW effect or other energy-dependent physical processes will affect the event rates in different experiments, we give the absorption cross sections in Table IX as a function of the incident neutrino energy for detectors composed of ^{2}H, ^{37}Cl, ^{40}Ar, ^{71}Ga, ^{81}Br, and ^{98}Mo.

We discuss in Secs. IV.C and IV.D possible *calibration experiments* with laboratory neutrino sources that could be used to test and improve the accuracy of the calculated neutrino absorption cross sections. We present in Sec. IV.C the cross sections and estimated uncertainties for experiments that could be performed with a ^{51}Cr source. We discuss in Sec. IV.D experiments that could be performed with a stopped muon beam.

We describe the *standard solar model* in Sec. V. In Sec. V.A, we outline the *basic aspects* of the standard solar model: the logic and the procedure. We present in Sec. V.B some of the *principal characteristics* of the standard model. Table X gives the distribution with mass and radius of the principal physical and chemical characteristics. The distribution within the sun of the energy generation and the neutrino fluxes is specified in Table XI. Figure 6 illustrates the dependence upon solar position of the energy generation, temperature, total density, and electron density. Figure 7 shows the dependence of the most important mass fractions upon solar position. We show in Table XII the evolution with time of the surface quantities: solar luminosity, radius, and effective temperature. In Table XIII of Sec. V.C, we give the best current values for the standard model *neutrino fluxes and their uncertainties.* The fluxes from a sequence of standard solar models are also discussed in Sec. V.C and compared, in Table XIV, with the values obtained in paper I. Figure 8 shows where the most important neutrino fluxes originate in the sun. The *primordial helium abundance* is derived in Sec. V.D and the surface *lithium abundance* is discussed in Sec. V.E.

We calculate in Sec. VI the fractional uncertainties in the individual neutrino fluxes by assuming that the uncertainties in each input parameter and in each calculat-

ed neutrino flux are all normally distributed. We present in Sec. VI.A the calculated *logarithmic derivatives* of each of the neutrino fluxes with respect to each of the important input parameters. These derivatives, which are summarized in Table XV, are used to evaluate the uncertainties in the predicted capture rates for different neutrino detectors and to indicate the dependence of the predicted rates on the parameters. We evaluate in Sec. VI.B the *fractional uncertainties* in each of the neutrino fluxes. The uncertainties are calculated using the logarithmic derivatives given in Table XV and the fractional uncertainties in each of the input parameters that are determined in Sec. II of this paper and in paper I. The uncertainties discussed in Sec. VI.B are independent of detector sensitivities.

We describe in Sec. VII the results obtained by constructing 1000 accurate solar models, the input parameters for which were drawn from normal distributions with means and standard deviations that are specified in Sec. II. Figure 9 compares the shape of the calculated distribution of ^{8}B fluxes for the 1000 models with the distribution obtained from a Gaussian with the same mean and standard deviation.

We give in Sec. VIII the *predicted capture rates and the estimated uncertainties* for the standard solar model for both radiochemical and direct counting experiments. We summarize the predictions for the radiochemical experiments, ^{37}Cl, ^{71}Ga, ^{98}Mo, ^{7}Li, ^{81}Br, and ^{205}Tl in Sec. VIII.A and for the direct counting experiments, electron scattering, ^{2}H, ^{40}Ar, ^{11}B, and ^{115}In detectors, in Sec. VIII.B. Table XVI displays the principal uncertainties in the calculated capture rate for each of the neutrino sources. The contributions of the separate neutrino sources to the total capture rate of each detector are shown in Table XVII. The existing experimental limit on the ratio of observed to predicted flux of ^{8}B neutrinos is shown to be between 0.0 and 0.5 [see Eq. (23)].

We describe in Sec. IX the results of detailed calculations of *nonstandard* solar models. In Sec. IX.A, we present the calculations for two classes of models with inhomogeneous primordial compositions, the "low-Z" and the "high-Y" models, and in Sec. IX.B, we describe the results for two illustrative models with nonstandard nuclear physics. In Table XVIII, we give the predicted capture rates for each of the nine nonstandard models in all of the detectors listed previously.

We devote Sec. X to a discussion of our results for *helioseismology*. Paying special attention to the modeling of the outer region of the sun, we calculate the frequencies directly from the solar models and then show how the systematic trends relate to the asymptotic theory. We do not follow the more standard practice of using asymptotic formulas to represent the calculated frequencies, thereby avoiding some uncertainties. In Sec. X.A, we provide a brief introduction to the theory and practice of helioseismology. We describe in Secs. X.B and X.C arguments suggesting that the frequency difference between the $l=0$ and the $l=2$ modes is relatively insensitive to poorly understood aspects of the solar surface and that this frequency difference offers therefore the best opportunity for using p-mode oscillations to study the solar interior. We discuss our numerical codes in Sec. X.D and Appendix C. We compare the calculated and observed eigenfrequencies in Secs. X.E–X.G, discussing both standard and nonstandard solar models.

We summarize in Sec. XI some of the principal results and conclusions of this article. We also emphasize those aspects of the subject that we feel are most important or most urgently require further work.

D. How?

How should this article be read? We recommend that the user turn first to the summary and conclusions that are given in Sec. XI and read this section quickly to find out what we think are the major new results and recommendations. Then we suggest you leaf through the different sections, looking mainly at the headings and glancing at what is contained in the tables and figures. This perusal will give you an idea of what you want to read in detail, if anything.

II. INPUT PARAMETERS FOR SOLAR MODELS

We discuss in this section those parameters for which improved data have become available since paper I was completed. Unless explicitly indicated in this section, we adopt the values given in paper I for both the best estimates of input parameters and their associated uncertainties.

A. Nuclear parameters

Table I lists the reaction parameters for the proton-proton chain. The first column shows the nuclear reaction; the second column gives a reaction number for reference. The third and fourth columns list Q, the nuclear energy released by the reaction, and $\langle q_\nu \rangle$, the average energy of the neutrino that is created. The values of $\langle q_\nu \rangle$ were computed by averaging over the neutrino spectra described in Bahcall (1978) and Bahcall and Holstein (1986). The familiar cross-section factors (Fowler, 1984), S_0 and dS/dE, are given in columns 5 and 6. Finally, we show in column 7 the order of magnitude of the lifetime for nuclear burning of each of the nuclear species, computed for typical solar core conditions ($T=1.5\times10^7$ K and $\rho=150$ gm cm^{-3}).

The reaction rates that are changed from what we used in paper I are the p-p reaction (reaction 1 of Table I), the pep reaction 2, the ^{3}He-^{3}He reaction 5, the ^{3}He-^{4}He reaction 6, and the ^{7}Be+p reaction 9. The value of $S_0(p\text{-}p)$ is increased by about 5% (and the uncertainty almost halved) because of the more precise determination of g_A/g_V from β-asymmetry measurements

TABLE I. Reaction parameters for the proton-proton chain. The uncertainties for the cross-section factors are indicated in parentheses; they correspond to 3σ errors and have been calculated using the data given in the original experimental papers (see Bahcall *et al.*, 1982; Parker, 1986 for discussions).

Reaction	Number	Q (MeV)	$<q_{\nu_e}>$ (MeV)	S_0 (keV barns)	(dS/dE) (barns)	Lifetime (yr)
$^1H(p,e^+\nu_e)^2H$	1	1.442	0.265	$4.07(1\pm0.051)\times10^{-22}$	4.52×10^{-24}	10^{10}
$^1H(p\ e^-,\nu_e)H$	2	1.442	1.442	[see Eq. (5), Paper I]		10^{12}
$^2H(p,\gamma)^3He$	3	5.494		2.5×10^{-4}	7.9×10^{-6}	10^{-8}
$^3He(p,e^+\nu_e)^4He$	4	19.795	9.625	8×10^{-20}		10^{12}
$^3He(^3He,2p)^4He$	5	12.860		$5.15(1\pm0.17)\times10^3$	-0.9	10^5
$^3He(^4He,\gamma)^7Be$	6	1.586		$0.54(1\pm0.06)$	-3.1×10^{-4}	10^6
$^7Be(e^-,\nu_e)^7Li$	7	0.862 0.384	0.862 0.384	[see Eq. (9), Paper I]		10^{-1}
$^7Li(p,\alpha)^4He$	8	17.347		$52(1\pm0.5)$	0	10^{-5}
$^7Be(p,\gamma)^8B$	9	0.137		$0.0243(1\pm0.22)$	-3×10^{-5}	10^2
$^8B(e^+\nu_e)^8Be^*$ $^8Be^*(\alpha)^4He$	10	17.980	6.710			10^{-8}

References: (1) Bahcall and May (1969); (2) Bahcall and May (1969); (3) Griffiths, Lal, and Scarfe (1963); (4) Werntz and Brennan (1973); Tegner and Bargholtz (1983); (5) Bahcall *et al.* (1987); Krauss, Becker, Trautvetter, and Rolfs (1987); (6) Alexander, Ball, Lennard, Geissel, and Mak (1984); Parker (1986); (7) Bahcall and Moeller (1969); (8) Rolfs and Kavanagh (1986); Fowler (1987); (9) Filippone, Elwyn, Davids, and Koetke (1983); Parker (1986); (10) Wilkinson and Alburger (1971); Warburton (1986).

($g_A/g_V=-1.262\pm0.005$; Bopp *et al.*, 1986). The largest uncertainties in the p-p rate arise from the estimates of the square of the nuclear matrix element (2.5%; see Bahcall and May, 1969) and the corrections for mesonic exchanges ($\sim2\%$). The only change in the pep rate occurs because of its proportionality to the rate of the p-p reaction $R_{p\text{-}p}$. The form of Eq. (5) of paper I remains the same; the value of $R_{p\text{-}p}$ which enters this equation is different because $S_{p\text{-}p}$ is changed. The best value for $S_{3\text{-}4}$ has also changed slightly (by about 4%) as a result of a number of important new measurements (Osborne *et al.*, 1982, 1984; Robertson *et al.*, 1983; Volk *et al.*, 1983; and Alexander *et al.*, 1984). The results for this reaction have been summarized by Parker (1986) in his Table III. Parker (1986) reanalyzed all of the available data (including the recent measurements of Filippone *et al.*, 1983) for the important reaction (10) that produces the relatively high-energy ^8B neutrinos. By a very different analysis, Kajino, Toki, and Austin (1987) have obtained a value (0.56 keV b) for $S_{3\text{-}4}$ that agrees well with Parker's value (0.54 keV b). The best estimate for $S_{1\text{-}7}$ has decreased by about 16%. The *low-energy cross-section factor for the* ^7Be+p *reaction remains the most important single parameter for the solar neutrino problem and the most uncertain nuclear quantity* (cf. Barker and Spear, 1986, and Kajino, Toki, and Austin, 1987). The 3σ uncertainty in this reaction rate is about 22% (see Table IV of Parker, 1986), including only recognized uncertainties.

Most of the solar models in this paper have been constructed using the value of S_0 for the ^3He-^3He reaction that is given in paper I: 4.7 MeV b. However, for our final standard solar model, labeled "Best" in Sec. V and Table XIV below, we have taken account of the recent and important experiment reported by Krauss, Becker, Trautvetter, and Rolfs (1987). These authors derive an S_0 equal to 5.6 ± 0.3 MeV b. We follow the analysis of Parker (1987) and adopt the average of the previous Caltech and the newer Munster results, namely, 5.15 ± 0.09 MeV b.

The cross section for the ^3He+p reaction (4) is especially uncertain because it is approximately proportional (see Tegner and Bargholtz, 1983) to the poorly known radiative capture cross section of thermal neutrons by ^3He. The quoted errors on the existing measurements are large (see Bollinger, Specht, and Thomas, 1973; Suffert and Berthollet, 1979; Alfimenkov *et al.* 1980); the experi-

ments should be repeated with higher accuracy. Tegner and Bargholtz (1983) quote an uncertainty of a factor of more than 6 in the cross-section factor. In the absence of further thermal neutron cross-section measurements, we continue to use the cross-section value calculated by Werntz and Brennan (1973), which is close to the geometrical mean of the extreme values obtained by Tegner and Bargholtz. We are not able to assign a meaningful quantitative estimate of the uncertainty in the adopted cross-section factor.

Appendix A describes how we have computed the generation of thermal energy from nuclear reactions and gives in Table XXI the *effective Q* values that apply when neutrino energy losses are included. Our calculations are the first that we know about in which the effect of the thermal motion of the reacting particles on the neutrino energy losses is evaluated explicitly [see Eqs. (A2)–(A4)].

B. Abundances

The present composition of the solar surface is presumed, in standard solar models, to reflect the initial abundances of all of the elements that are at least as heavy as carbon. The primordial ratio of heavy elements to hydrogen, Z/X, is one of the crucial input parameters in the determination of a solar model. The fractional abundances of each of the elements is also important in determining the stellar opacity, which is closely linked to the predicted neutrino fluxes. We include for the first time a treatment of the change in the opacity caused by the conversion of carbon and oxygen to nitrogen in the CNO cycle (see below).

In paper I we used the recommended elemental abundances from the review of solar abundances by Ross and Aller (1976) as the standard composition for which the radiative opacities were calculated. Since that work was completed, there has been a great deal of empirical and theoretical work on the individual abundances on the solar surfaces. This enormous joint effort of many different researchers has been ably summarized in two reviews (completed approximately at the same time) by Grevesse (1984) and Aller (1986). We have taken account of this improvement in our knowledge of the surface abundances and have adopted as standard values for the opacity used in this paper (see below) the abundances listed by Grevesse (1984).

Our abundance input procedure has been changed so that we input the published ratios of individual abundance to the hydrogen abundance rather than the mass fractions. This new procedure assures that the required (Z/X) is matched precisely and eliminates a potential source of error.

Table II lists the individual fractional abundances of the heavy elements that are recommended by Grevesse (1984), Aller (1986), and, for comparison, Ross and Aller (1976). The two recent studies are in excellent agreement. The best-estimate value of Z/X has increased considerably from the value of 0.0228 of the Ross-Aller (1976) mixture. The Grevesse (1984) value is $(Z/X)_{\text{Grevesse}}=0.027\,65$ and for the Aller (1986) mixture $(Z/X)_{\text{Aller}}=0.027\,39$. The difference between the Ross-Aller value of Z/X and the current value of Grevesse (1984) and Aller (1986) is about 19%, almost twice the uncertainty that we estimated in paper I. In accordance with the "rule of thumb" procedure that was described in paper I, we adopt as a total uncertainty

$$\Delta(Z/X)=0.19(Z/X)\ . \tag{1}$$

The uncertainty given in Eq. (1) is only slightly larger than that obtained from the papers of Grevesse (1984) and Aller (1986) if we interpret their listed uncertainties as 1σ errors and multiply by 3 in order to approximate an effective 3σ uncertainty.

C. Opacities

We have been fortunate to obtain detailed opacity tapes for the Grevesse mixture that is specified in Table II. The opacities were calculated with the programs of the Los Alamos Opacity Library and were made available to us through the generous cooperation of W. Huebner. A detailed description of the physics that underlies these calculations is given in Huebner (1986), and the most important opacity-related uncertainties are described in Sec. II.D of paper I.

In order that other workers can test their programs and compare with our results for the same input parameters, we give in Table III a numerical representation of the Los Alamos opacities for the Grevesse mixture. Table III covers the parameter range that is relevant for the calculation of standard solar models and contains all of the modifications described below except for the conversion of carbon and oxygen to nitrogen [see correction (3) below and Appendix B, Table XXII].

The Los Alamos Opacity Library can provide opacities for mixtures that contain arbitrary total heavy-element abundances Z. The detailed specification of Z is fixed by the initial mixing done at Los Alamos and is provided on one of three tapes that are combined by the library user to yield opacities for any desired mixture of X, Y, and Z. Because of our new method of defining the abundances in the model, the value of Z must change as Y is iterated to match the luminosity. Consequently, tables with at least two values of Z are needed. We have used the four combinations shown in Table III to compute standard solar models. The three models with low heavy-element abundance that are discussed in Sec. IX use opacities based upon a value of $Z=0.1\times Z_{\text{Grevesse}}$ as well as the normal opacities given in Table III.

The opacities that we are currently using differ from those discussed in paper I because of the four modifications described briefly below. To give the reader a feeling for the significance of these changes, we quote the fractional change in the ^{8}B neutrino flux that we have calculated by constructing detailed standard models with

TABLE II. Fractional abundances of heavy elements.

Element	Number fraction (Grevesse, 1984)	Number fraction (Aller, 1986)	Number fraction (Ross-Aller, 1976)
C	0.29661	0.27983	0.30279
N	0.05918	0.05846	0.06326
O	0.49226	0.49761	0.50249
Ne	0.06056	0.06869	0.02699
Na	0.00129	0.00125	0.00138
Mg	0.02302	0.02552	0.02892
Al	0.00179	0.00198	0.00241
Si	0.02149	0.02672	0.03244
P	0.00017	0.00018	0.00023
S	0.00982	0.01040	0.01151
Cl	0.00019	0.00019	0.00023
Ar	0.00230	0.00227	0.00073
Ca	0.00139	0.00134	0.00163
Ti	0.00006	0.00007	0.00008
Cr	0.00028	0.00035	0.00037
Mn	0.00017	0.00016	0.00019
Fe	0.02833	0.02382	0.02297
Ni	0.00108	0.00114	0.00138
Total	1.000	1.000	1.000

TABLE III. Rosseland mean opacities (cm^2g^{-1}). Here $E-X=10^{-X}$.

$\rho/(T6)^3$ T6	2.818E-2	3.981E-2	5.623E-2	2.818E-2	3.981E-2	5.623E-2	2.818E-2	3.981E-2	5.623E-2	2.818E-2	3.981E-2	5.623E-2
1.000	4.659E+1	5.802E+1	7.116E+1	4.407E+1	5.557E+1	6.892E+1	4.886E+1	6.085E+1	7.463E+1	4.609E+1	5.813E+1	7.208E+1
1.218	4.122E+1	5.168E+1	6.421E+1	3.823E+1	4.850E+1	6.075E+1	4.326E+1	5.424E+1	6.738E+1	4.002E+1	5.078E+1	6.359E+1
1.483	3.931E+1	4.931E+1	6.083E+1	3.592E+1	4.528E+1	5.681E+1	4.136E+1	5.188E+1	6.399E+1	3.772E+1	4.752E+1	5.963E+1
1.807	3.262E+1	4.050E+1	5.009E+1	2.989E+1	3.694E+1	4.555E+1	3.434E+1	4.267E+1	5.280E+1	3.140E+1	3.883E+1	4.791E+1
2.200	2.728E+1	3.286E+1	3.889E+1	2.464E+1	3.004E+1	3.588E+1	2.879E+1	3.470E+1	4.109E+1	2.595E+1	3.167E+1	3.786E+1
2.680	1.921E+1	2.214E+1	2.496E+1	1.760E+1	2.048E+1	2.335E+1	2.030E+1	2.342E+1	2.641E+1	1.859E+1	2.164E+1	2.468E+1
3.264	1.267E+1	1.433E+1	1.606E+1	1.160E+1	1.326E+1	1.494E+1	1.340E+1	1.515E+1	1.698E+1	1.226E+1	1.402E+1	1.579E+1
3.975	8.107E+0	9.145E+0	1.036E+1	7.404E+0	8.393E+0	9.451E+0	8.553E+0	9.644E+0	1.092E+1	7.814E+0	8.855E+0	9.966E+0
4.841	5.236E+0	5.940E+0	6.731E+0	4.703E+0	5.358E+0	6.115E+0	5.502E+0	6.238E+0	7.062E+0	4.947E+0	5.633E+0	6.422E+0
5.896	3.527E+0	4.017E+0	4.597E+0	3.137E+0	3.584E+0	4.118E+0	3.687E+0	4.197E+0	4.798E+0	3.284E+0	3.749E+0	4.303E+0
7.181	2.528E+0	2.895E+0	3.341E+0	2.205E+0	2.553E+0	2.957E+0	2.627E+0	3.008E+0	3.468E+0	2.295E+0	2.655E+0	3.074E+0
8.746	1.941E+0	2.240E+0	2.604E+0	1.680E+0	1.952E+0	2.279E+0	2.007E+0	2.315E+0	2.689E+0	1.739E+0	2.020E+0	2.356E+0
10.652	1.620E+0	1.875E+0	2.192E+0	1.397E+0	1.624E+0	1.910E+0	1.668E+0	1.930E+0	2.256E+0	1.440E+0	1.674E+0	1.968E+0
12.973	1.434E+0	1.666E+0	1.938E+0	1.237E+0	1.434E+0	1.672E+0	1.473E+0	1.712E+0	1.991E+0	1.272E+0	1.475E+0	1.720E+0
15.800	1.306E+0	1.484E+0	1.719E+0	1.122E+0	1.285E+0	1.474E+0	1.340E+0	1.523E+0	1.762E+0	1.153E+0	1.321E+0	1.514E+0
19.243	1.130E+0	1.285E+0	1.429E+0	9.754E-1	1.086E+0	1.242E+0	1.156E+0	1.313E+0	1.459E+0	1.000E+0	1.114E+0	1.270E+0
23.436	9.526E-1	1.053E+0	1.176E+0	8.077E-1	8.932E-1	1.000E+0	9.707E-1	1.072E+0	1.196E+0	8.246E-1	9.111E-1	1.019E+0
	X=0.7300, Z=0.0195			X=0.3500, Z=0.0195			X=0.7300, Z=0.0208			X=0.3500, Z=0.0208		

and without each modification (cf. Sec. VI). The fractional changes in other neutrino fluxes are generally less important and can be estimated approximately from the partial derivatives given in paper I (see also Sec. VI of this paper).

(1) *Abundances.* As described in the previous subsection (II.B), we currently use the abundances recommended by Grevesse (1984) (see also Aller, 1986, and Table II). The best estimate for Z/X has increased by about 19% (see Sec. II.B), largely as a result of small increases in the oxygen and carbon abundances and a substantial increase in the neon abundance. The adopted change in chemical abundances causes the ^{8}B neutrino flux to increase by about 28% compared to the value obtained with the Ross-Aller (1976) opacities used in paper I.

(2) *CNO conversion.* In the calculations described in this paper, we have taken account, for the first time, of the effect on the opacity of the conversion of carbon and oxygen to ^{14}N as a result of nuclear burning in the course of the evolution of the sun. The opacity of a star changes as a result of the gradual conversion of the CNO elements to nitrogen via the CNO nuclear burning cycle. Even though this process contributes only a small fraction of the solar luminosity, carbon and nitrogen nuclei in the solar core go through the catalytic cycle about a dozen times during the solar lifetime, and the oxygen nuclei go partially through the first cycle. Essentially all of the carbon, and about 6% of the oxygen, is converted to ^{14}N. The CNO atoms are important contributors to the opacity in the solar core, so that this interconversion alters the mean opacity.

Figure 1 shows the fractional increase, caused by the conversion process, in the opacity as a function of radius in a fully evolved standard model. The amplitude and sign of the opacity change depends upon details of the relevant atomic physics, including the relative strength and placement of absorption edges and lines for the CNO

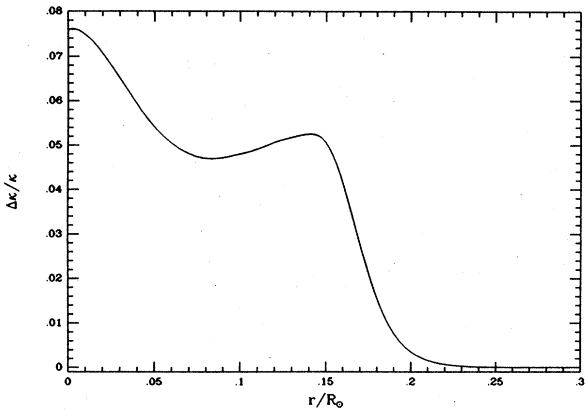

FIG. 1. The fractional increase in the opacity, $\delta\kappa/\kappa$, caused by the conversion of carbon and oxygen to ^{14}N, shown as a function of solar radius. The result illustrated applies to the model CNO Cor that we have adopted (see Sec. V.C) as our standard model and refers to the present epoch.

elements. We were unable to invent a reliable estimate of the effect prior to making a detailed calculation. All that one can say from general considerations is that it is plausible that the correction should be largest in the innermost regions, where the CNO cycle occurs often enough to reach a steady state, and should go to zero outside the region where the CNO cycle occurs. This general behavior is reflected in Fig. 1.

The CNO cycle conserves the number of heavy nuclei but changes their masses and hence alters the mass fraction of heavy elements Z. The value of Z is often thought of as loosely indicating the *number* abundance of heavy elements, so that a quick, but incorrect, interpretation of the CNO-induced change in Z would imply a change in heavy-element number abundance. In order to evaluate correctly the effect of CNO conversion on the opacity, we must utilize the information about the numbers of the individual heavy elements as a function of time that is available in the numerical calculations of the solar model. In the standard solar models the conversion of C and O to N during the CNO cycle increases the value of Z slightly from 0.0196 to 0.0202. However, this value of Z cannot be used directly for calculating the correction to the opacity with the original tables, since the tabulated distribution of heavy-element abundances does not take account of CNO conversion. In practice, all previous calculations of solar evolution have ignored this subtle point. In the present calculation of our best standard model, we recalculate Z at each point as the CNO conversion occurs and then use the procedure described in Appendix B to evaluate the correction to the tabulated opacity at the originally specified value of Z. For consistency, we must continue to use as our *uncorrected opacity* (see Appendix B and Fig. 1) the Los Alamos-supplied tables with the original value of Z that does not take account of CNO conversion.

A full treatment of this effect would require adding two more dimensions to the opacity lookup procedure, which is beyond the capabilities of our current code. We have therefore used an approximate treatment based upon the results of Huebner (1986), who fitted opacities to a power series in $\log(T)$ for a sequence of compositions of different mixtures. Huebner used the Ross-Aller mixture to calculate a fiducial opacity and then calculated the changes in the opacity induced by 25% variations, at constant Z, of the individual abundances of carbon, nitrogen, oxygen, neon, magnesium, and iron. We have applied the power-series expansions at temperatures between 1×10^6 and 16×10^6 K and have taken differences in order to derive the fractional changes that would result from converting all of the carbon and oxygen to nitrogen.

Table XXII of Appendix B can be used to make the opacity corrections caused by the conversion of carbon and oxygen to ^{14}N. The net result of including the conversion is an increase of the ^{8}B flux by 8% over what is obtained by ignoring this conversion.

(3) *Electron scattering.* Collective effects on the elec-

tron scattering cross section are included in the opacity library tables we currently receive from Los Alamos. In paper I, we used the expression derived by Diesendorf (1970), which implies a net decrease in the scattering cross section (compared to the Thompson value) of about 35% over most of the sun. We have compared opacity tables supplied by our Los Alamos collaborators that were computed with and without the collective corrections to the electron scattering cross section. This comparison shows that the Los Alamos calculation of collective effects, which is more complete, gives a decrease of only 18%, much smaller than implied by the Diesendorf formula.[1] The difference between the Los Alamos and the Diesendorf corrections amounts to only a 2.4% difference in the total opacity at the solar center. Boercker (1987) has shown that a large part of the discrepancy is due to the neglect by Diesendorf and Ninham (1969) of an angular dependence to the scattering cross section that integrates to zero for an electron in vacuum, but which causes the effect of electron correlations to be suppressed in a plasma. Using the Los Alamos estimate, we find an increase, over what we obtain with the Diesendorf correction, of 9% in the calculated ^{8}B neutrino flux.

(4) *Numerical representation.* We have restructured the grid in temperature T and density ρ (actually ρ/T^3) to ensure that the opacity changes by less than 40% between any adjacent points in the opacity table. This revision required doubling the number of grid points and resulted in an approximate 1% increase in the calculated ^{8}B neutrino flux. Our objective in increasing the density of points in the opacity table was to have a slow enough variation of the derived opacity from one table entry to the next that any reasonable interpolation scheme would give reliable results. We are, however, dependent on the basic opacity grid provided to us by our Los Alamos collaborators. The density of their table is comparable to ours in temperature but not in density. Whereas we have tabulated values of the opacity at density points close enough that the change in the opacity from one point to the next is less than about 20% in all cases, the Los Alamos grid involves opacity entry-to-entry changes of 55% to 65% in the density dimension. The changes in the temperature direction are consistent with our stated goal. The Los Alamos Library overcomes the sparseness of the opacity grid through the use of a spline interpolation procedure that depends on all available opacities. We have examined the spacing and distribution of the (LANL-supplied) data points that were interpolated to obtain the opacities given in Table III and have concluded that the spline interpolation should represent the data with an accuracy of about 3%.

[1]During this study, we discovered a related problem with the calculations carried out by Ulrich and Rhodes (1983) using a specially developed code (CATMOS; see Sec. VIII) that includes a detailed treatment of the solar envelope (in contrast to the schematic envelope treatment used in paper I and in previous versions of our solar neutrino code). In the Ulrich-Rhodes calculations, recent Los Alamos opacity library tapes were used that included the collective correction to the electron scattering cross section and that also inadvertently incorporated the same correction according to Diesendorf. Thus, in this code, there was a double correction for the collective effects. Fortunately, the solar oscillation frequencies are less sensitive to the interior opacity than are the neutrino fluxes, so that, although the standard model frequencies change by small amounts, none of the basic conclusions by Ulrich and Rhodes need to be modified.

III. NEUTRINO SOURCES AND SPECTRA

We summarize in this section the characteristics of the neutrino sources and their energy spectra.

A. Sources

There are five separate neutrino sources within the proton-proton chain (see Table I). Three of the sources produce continuum neutrino spectra, namely, p-p neutrinos (reaction 1, $q_{\max} \leq 0.420$ MeV), hep neutrinos (reaction 4, $q_{\max} = 18.773$ MeV), and the ^{8}B neutrinos (reaction 10, $q_{\max} < 15$ MeV). The p-p and ^{8}B neutrinos are familiar sources. The production rate of $^3\mathrm{He}+p$ (hep) neutrinos is expected to be much smaller than the flux of rare ^{8}B neutrinos. However, the hep neutrinos may be experimentally accessible, because of their large maximum energy, in detectors that count individual events (e.g., electron scattering experiments, ^{2}H, or the liquid-argon Icarus detector; see Sec. VIII.D).

There are also two sources of neutrino lines within the proton-proton chain: the pep neutrinos (reaction 2, $q = 1.442$ MeV) and the ^{7}Be neutrinos [reaction 7, $q = 0.862$ MeV (89.7%); 0.384 MeV (10.3%)]. These two sources produce neutrinos with discrete energies except for the small thermal broadening.

The most important reactions that are believed to produce solar neutrinos within the CNO cycle are

$$^{13}\mathrm{N} \rightarrow {}^{13}\mathrm{C} + e^+ + \nu_e (q \leq 1.199 \text{ MeV}) , \quad (2)$$

$$^{15}\mathrm{O} \rightarrow {}^{15}\mathrm{N} + e^+ + \nu_e (q \leq 1.732 \text{ MeV}) , \quad (3)$$

and

$$^{17}\mathrm{F} \rightarrow {}^{17}\mathrm{O} + e^+ + \nu_e (q \leq 1.740 \text{ MeV}) . \quad (4)$$

The ^{13}N and ^{15}O reactions [Eqs. (2) and (3)] provide information about the CNO cycle. The ^{17}F neutrinos [Eq. (4)] are potentially of great interest, since their flux is a measure of the primordial oxygen abundance in the solar interior. However, all three of the CNO neutrino sources will be difficult to detect experimentally if the standard solar models are correct.

B. Spectra

A measurement of the spectrum of neutrinos that reaches us from the sun will provide a decisive test of whether the solar neutrino problem is caused by our lack of understanding of the solar interior or by new physics. Whatever modification is made in the solar model, the calculated neutrino spectrum from each source will remain the same as long as no physical effects change the flavor or the energy distribution of the emitted neutrinos. We therefore provide in this subsection detailed information about the expected neutrino spectra.

Figure 2 shows the neutrino spectrum predicted for the standard solar model, Best, that is discussed in Sec. V (see row 6 of Table XIV). We include in this spectrum all of the important sources discussed in the previous subsection. The neutrino fluxes from continuum sources are given in units of number per cm^2 per s per MeV at one astronomical unit and the line fluxes are given in number per cm^2 per s.

Figures 3 and 4 show the energy spectra for the important p-p and ^8B neutrino sources. Figure 5 shows the spectra for the hep and ^{13}N sources.

Each of the spectra shown in Figs. 3–5 has a characteristic shape that is independent [up to terms of at least order $(kT/q_{\max})$, see Appendix A] of the conditions in the solar interior. The p-p spectrum rises slowly and peaks at about 0.31 MeV (which is $\approx\frac{3}{4}$ of the maximum neutrino energy), after which it is strongly cut off. The ^8B spectrum, on the other hand, is more nearly symmetric, with a peak at 6.4 MeV and a somewhat extended tail. The hep spectrum is rather symmetric and peaks at 9.6 MeV. The ^{13}N spectrum, like the p-p spectrum, rises slowly and then cuts off sharply; the ^{13}N peak is at 0.76 MeV.

Because of their importance for experiments that are planned or under way, we present in Tables IV–VI the calculated energy spectra for the p-p, ^8B, and hep neutrino sources. These tables should be useful in making detailed calculations of the implications of the MSW effect. The energy spectrum for the ^8B neutrinos is taken from Bahcall and Holstein (1986).

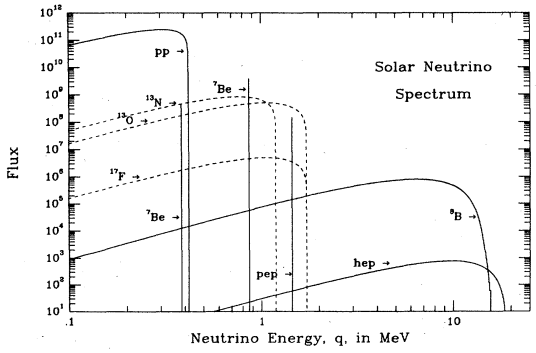

FIG. 2. The solar neutrino energy spectrum predicted by the standard solar model, Best discussed in Sec. V. The neutrino fluxes from continuum sources are given in units of number per cm^2 per s per MeV at one astronomical unit, and the line fluxes are given in number per cm^2 per s. Solid curves, spectra from the *pp* chain; dotted curves, CNO spectra.

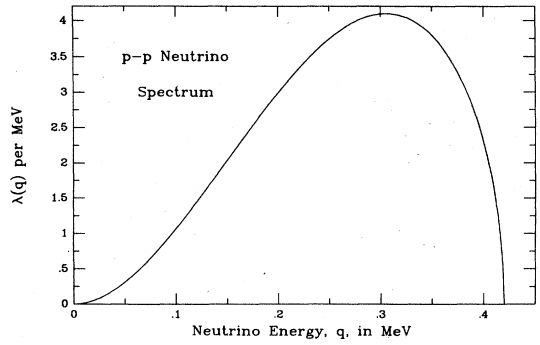

FIG. 3. Normalized energy spectrum, $\lambda(q)$, of p-p neutrinos. The integral of $\lambda(q)dq$ is normalized to unity for dq measured in MeV.

IV. NEUTRINO ABSORPTION CROSS SECTIONS

The rate at which events occur in a solar neutrino detector is determined by the summed product of individual neutrino fluxes times cross sections. In this section, we present new results on the cross sections for neutrino *absorption* by some of the most important experimental targets. Cross sections for neutrino scattering are given by Bahcall (1987).

The basic ingredients of these calculations are described by Bahcall (1978), although we include here in addition forbidden corrections to the allowed formulas in the approximation described by Bahcall and Holstein

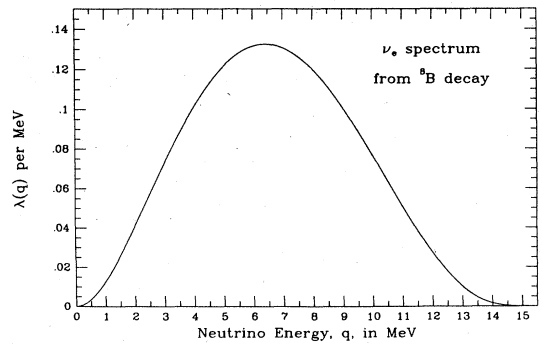

FIG. 4. Normalized energy spectrum, $\lambda(q)$, of ^8B neutrinos, from Bahcall and Holstein (1986). The integral of $\lambda(q)dq$ is normalized to unity for dq measured in MeV.

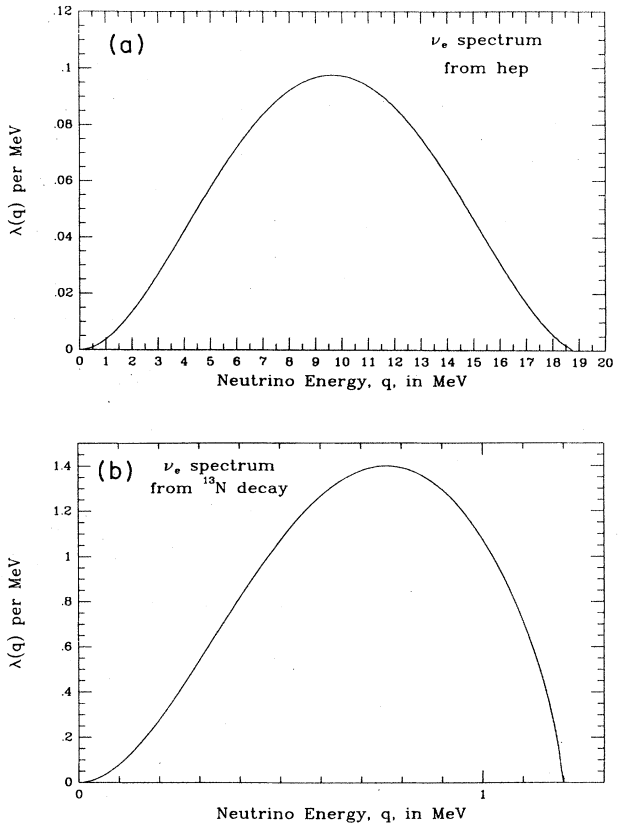

FIG. 5. The hep and ^{13}N neutrino spectra: (a) normalized energy spectrum $\lambda(q)$ of hep neutrinos; (b) normalized energy spectrum of ^{13}N neutrinos. The integral of $\lambda(q)dq$ is normalized to unity for dq measured in MeV.

(1986, see their Appendix).[2] We also use the recently derived ^{8}B neutrino spectrum (Bahcall and Holstein, 1986) to calculate more accurate cross sections for this important source. The only computational change from the earlier calculations is that the neutrino spectra are now evaluated by separate codes, which produce numerical files that are then used as input to a code that calculates the cross sections. The ^{2}H cross sections are based upon the work of Nozawa, Kohyama, Kaneta, and Kubodera (1986), who have included both exchange currents and forbidden corrections. We have used cross sections at individual energies that were generously supplied to us by Dr. Nozawa and Dr. Kubodera; these cross sections were then integrated over the appropriate neutrino spectra to form the weighted average cross sections, as a function of the minimum accepted electron recoil energy, that are given here (see Table XIV). The results agree to within a few percent with the calculation of Ellis and Bahcall (1968), who neglected forbidden corrections and exchange currents.

We use a number of important new experimental data, especially (p,n) measurements that have made it possible to calculate the cross sections for transitions to excited states of ^{71}Ga, ^{81}Br, ^{98}Mo, and ^{115}In. We use the (p,n) data of Krofcheck *et al.* (1985) and especially Krofcheck (1987) for ^{71}Ga, of Rapaport *et al.* (1985) for the ^{98}Mo and ^{115}In cross sections, and the data of Krofcheck *et al.* (1987) for ^{81}Br. In the region in which the energy resolution was not sufficient to separate contributions from different excited levels ($\gtrsim 1$ MeV), we performed the calculations in 0.5-MeV bins. Transitions were included up to the region in which the product nucleus became particle unstable (estimated to be $\sim 7.5 \pm 0.5$ MeV for all four targets). For the ^{71}Ga calculations, we have used the improved measurements of the half-life and Q value for ^{71}Ge that were determined, respectively, by Hampel and Remsberg (1985) and Hampel and Schlotz (1984), as well as the upper limit on the γ decay of the isobaric-analog state measured by Champagne *et al.* (1987). For the ^{81}Br cross sections, we used the improved Q value measured by Kouzes, Lowry, and Bennett (1982) [see also Lowry and Kouzes (1985)]. We have also used the important new measurements (Davids *et al.*, 1987; Lowry *et al.*, 1987) of the electron-capture branching ratio of metastable ^{81}Kr.

A. Values of the cross sections

Table VII gives the neutrino absorption cross sections, for each of the neutrino sources listed in Sec. II, on targets of ^{7}Li, ^{37}Cl, ^{71}Ga, ^{81}Br, ^{98}Mo, and ^{115}In. The results of Table VII apply if nothing happens to the neutrinos on the way to the Earth from the sun, i.e., if the spectrum of electron neutrinos is unchanged from what it is in the interior of the sun. The forbidden correction appropriate to Fermi transitions was used in calculating the ^{40}Ar cross sections.

The absorption cross sections for ^{8}B and hep neutrinos incident on ^{2}H and ^{40}Ar are given in Table VIII as a function of the minimum accepted kinetic energy of the recoil electron. The cross sections refer to transitions from the ground state of ^{40}Ar to the $T=2$ isobaric-analog state at 4.38 MeV in ^{40}K. The forbidden correction appropriate to Fermi transitions was used in computing the ^{40}Ar cross section.

For theoretical calculations of what is implied by different possible solutions of the solar neutrino problem, it is important to know the individual cross sections as a function of neutrino energy. Different solutions imply characteristic modifications of the neutrino energy spectra.

[2]Forbidden corrections cannot in general be calculated accurately. We evaluate them approximately in order to have a quantitative measure of the uncertainty they constitute. In order to simplify the analysis, we omit first forbidden corrections, which may be of the same order of magnitude as the forbidden corrections to allowed transitions that we evaluate explicitly (see appendix of Bahcall and Holstein, 1986).

TABLE IV. The p-p neutrino spectrum. The normalized neutrino energy spectrum $P(q)$ produced by reaction 1 is given in intervals of 10 keV. The neutrino energy q is expressed in MeV, and $P(q)$ is normalized per MeV.

q(MeV)	P(q)	q(MeV)	P(q)
0.01	0.0139	0.22	3.34
0.02	0.0542	0.23	3.49
0.03	0.119	0.24	3.63
0.04	0.205	0.25	3.75
0.05	0.312	0.26	3.86
0.06	0.436	0.27	3.95
0.07	0.576	0.28	4.02
0.08	0.731	0.29	4.07
0.09	0.897	0.30	4.10
0.10	1.07	0.31	4.10
0.11	1.26	0.32	4.08
0.12	1.45	0.33	4.02
0.13	1.64	0.34	3.93
0.14	1.84	0.35	3.80
0.15	2.04	0.36	3.63
0.16	2.24	0.37	3.41
0.17	2.44	0.38	3.13
0.18	2.63	0.39	2.76
0.19	2.82	0.40	2.28
0.20	3.00	0.41	1.60
0.21	3.17	0.42	0.00

Table IX gives the absorption cross sections for individual neutrino energies that are relevant for solar neutrino experiments or supernova detections. This table covers the following targets for which experiments are under way: ^{2}H, ^{37}Cl, ^{40}Ar, ^{71}Ga, ^{81}Br, and ^{98}Mo. Contributions from excited states and from forbidden effects have been included. For ^{40}Ar, the cross sections refer to transitions to the 4.38-MeV isobaric-analog state at ^{40}K. The individual cross sections given in Table IX are sufficient to reproduce the spectrum-averaged cross sections (given in Tables VII and VIII) to an accuracy of the order of 10%. These results will be useful for evaluating the effect of energy-dependent weak-interaction processes, such as the MSW effect, on the event rates in different detectors and in determining the potentialities of the detectors for observing supernovas. For completeness, we note that $\sigma(^{37}\mathrm{Cl})=2\times10^{-40}$ cm^2 at a neutrino energy of 50 MeV. [Readers who need even more detail can write to one of the authors (J.N.B.) for additional results.]

The ^{71}Ga detector is a special case. Two major experiments are under way (see Barabanov *et al.*, 1985; Hampel, 1985; Kirsten, 1986). Somewhat paradoxically, a majority of the captures expected on the basis of the standard model are from low-energy neutrinos (especially p-p neutrinos), while most of the uncertainty is caused by transitions to excited states (see Sec. VIII.A.2). We therefore give here the cross sections for transitions between the ground state of ^{71}Ga and the ground state of ^{71}Ge, which can be useful in estimating the capture rates and uncertainties for hypotheses in which the incident

TABLE V. The spectrum of solar neutrinos from the decay of ^{8}B. The neutrino energy q is in MeV, and $P(q)$ is the probability that a neutrino with energy q is emitted between $q \pm 0.5$ MeV.

q	P(q)	q	P(q)	q	P(q)	q	P(q)	q	P(q)
0.1	0.00022	3.1	0.07625	6.1	0.13211	9.1	0.09832	12.1	0.02526
0.2	0.00079	3.2	0.07929	6.2	0.13239	9.2	0.09603	12.2	0.02328
0.3	0.00152	3.3	0.08227	6.3	0.13256	9.3	0.09368	12.3	0.02137
0.4	0.00257	3.4	0.08521	6.4	0.13262	9.4	0.09130	12.4	0.01952
0.5	0.00386	3.5	0.08808	6.5	0.13258	9.5	0.08888	12.5	0.01776
0.6	0.00537	3.6	0.09089	6.6	0.13242	9.6	0.08643	12.6	0.01607
0.7	0.00709	3.7	0.09364	6.7	0.13216	9.7	0.08394	12.7	0.01446
0.8	0.00899	3.8	0.09631	6.8	0.13180	9.8	0.08143	12.8	0.01294
0.9	0.01105	3.9	0.09891	6.9	0.13133	9.9	0.07890	12.9	0.01150
1.0	0.01328	4.0	0.10144	7.0	0.13075	10.0	0.07634	13.0	0.01015
1.1	0.01565	4.1	0.10388	7.1	0.13007	10.1	0.07377	13.1	0.00889
1.2	0.01815	4.2	0.10623	7.2	0.12930	10.2	0.07119	13.2	0.00771
1.3	0.02077	4.3	0.10850	7.3	0.12842	10.3	0.06860	13.3	0.00664
1.4	0.02349	4.4	0.11068	7.4	0.12745	10.4	0.06601	13.4	0.00565
1.5	0.02630	4.5	0.11277	7.5	0.12638	10.5	0.06342	13.5	0.00476
1.6	0.02920	4.6	0.11476	7.6	0.12522	10.6	0.06083	13.6	0.00396
1.7	0.03217	4.7	0.11665	7.7	0.12397	10.7	0.05826	13.7	0.00325
1.8	0.03520	4.8	0.11845	7.8	0.12263	10.8	0.05569	13.8	0.00263
1.9	0.03828	4.9	0.12014	7.9	0.12120	10.9	0.05314	13.9	0.00210
2.0	0.04140	5.0	0.12173	8.0	0.11969	11.0	0.05061	14.0	0.00166
2.1	0.04455	5.1	0.12322	8.1	0.11810	11.1	0.04811	14.1	0.00129
2.2	0.04773	5.2	0.12460	8.2	0.11643	11.2	0.04563	14.2	0.00099
2.3	0.05093	5.3	0.12587	8.3	0.11468	11.3	0.04319	14.3	0.00075
2.4	0.05414	5.4	0.12703	8.4	0.11286	11.4	0.04078	14.4	0.00056
2.5	0.05735	5.5	0.12809	8.5	0.11097	11.5	0.03841	14.5	0.00042
2.6	0.06055	5.6	0.12904	8.6	0.10902	11.6	0.03609	14.6	0.00030
2.7	0.06374	5.7	0.12987	8.7	0.10699	11.7	0.03381	14.7	0.00022
2.8	0.06691	5.8	0.13060	8.8	0.10491	11.8	0.03159	14.8	0.00016
2.9	0.07006	5.9	0.13121	8.9	0.10277	11.9	0.02942	14.9	0.00011
3.0	0.07317	6.0	0.13171	9.0	0.10057	12.0	0.02731	15.0	0.00008

neutrino spectrum is different from the standard one shown in Fig. 2. For the p-p, pep, hep, ^{7}Be, ^{8}B, ^{13}N, ^{15}O, and ^{17}F neutrino sources, respectively, the ground-state-to-ground-state absorption cross sections are (unit is 10^{-46} cm^2): 11.8, 170, 5.44×10^3, 69.1, 2.85×10^3, 58.1, 100.1, and 100.5. Note that ground-state-to-ground-state transitions are dominant for all except the ^{8}B and hep neutrino sources (cf. Table VII).

B. Uncertainties

1. General considerations

There are two major sources of uncertainties in the absorption cross sections: (1) transitions to excited states and (2) forbidden corrections.

For the ^{37}Cl detector alone, it is possible (see Bahcall, 1978) to evaluate rather accurately the allowed matrix elements that connect the ground state of the target nucleus to the excited states of ^{37}Ar. This special calibration is accomplished by using data obtained from the decay of ^{37}Ca, the isotopic analog of the neutrino capture process. The uncertainties for this important detector are discussed separately below (see Sec. IV.B.2).

More generally, *we adopt a factor-of-2 uncertainty, total theoretical range, for transitions to excited states whose matrix elements must be inferred from (p,n) measurements.* Specifically, we assume that the lower limit for such transitions is one-half the value obtained from the (p,n) measurements by the standard methods and that the upper limit is twice the value found by using the

TABLE VI. The hep neutrino spectrum. The normalized neutrino energy spectrum $P(q)$ produced by reaction 1 is given in intervals of 0.447 MeV. The neutrino energy q is expressed in MeV, and $P(q)$ is normalized per MeV.

q(MeV)	P(q)	q(MeV)	P(q)
0.447	8.00E-04	9.83	9.74E-02
0.894	3.05E-03	10.3	9.66E-02
1.341	6.53E-03	10.7	9.50E-02
1.788	1.10E-02	11.2	9.25E-02
2.235	1.64E-02	11.6	8.93E-02
2.682	2.24E-02	12.1	8.54E-02
3.129	2.88E-02	12.5	8.08E-02
3.576	3.56E-02	13.0	7.56E-02
4.023	4.25E-02	13.4	6.98E-02
4.470	4.95E-02	13.9	6.36E-02
4.917	5.63E-02	14.3	5.70E-02
5.364	6.29E-02	14.8	5.02E-02
5.811	6.92E-02	15.2	4.32E-02
6.258	7.50E-02	15.6	3.62E-02
6.705	8.03E-02	16.1	2.94E-02
7.152	8.49E-02	16.5	2.29E-02
7.599	8.89E-02	17.0	1.68E-02
8.046	9.22E-02	17.4	1.13E-02
8.493	9.47E-02	17.9	6.62E-03
8.940	9.64E-02	18.3	2.92E-03
9.387	9.73E-02	18.8	0.00E+00

TABLE VII. Neutrino absorption cross sections, given in units of 10^{-46} cm^2 and averaged over the experimental spectra. Contributions from excited states and from forbidden effects are included. Uncertainties are discussed in the text.

Target	p-p	pep	hep	^{7}Be	^{8}B	^{13}N	^{15}O	^{17}F
^{7}Li	0.0	655	8.4×10^4	9.6	3.9×10^4	42.4	246	249
^{37}Cl	0.0	16	3.9×10^4	2.4	1.06×10^4	1.7	6.8	6.9
^{71}Ga	11.8	215	7.3×10^4	73.2	2.43×10^4	61.8	116	117
^{81}Br	0.0	75	9.0×10^4	18.3	2.7×10^4	14.5	36.7	37.0
^{98}Mo	0.0	0.0	1.0×10^5	0.0	3.0×10^4	0.0	0.0	0.0
^{115}In	78.0	576	6.1×10^4	248	2.5×10^4	224	355	356

TABLE VIII. Absorption cross sections for ^{8}B and hep neutrinos incident on ^{2}H and ^{40}Ar. The absorption cross sections are given for different values of the minimum accepted kinetic energy T_{min} of the recoil electrons. The deuterium values were computed using cross sections determined for individual energies by Nozawa (1987) (see Nozawa *et al.*, 1986) that were then averaged over the appropriate neutrino spectra (see Bahcall and Holstein, 1986, and Sec. III). The cross sections for argon refer to transitions from the ground state of ^{40}Ar to the $T=2$ isotopic-analog state at 4.38 MeV excitation in ^{40}K. The unit is 10^{-46} cm^2.

T_{min}	$\sigma(^8B)$		σ(hep)	
	^{2}H	^{40}Ar	^{2}H	^{40}Ar
0.0	1.17E+04	7.85E+03	3.03E+04	3.07E+04
1.0	1.17E+04	7.70E+03	3.03E+04	3.06E+04
2.0	1.17E+04	7.16E+03	3.03E+04	3.03E+04
3.0	1.15E+04	6.11E+03	3.02E+04	2.94E+04
4.0	1.11E+04	4.60E+03	3.01E+04	2.78E+04
4.5	1.08E+04	3.76E+03	2.99E+04	2.67E+04
5.0	1.04E+04	2.92E+03	2.96E+04	2.53E+04
5.5	9.83E+03	2.12E+03	2.93E+04	2.37E+04
6.0	9.17E+03	1.42E+03	2.89E+04	2.20E+04
6.5	8.40E+03	8.57E+03	2.83E+04	2.01E+04
7.0	7.53E+03	4.46E+02	2.76E+04	1.79E+04
7.5	6.59E+03	1.90E+02	2.68E+04	1.57E+04
8.0	5.60E+03	6.20E+01	2.58E+04	1.35E+04
8.5	4.59E+03	1.54E+01	2.46E+04	1.12E+04
9.0	3.62E+03	2.89E+00	2.33E+04	8.98E+03
9.5	2.71E+03	2.91E-01	2.18E+04	6.94E+03
10.0	1.90E+03	0.00E+00	2.02E+04	5.09E+03
11.0	7.14E+02	0.00E+00	1.66E+04	2.09E+03
12.0	1.45E+02	0.00E+00	1.27E+04	4.23E+02
12.5	4.50E+01	0.00E+00	1.07E+04	8.46E+01
13.0	1.07E+01	0.00E+00	8.81E+03	0.00E+00
13.5	1.95E+00	0.00E+00	6.99E+03	0.00E+00
14.0	2.28E−01	0.00E+00	5.31E+03	0.00E+00
14.5	1.10E−02	0.00E+00	3.81E+03	0.00E+00
15.0	0.00E−00	0.00E+00	2.54E+03	0.00E+00

(p,n) experiments. Thus, if the cross section inferred from (p,n) measurements is X, we take the upper limit to be $2X$ and the lower limit $0.5X$, which causes a difference in the upper and lower error estimates for some of the detectors discussed in Sec. VI. In computing the uncertainties from excited levels, we sum the contributions from individual excited states and neutrino sources and then square the result to obtain the quantity that is added in quadrature to the other estimated uncertainties discussed in Sec. V. We believe this conservative procedure

TABLE IX. Absorption cross sections for specific energies that are relevant for solar neutrino experiments. The unit is 10^{-46} cm^2. Contributions from excited states and from forbidden effects are included.

q(MeV)	$\sigma(^2H)$	$\sigma(^{37}Cl)$	$\sigma(^{40}Ar)$	$\sigma(^{71}Ga)$	$\sigma(^{81}Br)$	$\sigma(^{98}Mo)$
0.130	0.00E+00	0.00E+00	0.00E+00	0.00E+00	0.00E+00	0.00E+00
0.150	0.00E+00	0.00E+00	0.00E+00	0.00E+00	0.00E+00	0.00E+00
0.200	0.00E+00	0.00E+00	0.00E+00	0.00E+00	0.00E+00	0.00E+00
0.250	0.00E+00	0.00E+00	0.00E+00	1.39E+01	0.00E+00	0.00E+00
0.275	0.00E+00	0.00E+00	0.00E+00	1.53E+01	0.00E+00	0.00E+00
0.300	0.00E+00	0.00E+00	0.00E+00	1.70E+01	0.00E+00	0.00E+00
0.325	0.00E+00	0.00E+00	0.00E+00	1.88E+01	0.00E+00	0.00E+00
0.350	0.00E+00	0.00E+00	0.00E+00	2.06E+01	0.00E+00	0.00E+00
0.375	0.00E+00	0.00E+00	0.00E+00	2.26E+01	0.00E+00	0.00E+00
0.400	0.00E+00	0.00E+00	0.00E+00	2.46E+01	0.00E+00	0.00E+00
0.425	0.00E+00	0.00E+00	0.00E+00	2.71E+01	0.00E+00	0.00E+00
1.000	0.00E+00	5.21E+00	0.00E+00	1.01E+02	2.90E+01	0.00E+00
2.000	3.30E+01	3.70E+01	0.00E+00	4.06E+02	1.78E+02	1.16E+02
3.000	4.37E+02	1.15E+02	0.00E+00	1.01E+03	5.20E+02	9.64E+02
4.000	1.46E+03	2.63E+02	0.00E+00	2.18E+03	1.31E+03	2.65E+03
5.000	3.24E+03	5.63E+02	0.00E+00	4.48E+03	3.18E+03	5.67E+03
6.000	5.87E+03	1.52E+03	3.20E+02	8.62E+03	7.04E+03	1.04E+04
7.000	9.41E+03	4.76E+03	2.73E+03	1.56E+04	1.43E+04	1.77E+04
8.000	1.39E+04	1.02E+04	7.09E+03	2.63E+04	2.64E+04	2.91E+04
9.000	1.94E+04	1.79E+04	1.35E+04	4.06E+04	4.41E+04	4.67E+04
10.00	2.59E+04	2.77E+04	2.18E+04	5.84E+04	6.70E+04	7.16E+04
11.00	3.35E+04	3.97E+04	3.21E+04	7.96E+04	9.51E+04	1.03E+05
12.00	4.22E+04	5.38E+04	4.42E+04	1.04E+05	1.28E+05	1.42E+05
13.00	5.21E+04	7.00E+04	5.82E+04	1.32E+05	1.66E+05	1.86E+05
14.00	6.31E+04	8.83E+04	7.40E+04	1.62E+05	2.08E+05	2.36E+05
15.00	7.53E+04	1.09E+05	9.15E+04	1.95E+05	2.54E+05	2.92E+05
16.00	8.87E+04	1.31E+05	1.11E+05	2.32E+05	3.04E+05	3.52E+05
18.00	1.18E+05	1.81E+05	1.54E+05	3.11E+05	4.14E+05	4.84E+05
20.00	1.5E+05	2.38E+05	2.04E+05	3.99E+05	5.36E+05	6.30E+05
30.00		6.11E+05	5.25E+05	8.99E+05	1.21E+06	1.39E+06

is justified, since the most likely large error would result from an inapplicable extrapolation of the low A calibration of the average relation between (p,n) and neutrino capture cross sections (see Taddeucci *et al.*, 1987) to a particular large A nucleus. A calibration error would cause all of the transitions to move up or down together (in rate).

These conservative error limits represent an attempt to

take account of possible systematic effects that can occur in the calibration and application of the (p,n) experiments to the calculation of weak-interaction matrix elements, as well as the sometimes smaller statistical errors. Much more experimental and theoretical work is required on the relation between (p,n) cross sections and weak-interaction matrix elements in order to understand and, hopefully, reduce the uncertainties. The most urgently required experiments are measurements in the mass range A from ~ 70 to ~ 120, for which weak-interaction matrix elements are already known from β-decay experiments. A calibration sample that included of order ten targets in this mass range would provide a much improved basis for estimating the errors. It would be particularly desirable to measure the (p,n) cross sections for a number of different Gamow-Teller transitions *between the same pair of nuclei,* all of whose B(GT) values are known from β-decay experiments. There is some evidence (see Taddeucci *et al.*, 1987) that, for several targets with $A \lesssim 42$, the ratios of B(GT)'s with significant single-particle strength to a given daughter nucleus are determined to an accuracy of order 10% by the (p,n) measurements. However, there are only two well-studied targets, both with moderate mass numbers (^{26}Mg and ^{27}Al), in which as many as three ratios could be considered in the same nucleus (see Table III of Taddeucci *et al.*, 1987). It is therefore not clear that this regularity also applies for the larger mass numbers that are mainly of interest in the present paper.

We assume an uncertainty due to forbidden corrections that is 3 times larger than the best-estimate value given by Bahcall and Holstein (1986), (which is based upon dimensional analysis since the forbidden matrix elements cannot be reliably calculated). In addition, for the ^{8}B neutrinos, there is a further uncertainty that arises from the imprecisely known shape of the ^{8}B neutrino spectrum. We adopt for this latter effect, which refers only to ^{8}B neutrino absorption cross sections, a value of 3% (see Bahcall and Holstein, 1986).

How do we combine the cross-section uncertainties for different neutrino sources that contribute to the capture rate in a given detector? We have, for this purpose, divided up the sources into two groups, a high-energy group which contains only ^{8}B and hep neutrinos and a second group containing everything else. The most likely errors (calibration errors, forbidden corrections, uncertain decay rates) will usually affect in the same way sources within each group, but will affect differently the high-energy and the lower-energy sources. We have therefore combined the uncertainties coherently within each group (summed before we square) and incoherently between the two groups (square and then sum to compute the quadratic sum). For the ^{115}In experiment, we have chosen to combine coherently all of the cross-section uncertainties, since in this case every transition probability was calculated using the (p,n) data.

The uncertainties adopted here for neutrino absorption cross sections represent the intent of the "effective 3σ" uncertainties defined in paper I or the equivalent *"total theoretical range"* that is described in Sec. I.B of the Introduction to this paper. The uncertainties for the cross sections have to be evaluated separately for each neutrino source and for each target.

2. Uncertainties for individual detectors

For the ^{2}H detector, we assign an uncertainty of 10%. This uncertainty is the same as was given by Ellis and Bahcall (1968) in an earlier calculation of the ^{2}H cross sections. The work of Nozawa *et al.* (1986) includes forbidden corrections and exchange currents, both of which effects were explicitly omitted from the Ellis and Bahcall calculation. The nuclear models that were considered by Nozawa *et al.* yield results, including electron recoils of all energies, that have a range of $\pm 6\%$. However, Nozawa *et al.* did not attempt to estimate the *maximum* range for the values of the cross sections, but instead adopted nuclear models that were readily available. We have therefore adopted the original uncertainty estimate of Ellis and Bahcall, even though this somewhat exceeds the range in quoted cross-section values given by Nozawa *et al.* (1986).

For the ^{7}Li detector, we have extracted the nuclear matrix elements from the superallowed β decay of ^{7}Be, which is well studied in the laboratory. The major uncertainties are from forbidden corrections. We estimate the following percentage uncertainties for the different sources: pep (6%), hep (21%), ^{7}Be (5%), ^{8}B (17%), ^{13}N (5.5%), ^{15}O (6%), and ^{17}F (6%).

For the ^{37}Cl detector, only ^{8}B and hep neutrinos have enough energy to populate excited states. All the other sources have cross sections to which we assign uncertainties (as defined above) of 6%. For ^{8}B and hep neutrinos, the cross section is uncertain by about 10% (Bahcall and Holstein, 1986; Adelberger and Haxton, 1987).

For the ^{40}Ar detector, forbidden corrections constitute the dominant uncertainty, since the superallowed transition to the isobaric-analog state of ^{40}K can be calculated with high precision. The forbidden corrections are rather large for the high-energy neutrinos from ^{8}B and hep that are absorbed by ^{40}Ar. For a minimum electron kinetic energy $T_{\min}=0$, 5, or 7 MeV, the 1σ uncertainty for ^{8}B neutrino absorption is 2%, 2.5%, or 3%, respectively, implying an effective 3σ uncertainty $\sim 8\%$ for $T_{\min}=5$ MeV.

For the ^{71}Ga detector, the uncertainties in the cross sections are dominated by transitions to excited states for all but the p-p, ^{7}Be, and ^{13}N sources. For p-p neutrinos, the uncertainties are determined almost entirely by the forbidden corrections. Transitions to excited states are relatively infrequent also for ^{7}Be and ^{13}N neutrinos because of the small amount of energy available above threshold and, in both cases, lead to estimated uncertainties that are comparable to the uncertainties caused by

forbidden corrections. We adopt the following upper-limit uncertainties in absorption cross sections (uncertainty in parentheses): p-p, (7%), pep (22%), ^{7}Be (9%), ^{13}N (9%), ^{15}O (19%), and ^{17}F (19%). The corresponding lower-limit uncertainties are 7%, 13%, 8%, 8%, 11%, and 11%. The ^{8}B and hep absorption cross sections are determined almost entirely from the (p,n) measurements. The upper and lower uncertainties for absorption of ^{8}B neutrinos are 88% and 45%, respectively, and for hep neutrinos, 93% and 47%. (About 12% of the total cross section for the ^{8}B neutrinos is due to the ground-state-to-ground-state transition; the corresponding number for hep neutrinos is 7.5%.) The cross section that is calculated for ^{8}B neutrinos using the lower-background data presented by Krofcheck (1987) is 30% smaller than that obtained using the data of Krofcheck *et al.* (1985); the corresponding decrease for the hep cross section is 33%. All of the other cross sections are changed by less than 2% when the Krofcheck *et al.* (1985) data are replaced by the Krofcheck (1987) data.

All of the allowed transitions for the ^{81}Br detector are to excited states of ^{81}Kr. Transitions to the level of ^{81}Kr at 190-keV excitation energy dominate the absorption cross sections for all the following sources (percentage of the total cross section that is from the 190-keV level is given in parentheses): pep (57%), ^{7}Be (76%), ^{13}N (78%), ^{15}O (62%), and ^{17}F (62%). The uncertainty from forbidden corrections is between 6% and 7% for all of these sources. The total adopted uncertainties for the upper limit are, in the same order of sources, 46%, 33%, 32%, 42%, and 42% (cf. the discussion of a ^{81}Br detector in Sec. IV.C); the uncertainties for the lower limit are 27%, 26%, 26%, 27%, and 27%. The upper and lower uncertainties for absorption of ^{8}B neutrinos are 97% and 48%, respectively, and for hep neutrinos, 97% and 49%.

For ^{98}Mo, only ^{8}B and hep neutrinos are energetic enough to cause allowed transitions to ^{98}Tc. The experimental 1σ uncertainties in the (p,n) measurements (Rapaport *et al.*, 1985) are by themselves $\pm 30\%$, so that the total theoretical range in the predicted capture rate for this detector due to the neutrino absorption cross sections is at least a factor of 2. For definiteness, we adopt a factor-of-2 uncertainty.

For the ^{115}In detector, all of the relevant transitions are to excited states [see Bahcall (1978) for a discussion of the difficulties of calculating the capture rates for this nucleus]. The best estimate furnished by the (p,n) experiments (Rapaport *et al.*, 1985) for the matrix element to the lowest excited state at 0.61 MeV in ^{115}Sn is in remarkably good agreement with an insightful estimate made by Raghavan (1976) in his original paper on this subject. However, the available (p,n) measurements for all of the relevant transitions have large measuring errors, 1σ uncertainties of order 30%. In addition, the calibration is uncertain for the usual reasons discussed in the previous subsection. Thus the total theoretical range in the predicted capture rate for this detector due to the neutrino cross sections is also about a factor of 2.

C. Calibration experiments with a ^{51}Cr source

Systematic errors are difficult to estimate in any solar neutrino experiment. The confidence with which one regards the final measured number could be increased significantly by performing calibration experiments in the laboratory using megacurie amounts of radioactive sources. The most promising source appears to be ^{51}Cr.

The throughput efficiency of a ^{71}Ga detector can be tested by using a ^{51}Cr calibration source (Bahcall *et al.*, 1978). The total cross section for this source is

$$\sigma(^{51}\text{Cr on } ^{71}\text{Ga}) = 59.2(1\pm 0.1)\times 10^{-46} \text{ cm}^2 . \quad (5)$$

The ratio of cross sections computed with and without contributions from excited states is $\sigma(\text{total})/\sigma(\text{ground state}) = 1.05$. In computing the ^{71}Ga cross sections given in Table IV and Eq. (5), we have assumed that the B(GT) value to the 0.175-MeV excited state of ^{71}Ge is one-half the upper limit determined by Krofcheck (1987). The forbidden corrections to the capture rate increase the ^{71}Ga cross sections by about 2.25% (total theoretical uncertainty of 6.7%). The total formal uncertainties, computed according to the prescription given in Sec. IV.B.1, are $+8\%$ and -7%.

A calibration of the ^{81}Br detector with a ^{51}Cr source would be important because of the uncertain contribution for the ^{7}Be neutrinos of the 457 excited state of ^{81}Kr (see Bahcall, 1981), which cannot be studied by weak-interaction experiments in the laboratory. We have estimated the total cross section for ^{51}Cr neutrinos incident on ^{81}Br by combining the electron-capture measurements on ^{81}Br with the (p,n) experiments on ^{81}Br (Krofcheck *et al.* 1987). For the transition to the 190-keV excited state of ^{81}Kr, we adopt the weighted average B(GT) value, $0.0264(1\pm 0.1)$, 1σ error, that is determined jointly by the recent remeasurements of the electron-capture branching ratio of ^{81}Kr by Davids *et al.* (1987) and Lowry *et al.* (1987) and by the (p,n) experiments. For transitions to the other excited states, we use the B(GT) values that were determined in the (p,n) experiments. We find for the total cross section

$$\sigma(^{51}\text{Cr on } ^{81}\text{Br}) = 13.4(1\pm 0.3)\times 10^{-46} \text{ cm}^2 , \quad (6)$$

where the estimated uncertainty corresponds to the total theoretical range (cf. discussion in Sec. IV.B,2). The cross section given in Eq. (6) includes a 21% contribution from the 457 excited state of ^{81}Kr and a 2% forbidden correction.

For ^{115}In the calibration with a radioactive source is almost essential since the uncertainty (of order a factor of 2; see Sec. IV.B) in the absorption cross section is much larger than any of the astrophysical uncertainties (see Secs. VI and VII). Fortunately, a calibration experiment with a ^{51}Cr source would provide exactly the required information. A ^{51}Cr source would excite only the 0.61-MeV level of ^{115}Sn in the allowed approximation. The p-p and ^{7}Be neutrinos, which according to the standard

solar neutrino spectrum provide about 91% of the expected capture rate in a ^{115}In detector, also excite only the 0.61-MeV level. The neutrino sources that provide the remaining 9% of the expected capture rate only occasionally excite levels above the 0.61-MeV state. The total contribution of states above 0.61 MeV to the capture rate is primarily from ^{8}B neutrinos and is calculated to be of order 2% for the standard solar neutrino spectrum. Using the calibration inferred from the (p,n) data of Krofcheck *et al.* (1985), we estimate

$$\sigma(^{51}\text{Cr on } ^{115}\text{In}) = 222^{+222}_{-111} \times 10^{-46} \text{ cm}^2 , \quad (7)$$

where the total uncertainty was obtained according to the prescription given in Sec. IV.B.2. A measurement of the ^{51}Cr neutrino absorption cross section on ^{115}In would provide a valuable test of the validity of the (p,n) method for determining GT matrix elements.

D. Calibration experiments with a muon beam

The neutrinos from the decay of μ^+'s that are stopped in the beam dump of a meson factory such as the Los Alamos Meson Factory can be used in principle to calibrate the overall performance of solar neutrino detectors. The possibility of making such fundamental checks of the ^{37}Cl and the ^{71}Ga solar neutrino experiments has been discussed on a number of occasions (see, for example, Davis *et al.*, 1973; Evans *et al.*, 1980; Bowles, Cleveland, and Robertson, 1986).

We have calculated the expected total cross sections for neutrinos from stopped-muon decay using the known (Bahcall, 1978) β-decay matrix elements for transitions between ^{37}Cl and ^{37}Ar and the recent determination (Krofcheck *et al.*, 1985 and Krofcheck, 1987) by (p,n) measurements of the B(GT) values for the ^{71}Ga-to-^{71}Ge transitions. The matrix elements that are most important for the stopped-muon decay spectrum are the same ones that are dominant for the absorption of ^{8}B neutrinos. The B(GT) values increase relatively rapidly up to the neutrino separation energy, so that for both the ^{37}Cl and the ^{71}Ga detectors the largest contributions come, for both muon and ^{8}B neutrinos, from transitions to excited states at several MeV (typically $\sim$5 MeV) above the ground state.

We have made two calculations for each detector: (1) including corrections for forbidden terms in an expansion of the weak-interaction Hamiltonian according to a recently derived plausible prescription (Bahcall and Holstein, 1986); and (2) ignoring all forbidden corrections. Our goal is to show that the uncertainties are large because of terms that cannot be reliably calculated. For simplicity, we have omitted contributions of the *opposite* sign, but the same order of magnitude, as the contributions from the forbidden corrections to allowed capture that are considered here. The omitted terms are expected (Haxton, 1987) to arise from first forbidden corrections to allowed neutrino capture [see the estimate given in Appendix A of Bahcall and Holstein, 1986, Eqs. (A17)–(A21)].

For the ^{37}Cl detector, we find

$$\sigma(^{37}\text{Cl})_{\text{incl. forbid.}} = 0.93 \times 10^{-40} \text{ cm}^2 \quad (8)$$

when forbidden corrections are included and

$$\sigma(^{37}\text{Cl})_{\text{no forbid.}} = 1.24 \times 10^{-40} \text{ cm}^2 \quad (9)$$

when forbidden corrections are ignored.

Similarly, for the ^{71}Ga detector we find

$$\sigma(^{71}\text{Ga})_{\text{incl. forbid.}} = 9.9 \times 10^{-41} \text{ cm}^2 \quad (10)$$

including forbidden corrections and

$$\sigma(^{71}\text{Ga})_{\text{no forbid.}} = 2.0 \times 10^{-40} \text{ cm}^2 \quad (11)$$

without forbidden corrections.

The difference between cross sections calculated with and without forbidden corrections is much larger for neutrinos from μ^+ decay than was found by Bahcall and Holstein (1986) for the solar neutrino spectrum from ^{8}B. The reason is that many of the most important forbidden terms scale as (neutrino energy $\times$ nuclear radius)^2.

The calculated forbidden terms include corrections to allowed transitions measured either by the decay of ^{37}Ca (for the case of ^{37}Cl) or by (p,n) measurements (for the ^{71}Ga detector). However, other correction terms that are potentially of the same order are not included. The terms that are omitted are the so-called first forbidden transitions in nuclear β decay, which would not show up in either the β decay or the (p,n) measurements. We do not know of a reliable way to estimate their nuclear matrix elements. Moreover, the prescription (Bahcall and Holstein, 1986) adopted for evaluating the forbidden terms that are included provides only a plausible estimate, not a rigorous determination.

We therefore regard the difference between the two ways of calculating the absorption cross sections, with and without forbidden corrections, as a measure of the theoretical uncertainty. The neutrinos from muon decay can be used to calibrate the overall performance of the solar neutrino detectors to an accuracy of a factor of 2 or better, but not to an accuracy of 10%.

V. THE STANDARD SOLAR MODEL

A. The basics

The "standard solar model" is the result of the best physics and input parameters that are available at the time the model is constructed. Thus the set of numbers that correspond to the standard solar model vary with time, hopefully (nearly) always getting closer to the "true" standard model. In the quarter of a century that we have been working on this problem, we have made many hundreds of improvements and changes in the standard model. It would be impossible to summarize

them all here. The reader who wants to investigate standard models in more detail can consult the references listed in the caption to Fig. 10.

We continually upgrade our computer codes to include more accurate physics and better input data. The complications in the coding that are introduced by this (seemingly) endless process of iterations make it difficult for many of our colleagues to check directly our most detailed numerical evaluations. However, we believe that difficulty in replication is not too expensive a price to pay for precision, especially when one wishes to compare with solar neutrino experiments or measurements of solar oscillation frequencies. Some seemingly esoteric aspects of our codes make noticeable differences in the predictions of neutrino fluxes or oscillation frequencies.

The most important input data used in constructing standard solar models are nuclear reaction cross sections, the solar luminosity, the solar age, the equation of state, the elemental abundances, and the radiative opacity. Our best estimates for all of these quantities are described in Sec. II of paper I and in Sec. II of the present paper.

Some of the principal approximations used in constructing standard models deserve special attention since they have been investigated particularly thoroughly or often for possible sources of departure from the standard scenario. (The interested reader can find detailed discussions of the validity of these approximations, as well as estimates of the small expected effects of departures from the standard assumptions, in the references listed in Fig. 10 and in the reviews of nonstandard models listed at the end of this subsection.) (1) Hydrostatic equilibrium. The sun is assumed to be in hydrostatic equilibrium; the radiative and particle pressures of the model exactly balance gravity. Observationally, this is known to be an excellent approximation, since a gross departure from hydrostatic equilibrium would cause the sun to collapse in a free-fall time, which is less than 1 h. We also neglect pulsation, rotation, and pressure due to magnetic fields. (2) Energy transport by photons or convective currents. In the deep interior, which is most important for the solar neutrino problem, the energy transport is primarily by photon diffusion and is described in terms of the Rosseland mean opacity. For regions that are unstable against convective motions, the temperature gradient is taken to be the adiabatic gradient except very near the surface (important for the helioseismological calculations), where mixing-length theory is used. We neglect transport due to acoustic or gravity waves or to possible weakly interacting massive particles (WIMP's). (3) Energy generation by nuclear reactions. The primary energy source for the radiated photons and neutrinos is nuclear fusion, although we include the small effects of gravitational contraction (actually expansion at the present epoch). We also include small departures from equilibrium that are caused by the fusion processes themselves, i.e., nuclear burning. We do not include, for example, hypothetical transient events caused by large, abrupt mixing of the solar interior nor accretion onto a conjectured central black hole. (4) Abundance changes caused solely by nuclear reactions. We assume that the primordial solar interior was chemically homogeneous. Changes in the local abundances of individual isotopes occur only by nuclear reactions in those regions of the model that are convectively stable. We neglect thermal and gravitational diffusion, as well as meridional currents or low-amplitude pulsations.

A standard solar model is really a sequence of models. We generally begin with a main sequence star that has a homogeneous composition. Hydrogen burns in the core of the model, supplying both the radiated luminosity and the local heat (thermal pressure) which supports the star against gravitational collapse. Successive models are calculated by allowing for composition changes caused by nuclear reactions, as well as the mild evolution of other parameters; the integration of the nuclear abundance equations entails some numerical complications (see Appendix B of paper I). The nuclear interaction rates are interpolated between the previous and new models and multiplied by a time step (usually of order 5×10^8 or 10^9 yr), in order to determine the new chemical composition as a function of mass fraction included. The model at the advanced time is computed using the new composition. The later models in an evolutionary sequence have very inhomogeneous compositions, the innermost mass fraction of hydrogen being about one-half the surface (primordial) value.

The stellar evolution models are constructed by integrating from the center outward and from the surface inward, requiring that the two solutions match at a convenient point that is typically at about $0.2M_\odot$. Details of how our codes work are provided in Appendix C of this paper. Bahcall and Sears (1972) described and compared many of the earlier standard solar models and the methods by which they were derived. Evolutionary codes have been developed recently by a number of different groups (for example, Gilliland, 1982; Cassé, Cahen, and Doom, 1986); when adjusted for differences in input parameters, all of the codes yield solar neutrino fluxes that are in agreement with each other to of order 10% or better.

How does one proceed in practice? Guess an initial set of parameters; march the models along in time using difference equations to represent the equations of stellar evolution; calculate the predicted characteristics of the present sun; and then iterate the results until good numerical agreement is obtained between the model and the observed sun. In our models, we begin by guessing primordial values of X, the initial homogeneous hydrogen abundance, and S, the entropylike variable discussed in Appendix A of paper I. [S defines the adiabat of the convection zone; cf. discussion given below of the variables listed in Table X. In earlier treatments of the problem, one adjusted the constant $K=P/T^{2.5}$, which gives the relation between pressure and temperature in the convective envelope (see Sears, 1964, or Bahcall and Shaviv, 1968).] Typically, an evolutionary sequence requires of order five-to-seven solar models of progressively greater

ages to match the luminosity and radius to the desired one part in 10^5.

The primordial helium abundance of the model is determined in the process of iteration (see Sec. V.D for our best current estimate of the primordial helium abundance). The other two composition parameters are fixed by the surface (primordial) ratio of Z/X that is taken from observations (see Sec. II.B) and by the fact that the sum of all the mass fractions is equal to unity, i.e., $X+Y+Z=1.0$.

Constructing a solar model is an eigenvalue problem, with fixed boundary conditions. We seek a model with a total luminosity (in photons) equal to $L_{\rm solar}$ and an outer radius $R_{\rm solar}$ at an elapsed time of 4.6×10^9 yr. The initially assumed values of X and S are iterated until an eigenvalue is obtained. Empirical relations have been derived which can be used as guides in this iterative process [see Eq. (15) of paper I].

The luminosity boundary condition has an especially strong effect on the calculated neutrino fluxes. The reason is that both the luminosity and the neutrino fluxes are produced by nuclear reactions in the solar core. [The interplay between the energy generation and the neutrino fluxes can be seen most easily by comparing Figs. 6(a) and 8, below.] The strong coupling between the luminosity and the neutrino fluxes has resulted in some groups' deriving incorrect results because they have not iterated the models sufficiently.

An eigenvalue solution determines the primordial values for the mass fractions of hydrogen, helium, and heavy elements (respectively, X, Y, and Z), the present complete run of physical variables inside the sun, the spectrum of oscillation frequencies, and, of course, the neutrino fluxes.

What are nonstandard solar models? "Nonstandard" solar models are, by definition, constructed by changing something, physics or input data, from the current best guess to something that is less plausible. Most of the nonstandard solar models that have been published were invented in order to "solve" the solar neutrino problem [systematic investigations and reviews of many of the nonstandard models have been given by Bahcall, Bahcall, and Ulrich (1969), Rood (1978), Boyd *et al.* (1985), Roxburgh (1985a, 1985b), Schatzman (1985), and Newman (1986)]. If the physics or input parameters used in the nonstandard models were believed to be correct, then we would have incorporated the "nonstandard" features into the standard model.

B. Physical characteristics

We have constructed new standard solar models using the best estimates for all of the parameters given in this paper and in paper I. We derived evolutionary sequences for the sun beginning with a zero-age main sequence model with a homogeneous composition. Successive models embody composition changes caused by the nuclear reactions. The models were iterated until agreement with an accuracy of one part in 10^4 was achieved between the model and the observations of the solar luminosity and the solar radius. The adopted ratio of heavy-element-to-hydrogen abundance was maintained precisely throughout the calculations. Details of the calculational procedure are described in paper I, Appendix C of this paper, and in the references contained therein.

There are a number of characteristics of the standard model that are of general interest. For example, the fraction of the photon luminosity that originates in the *p-p* chain is 0.984; the corresponding fraction for the CNO cycle is 0.016. The gravitational expansion at the present epoch corresponds to a luminosity fraction of -0.0003. The convection zone terminates at 1.92×10^6 K, corresponding to a radius of $0.74R_\odot$ and a density of 0.12 g cm^{-3}; the convection zone comprises the outer 1.5% of the solar mass.[3] One-half of the luminosity (or the flux of *p-p* neutrinos) is produced within the inner $0.09M_\odot$ ($R\leq0.11R_\odot$); 95% of the luminosity is produced within the inner $0.36M_\odot$ ($R\leq0.21R_\odot$).

The neutrino luminosity is 2.3% of the photon luminosity, which corresponds to an average amount of energy lost in neutrinos per termination of the *p-p* chain of 0.572 MeV. The *p-p* chain is terminated 84.5% of the time by the ^{3}He-^{3}He reaction (number 5 in Table I) and 14.5% in the time by the ^{3}He-^{4}He reaction (number 6 in Table I).

Tables X and XI provide a detailed numerical description of the solar interior of the standard model. Table X lists the principal physical and chemical characteristics of the standard solar model. The first seven columns present the physical variables that define the model: the zone number, the mass included in the current and all inner zones (in units of $M_\odot$), the radius (in units of $R_\odot$), the temperature (in degrees K), the density (in units of g cm^{-3}), the pressure (in units of ergs cm^{-3}), the lumi-

[3]The precise parameters for the convective zone are unimportant for the solar neutrino problem (see the end of Sec. X.D), although they are relevant for the calculation of the *p*-mode oscillation frequencies (see Sec. X). The parameters for the convection zone given here differ slightly from those obtained by Christensen-Dalsgaard (1982), who finds a convection zone that extends somewhat deeper (to $0.71R_\odot$). The asymptotic inversions given by Christensen-Dalsgaard *et al.* (1985) and discussed by Gough (1986) suggest that the depth of the solar convection zone is closer to 0.71 $R_\odot$ than to $0.74R_\odot$ (our value). The significance of this result is unclear, however, since the Christensen-Dalsgaard (1982) model was derived using an opacity that is not up to date. Moreover, the equation of state used by Christensen-Dalsgaard (1982) introduces significant uncertainties because it is based upon the Eggleton, Faulkner, and Flannery (1973) treatment of pressure ionization, which contains an arbitrary function. The influence of this unknown function on the derived properties of solar models has not yet been studied systematically.

TABLE X. Model physical and chemical characteristics.

$M/M_\odot$	$R/R_\odot$	T	ρ	P	$L/L_\odot$	S_{crit}	$X(^1\mathrm{H})$	$X(^3\mathrm{He})$	$X(^4\mathrm{He})$	$X(^7\mathrm{Be})$	$X(^{12}\mathrm{C})$	$X(^{14}\mathrm{N})$	$X(^{16}\mathrm{O})$
0.00000	0.0000	1.56E+07	1.48E+02	2.29E+17	0.000	-0.127	0.34111	7.74E-06	0.63867	1.65E-11	2.61E-05	6.34E-03	8.48E-03
0.00001	0.0039	1.56E+07	1.48E+02	2.29E+17	0.000	-0.124	0.34103	7.73E-06	0.63875	1.65E-11	2.61E-05	6.34E-03	8.48E-03
0.00005	0.0083	1.56E+07	1.47E+02	2.28E+17	0.000	-0.127	0.34317	7.88E-06	0.63661	1.64E-11	2.60E-05	6.33E-03	8.50E-03
0.00017	0.0120	1.56E+07	1.46E+02	2.27E+17	0.001	-0.130	0.34546	8.04E-06	0.63432	1.62E-11	2.59E-05	6.31E-03	8.52E-03
0.00040	0.0158	1.56E+07	1.45E+02	2.26E+17	0.003	-0.132	0.34885	8.29E-06	0.63092	1.59E-11	2.56E-05	6.29E-03	8.54E-03
0.00078	0.0197	1.55E+07	1.44E+02	2.24E+17	0.007	-0.134	0.35328	8.63E-06	0.62649	1.56E-11	2.54E-05	6.26E-03	8.58E-03
0.00135	0.0237	1.55E+07	1.42E+02	2.21E+17	0.012	-0.137	0.35868	9.06E-06	0.62108	1.52E-11	2.50E-05	6.22E-03	8.62E-03
0.00214	0.0277	1.54E+07	1.40E+02	2.18E+17	0.018	-0.141	0.36499	9.58E-06	0.61476	1.47E-11	2.47E-05	6.18E-03	8.66E-03
0.00320	0.0317	1.53E+07	1.37E+02	2.15E+17	0.027	-0.144	0.37217	1.02E-05	0.60758	1.41E-11	2.43E-05	6.14E-03	8.71E-03
0.00456	0.0358	1.52E+07	1.35E+02	2.12E+17	0.038	-0.147	0.38016	1.09E-05	0.59958	1.34E-11	2.38E-05	6.10E-03	8.76E-03
0.00625	0.0400	1.51E+07	1.32E+02	2.08E+17	0.051	-0.150	0.38890	1.18E-05	0.59084	1.27E-11	2.34E-05	6.06E-03	8.81E-03
0.00832	0.0442	1.50E+07	1.29E+02	2.03E+17	0.067	-0.155	0.39833	1.28E-05	0.58140	1.19E-11	2.29E-05	6.02E-03	8.86E-03
0.01080	0.0484	1.49E+07	1.26E+02	1.99E+17	0.085	-0.160	0.40839	1.39E-05	0.57133	1.11E-11	2.24E-05	5.98E-03	8.90E-03
0.01373	0.0528	1.48E+07	1.23E+02	1.94E+17	0.106	-0.163	0.41903	1.52E-05	0.56069	1.02E-11	2.19E-05	5.94E-03	8.94E-03
0.01715	0.0572	1.46E+07	1.19E+02	1.89E+17	0.130	-0.167	0.43017	1.67E-05	0.54954	9.33E-12	2.13E-05	5.91E-03	8.98E-03
0.02109	0.0616	1.45E+07	1.16E+02	1.83E+17	0.157	-0.171	0.44176	1.85E-05	0.53794	8.44E-12	2.08E-05	5.88E-03	9.01E-03
0.02560	0.0662	1.43E+07	1.12E+02	1.78E+17	0.186	-0.176	0.45428	2.05E-05	0.52542	7.55E-12	2.03E-05	5.86E-03	9.04E-03
0.03071	0.0708	1.42E+07	1.08E+02	1.72E+17	0.217	-0.179	0.46672	2.28E-05	0.51297	6.69E-12	1.98E-05	5.84E-03	9.06E-03
0.03645	0.0756	1.40E+07	1.05E+02	1.66E+17	0.251	-0.183	0.47942	2.54E-05	0.50026	5.86E-12	1.92E-05	5.82E-03	9.08E-03
0.04287	0.0804	1.38E+07	1.01E+02	1.60E+17	0.287	-0.188	0.49233	2.85E-05	0.48735	5.08E-12	1.87E-05	5.81E-03	9.10E-03
0.05000	0.0853	1.37E+07	9.70E+01	1.53E+17	0.325	-0.192	0.50536	3.20E-05	0.47431	4.35E-12	1.82E-05	5.80E-03	9.11E-03
0.05769	0.0902	1.35E+07	9.33E+01	1.47E+17	0.363	-0.196	0.51817	3.60E-05	0.46150	3.70E-12	1.76E-05	5.79E-03	9.12E-03
0.06538	0.0948	1.33E+07	8.99E+01	1.41E+17	0.400	-0.200	0.52988	4.02E-05	0.44978	3.16E-12	1.71E-05	5.78E-03	9.13E-03
0.07308	0.0992	1.31E+07	8.68E+01	1.36E+17	0.434	-0.205	0.54066	4.46E-05	0.43900	2.71E-12	1.67E-05	5.78E-03	9.14E-03
0.08077	0.1033	1.30E+07	8.40E+01	1.31E+17	0.466	-0.208	0.55064	4.93E-05	0.42902	2.33E-12	1.62E-05	5.78E-03	9.14E-03
0.08846	0.1073	1.28E+07	8.13E+01	1.26E+17	0.497	-0.213	0.55990	5.42E-05	0.41975	2.01E-12	1.58E-05	5.78E-03	9.14E-03
0.09615	0.1111	1.27E+07	7.88E+01	1.22E+17	0.525	-0.216	0.56853	5.95E-05	0.41111	1.74E-12	1.54E-05	5.77E-03	9.14E-03
0.10385	0.1147	1.25E+07	7.64E+01	1.18E+17	0.553	-0.219	0.57659	6.51E-05	0.40304	1.50E-12	1.50E-05	5.77E-03	9.15E-03
0.11154	0.1182	1.24E+07	7.42E+01	1.14E+17	0.579	-0.224	0.58414	7.10E-05	0.39549	1.30E-12	1.47E-05	5.77E-03	9.15E-03
0.11923	0.1217	1.22E+07	7.20E+01	1.10E+17	0.603	-0.228	0.59121	7.73E-05	0.38841	1.13E-12	1.43E-05	5.77E-03	9.15E-03
0.12692	0.1250	1.21E+07	7.00E+01	1.06E+17	0.626	-0.233	0.59785	8.40E-05	0.38177	9.86E-13	1.40E-05	5.77E-03	9.15E-03
0.13462	0.1283	1.20E+07	6.81E+01	1.03E+17	0.648	-0.237	0.60409	9.11E-05	0.37552	8.59E-13	1.39E-05	5.77E-03	9.15E-03
0.14231	0.1315	1.18E+07	6.63E+01	9.92E+16	0.668	-0.241	0.60996	9.86E-05	0.36964	7.50E-13	1.45E-05	5.77E-03	9.15E-03
0.15000	0.1346	1.17E+07	6.45E+01	9.60E+16	0.688	-0.246	0.61549	1.07E-04	0.36410	6.56E-13	1.68E-05	5.77E-03	9.15E-03
0.15600	0.1370	1.16E+07	6.32E+01	9.36E+16	0.702	-0.250	0.61958	1.13E-04	0.36001	5.91E-13	2.14E-05	5.76E-03	9.15E-03
0.16200	0.1393	1.15E+07	6.20E+01	9.12E+16	0.716	-0.254	0.62349	1.20E-04	0.35610	5.33E-13	3.07E-05	5.75E-03	9.15E-03
0.16800	0.1417	1.14E+07	6.07E+01	8.89E+16	0.729	-0.259	0.62722	1.27E-04	0.35236	4.81E-13	4.76E-05	5.73E-03	9.15E-03
0.17400	0.1440	1.13E+07	5.95E+01	8.67E+16	0.742	-0.264	0.63079	1.35E-04	0.34879	4.34E-13	7.59E-05	5.70E-03	9.15E-03
0.18000	0.1462	1.13E+07	5.84E+01	8.46E+16	0.754	-0.268	0.63420	1.43E-04	0.34537	3.92E-13	1.20E-04	5.65E-03	9.15E-03
0.18600	0.1485	1.12E+07	5.72E+01	8.25E+16	0.766	-0.275	0.63747	1.51E-04	0.34211	3.54E-13	1.84E-04	5.57E-03	9.15E-03
0.19200	0.1507	1.11E+07	5.61E+01	8.05E+16	0.777	-0.281	0.64059	1.60E-04	0.33899	3.20E-13	2.72E-04	5.47E-03	9.15E-03
0.19800	0.1529	1.10E+07	5.50E+01	7.85E+16	0.788	-0.287	0.64359	1.69E-04	0.33600	2.90E-13	3.87E-04	5.34E-03	9.15E-03
0.20400	0.1551	1.09E+07	5.40E+01	7.66E+16	0.798	-0.295	0.64646	1.79E-04	0.33315	2.63E-13	5.28E-04	5.17E-03	9.15E-03
0.21000	0.1572	1.08E+07	5.30E+01	7.47E+16	0.807	-0.304	0.64922	1.89E-04	0.33041	2.38E-13	6.94E-04	4.98E-03	9.15E-03
0.21600	0.1594	1.08E+07	5.20E+01	7.29E+16	0.817	-0.312	0.65185	2.00E-04	0.32779	2.16E-13	8.82E-04	4.76E-03	9.15E-03
0.22200	0.1615	1.07E+07	5.10E+01	7.11E+16	0.826	-0.321	0.65438	2.11E-04	0.32529	1.96E-13	1.09E-03	4.52E-03	9.15E-03
0.22800	0.1636	1.06E+07	5.00E+01	6.94E+16	0.834	-0.329	0.65681	2.22E-04	0.32289	1.78E-13	1.30E-03	4.26E-03	9.15E-03
0.23400	0.1657	1.05E+07	4.91E+01	6.77E+16	0.842	-0.337	0.65913	2.34E-04	0.32058	1.61E-13	1.53E-03	4.00E-03	9.15E-03
0.24000	0.1678	1.04E+07	4.82E+01	6.61E+16	0.850	-0.346	0.66136	2.47E-04	0.31838	1.47E-13	1.75E-03	3.74E-03	9.15E-03
0.24600	0.1699	1.04E+07	4.73E+01	6.45E+16	0.857	-0.352	0.66349	2.60E-04	0.31627	1.33E-13	1.98E-03	3.48E-03	9.15E-03
0.25200	0.1719	1.03E+07	4.64E+01	6.29E+16	0.865	-0.364	0.66550	2.73E-04	0.31429	1.22E-13	2.18E-03	3.24E-03	9.15E-03
0.25800	0.1740	1.02E+07	4.55E+01	6.14E+16	0.872	-0.373	0.66746	2.87E-04	0.31235	1.11E-13	2.39E-03	3.00E-03	9.15E-03
0.26400	0.1760	1.02E+07	4.47E+01	5.99E+16	0.878	-0.381	0.66934	3.03E-04	0.31049	1.01E-13	2.58E-03	2.78E-03	9.15E-03
0.27000	0.1781	1.01E+07	4.38E+01	5.84E+16	0.885	-0.390	0.67113	3.18E-04	0.30871	9.22E-14	2.75E-03	2.58E-03	9.15E-03
0.27600	0.1801	1.00E+07	4.30E+01	5.70E+16	0.891	-0.399	0.67285	3.35E-04	0.30700	8.40E-14	2.91E-03	2.39E-03	9.15E-03
0.28200	0.1821	9.95E+06	4.22E+01	5.56E+16	0.896	-0.406	0.67450	3.52E-04	0.30536	7.65E-14	3.06E-03	2.21E-03	9.15E-03
0.28800	0.1841	9.88E+06	4.14E+01	5.42E+16	0.902	-0.414	0.67607	3.71E-04	0.30379	6.97E-14	3.19E-03	2.06E-03	9.15E-03
0.29400	0.1861	9.81E+06	4.06E+01	5.29E+16	0.907	-0.423	0.67758	3.90E-04	0.30228	6.36E-14	3.31E-03	1.92E-03	9.15E-03
0.30000	0.1881	9.74E+06	3.99E+01	5.16E+16	0.912	-0.430	0.67902	4.10E-04	0.30084	5.80E-14	3.42E-03	1.80E-03	9.15E-03
0.31000	0.1914	9.63E+06	3.86E+01	4.95E+16	0.919	-0.446	0.68129	4.45E-04	0.29856	4.98E-14	3.57E-03	1.62E-03	9.15E-03
0.32000	0.1948	9.52E+06	3.74E+01	4.75E+16	0.926	-0.459	0.68339	4.84E-04	0.29644	4.27E-14	3.69E-03	1.48E-03	9.15E-03
0.33000	0.1981	9.41E+06	3.63E+01	4.55E+16	0.933	-0.473	0.68535	5.26E-04	0.29445	3.67E-14	3.79E-03	1.37E-03	9.15E-03
0.34000	0.2014	9.31E+06	3.51E+01	4.36E+16	0.939	-0.488	0.68716	5.71E-04	0.29261	3.15E-14	3.86E-03	1.28E-03	9.15E-03
0.35000	0.2047	9.20E+06	3.40E+01	4.18E+16	0.945	-0.502	0.68885	6.20E-04	0.29088	2.71E-14	3.92E-03	1.21E-03	9.15E-03
0.36000	0.2080	9.10E+06	3.29E+01	4.01E+16	0.950	-0.517	0.69042	6.74E-04	0.28927	2.33E-14	3.97E-03	1.16E-03	9.15E-03

TABLE X. (*Continued*).

$M/M_\odot$	$R/R_\odot$	T	ρ	P	$L/L_\odot$	S_{crit}	$X(^1H)$	$X(^3He)$	$X(^4He)$	$X(^7Be)$	$X(^{12}C)$	$X(^{14}N)$	$X(^{16}O)$
0.37000	0.2113	9.00E+06	3.18E+01	3.84E+16	0.954	-0.533	0.69187	7.32E-04	0.28776	2.00E-14	4.01E-03	1.11E-03	9.15E-03
0.38000	0.2146	8.90E+06	3.08E+01	3.67E+16	0.959	-0.548	0.69322	7.95E-04	0.28636	1.72E-14	4.04E-03	1.08E-03	9.15E-03
0.39000	0.2179	8.80E+06	2.98E+01	3.52E+16	0.963	-0.564	0.69447	8.64E-04	0.28504	1.48E-14	4.06E-03	1.05E-03	9.15E-03
0.40000	0.2212	8.70E+06	2.88E+01	3.36E+16	0.966	-0.580	0.69563	9.38E-04	0.28381	1.27E-14	4.08E-03	1.03E-03	9.15E-03
0.41000	0.2246	8.60E+06	2.78E+01	3.22E+16	0.970	-0.589	0.69670	1.02E-03	0.28266	1.09E-14	4.09E-03	1.02E-03	9.15E-03
0.42000	0.2279	8.51E+06	2.69E+01	3.08E+16	0.973	-0.600	0.69770	1.11E-03	0.28158	9.38E-15	4.10E-03	1.00E-03	9.15E-03
0.43000	0.2313	8.41E+06	2.60E+01	2.94E+16	0.976	-0.610	0.69862	1.21E-03	0.28056	8.06E-15	4.11E-03	9.93E-04	9.15E-03
0.44000	0.2347	8.32E+06	2.51E+01	2.81E+16	0.978	-0.622	0.69946	1.32E-03	0.27960	6.91E-15	4.12E-03	9.86E-04	9.15E-03
0.45000	0.2381	8.22E+06	2.42E+01	2.68E+16	0.981	-0.633	0.70024	1.44E-03	0.27871	5.93E-15	4.12E-03	9.80E-04	9.15E-03
0.46000	0.2415	8.13E+06	2.34E+01	2.56E+16	0.983	-0.644	0.70096	1.57E-03	0.27786	5.08E-15	4.12E-03	9.76E-04	9.15E-03
0.47000	0.2450	8.04E+06	2.25E+01	2.44E+16	0.985	-0.658	0.70161	1.72E-03	0.27705	4.35E-15	4.13E-03	9.73E-04	9.15E-03
0.48000	0.2485	7.95E+06	2.17E+01	2.32E+16	0.987	-0.667	0.70221	1.88E-03	0.27629	3.72E-15	4.13E-03	9.70E-04	9.15E-03
0.49000	0.2520	7.86E+06	2.09E+01	2.21E+16	0.989	-0.682	0.70275	2.07E-03	0.27557	3.18E-15	4.13E-03	9.68E-04	9.15E-03
0.50000	0.2555	7.76E+06	2.01E+01	2.10E+16	0.990	-0.694	0.70324	2.26E-03	0.27488	2.71E-15	4.13E-03	9.67E-04	9.15E-03
0.51000	0.2591	7.67E+06	1.94E+01	2.00E+16	0.992	-0.707	0.70368	2.47E-03	0.27423	2.29E-15	4.13E-03	9.66E-04	9.15E-03
0.52000	0.2628	7.58E+06	1.86E+01	1.90E+16	0.993	-0.721	0.70409	2.69E-03	0.27361	1.93E-15	4.13E-03	9.65E-04	9.15E-03
0.53000	0.2664	7.49E+06	1.79E+01	1.81E+16	0.994	-0.736	0.70446	2.90E-03	0.27303	1.60E-15	4.13E-03	9.64E-04	9.15E-03
0.54000	0.2702	7.41E+06	1.72E+01	1.71E+16	0.995	-0.751	0.70480	3.08E-03	0.27251	1.31E-15	4.13E-03	9.64E-04	9.15E-03
0.55000	0.2739	7.32E+06	1.65E+01	1.62E+16	0.996	-0.766	0.70512	3.22E-03	0.27204	1.05E-15	4.13E-03	9.64E-04	9.15E-03
0.58500	0.2876	7.01E+06	1.42E+01	1.34E+16	0.998	-0.815	0.70621	3.18E-03	0.27100	4.01E-16	4.13E-03	9.63E-04	9.15E-03
0.62000	0.3020	6.70E+06	1.20E+01	1.09E+16	0.999	-0.854	0.70723	2.49E-03	0.27066	1.15E-16	4.14E-03	9.63E-04	9.15E-03
0.65500	0.3176	6.39E+06	1.01E+01	8.69E+15	1.000	-0.896	0.70806	1.74E-03	0.27059	2.74E-17	4.14E-03	9.63E-04	9.15E-03
0.69000	0.3344	6.08E+06	8.34E+00	6.82E+15	1.000	-0.946	0.70866	1.15E-03	0.27058	5.69E-18	4.14E-03	9.63E-04	9.15E-03
0.72500	0.3529	5.76E+06	6.75E+00	5.22E+15	1.000	-0.996	0.70907	7.40E-04	0.27058	1.04E-18	4.14E-03	9.63E-04	9.15E-03
0.76000	0.3737	5.44E+06	5.32E+00	3.88E+15	1.000	-1.029	0.70934	4.67E-04	0.27058	1.61E-19	4.14E-03	9.63E-04	9.15E-03
0.79500	0.3975	5.09E+06	4.06E+00	2.77E+15	1.001	-1.065	0.70952	2.95E-04	0.27058	2.06E-20	4.14E-03	9.63E-04	9.15E-03
0.83000	0.4255	4.73E+06	2.96E+00	1.88E+15	1.001	-1.101	0.70962	1.93E-04	0.27058	2.11E-21	4.14E-03	9.63E-04	9.15E-03
0.86500	0.4597	4.33E+06	2.03E+00	1.18E+15	1.001	-1.111	0.70967	1.38E-04	0.27057	1.58E-22	4.14E-03	9.63E-04	9.15E-03
0.90000	0.5038	3.88E+06	1.27E+00	6.59E+14	1.001	-1.093	0.70970	1.12E-04	0.27058	6.87E-24	4.14E-03	9.63E-04	9.15E-03
0.92373	0.5431	3.53E+06	8.42E-01	3.98E+14	1.001	-1.048	0.70970	1.04E-04	0.27058	4.48E-25	4.14E-03	9.63E-04	9.15E-03
0.94183	0.5818	3.20E+06	5.72E-01	2.45E+14	1.001	-0.974	0.70970	1.02E-04	0.27058	2.90E-26	4.14E-03	9.63E-04	9.15E-03
0.95563	0.6195	2.91E+06	3.96E-01	1.55E+14	1.000	-0.874	0.70970	1.01E-04	0.27058	1.76E-27	4.14E-03	9.63E-04	9.15E-03
0.96616	0.6559	2.64E+06	2.81E-01	9.94E+13	1.000	-0.700	0.70970	1.00E-04	0.27058	9.11E-29	4.14E-03	9.63E-04	9.15E-03
0.97419	0.6906	2.38E+06	2.05E-01	6.53E+13	1.000	-0.499	0.70970	1.00E-04	0.27058	3.55E-30	4.14E-03	9.63E-04	9.15E-03
0.98032	0.7230	2.11E+06	1.54E-01	4.37E+13	1.000	-0.167	0.70970	1.00E-04	0.27059	2.23E-30	4.14E-03	9.63E-04	9.15E-03
0.98499	0.7523	1.82E+06	1.22E-01	2.98E+13	1.000	0.285	0.70970	1.00E-04	0.27059	2.23E-30	4.14E-03	9.63E-04	9.15E-03
0.98855	0.7783	1.57E+06	9.81E-02	2.06E+13	1.000	0.556	0.70970	1.00E-04	0.27059	2.23E-30	4.14E-03	9.63E-04	9.15E-03
0.99127	0.8015	1.36E+06	7.92E-02	1.44E+13	1.000	0.708	0.70970	1.00E-04	0.27059	2.23E-30	4.14E-03	9.63E-04	9.15E-03
0.99334	0.8221	1.19E+06	6.42E-02	1.01E+13	1.000	0.801	0.70970	1.00E-04	0.27059	2.23E-30	4.14E-03	9.63E-04	9.15E-03
0.99492	0.8406	1.03E+06	5.22E-02	7.19E+12	1.000	0.867	0.70970	1.00E-04	0.27059	2.23E-30	4.14E-03	9.63E-04	9.15E-03
0.99612	0.8573	9.04E+05	4.26E-02	5.12E+12	1.000	0.910	0.70970	1.00E-04	0.27059	2.23E-30	4.14E-03	9.63E-04	9.15E-03
0.99704	0.8722	7.91E+05	3.48E-02	3.65E+12	1.000	0.937	0.70970	1.00E-04	0.27059	2.23E-30	4.14E-03	9.63E-04	9.15E-03
0.99775	0.8858	6.92E+05	2.84E-02	2.60E+12	1.000	0.956	0.70970	1.00E-04	0.27059	2.23E-30	4.14E-03	9.63E-04	9.15E-03
0.99828	0.8981	6.04E+05	2.31E-02	1.84E+12	1.000	0.969	0.70970	1.00E-04	0.27059	2.23E-30	4.14E-03	9.63E-04	9.15E-03
0.99869	0.9093	5.25E+05	1.87E-02	1.29E+12	1.000	0.978	0.70970	1.00E-04	0.27059	2.23E-30	4.14E-03	9.63E-04	9.15E-03
0.99900	0.9197	4.54E+05	1.50E-02	8.95E+11	1.000	0.984	0.70970	1.00E-04	0.27059	2.23E-30	4.14E-03	9.63E-04	9.15E-03
1.00000	1.0000	5.77E+03	0.00E+00	0.00E+00	1.000	-1.000	0.70970	1.00E-04	0.27059	2.23E-30	4.14E-03	9.63E-04	9.15E-03

nosity integrated up to and including the current zone (in units $L_\odot$), and $S_{\rm crit}=(1-\nabla_{\rm ad}/\nabla_{\rm rad})$. The last seven columns give the most important isotopic abundances, the fractions by mass of ^{1}H, ^{3}He, ^{4}He, ^{7}Be, ^{12}C, ^{14}N, and ^{16}O. The primordial heavy-element abundance Z is 0.019 61.

For some purposes, it is useful to have approximate relations between the physical variables. Using the values given in Table X, we find that the relation between the density ρ (in units of g cm^{-3}) and temperature T_6 (in units of 10^6 K) is close to a polytrope of index 3 in the inner 65% by mass of the sun. We find

$$\rho=0.041(1\pm0.07)T_6^3\ , \tag{12}$$

for $T_6>6.5$.

Table XI gives the local production rates in the sun for nuclear energy and for individual neutrino fluxes. The first four columns list the radius, the temperature (in units of 10^6 K), the logarithm (to the base 10) of the electron density (in units of cm$^{-3}/N_A$, where N_A is Avogadro's number), and the mass of the zone (in units of $M_\odot$). The fifth column gives the fraction of the energy that is generated in the zone. The last eight columns give the fraction of each neutrino flux produced in the zone.

TABLE XI. Rates of neutrino and energy production.

$R/R_\odot$	T_6	$\log(\rho)$	$d(Mass)$	$d(energy)$	$d\varphi$(pp)	$d\varphi(^8\mathrm{B})$	$d\varphi(^{13}\mathrm{N})$	$d\varphi(^{15}\mathrm{O})$	$d\varphi(^{17}\mathrm{F})$	$d\varphi(^7\mathrm{Be})$	$d\varphi$(pep)	$d\varphi$(hep)
0.001953	15.6443	1.9939	0.000006	0.000055	0.000038	0.000497	0.000386	0.000450	0.000462	0.000196	0.000059	0.000015
0.006088	15.6305	1.9931	0.000044	0.000384	0.000265	0.003419	0.002651	0.003095	0.003177	0.001364	0.000411	0.000107
0.010122	15.6073	1.9916	0.000119	0.001037	0.000721	0.009025	0.006981	0.008150	0.008381	0.003655	0.001114	0.000294
0.013896	15.5773	1.9897	0.000231	0.002005	0.001407	0.016947	0.013073	0.015262	0.015731	0.006999	0.002167	0.000581
0.017775	15.5360	1.9870	0.000381	0.003273	0.002327	0.026547	0.020413	0.023830	0.024634	0.011270	0.003564	0.000974
0.021711	15.4836	1.9837	0.000569	0.004822	0.003483	0.037078	0.028423	0.033181	0.034405	0.016305	0.005298	0.001484
0.025693	15.4206	1.9796	0.000794	0.006628	0.004876	0.047718	0.036493	0.042602	0.044307	0.021905	0.007356	0.002122
0.029718	15.3474	1.9749	0.001056	0.008664	0.006505	0.057648	0.044046	0.051419	0.053611	0.027844	0.009720	0.002898
0.033788	15.2640	1.9695	0.001356	0.010899	0.008364	0.066110	0.050574	0.059040	0.061660	0.033868	0.012362	0.003825
0.037907	15.1708	1.9635	0.001694	0.013299	0.010445	0.072499	0.055686	0.065008	0.067924	0.039720	0.015249	0.004912
0.042079	15.0679	1.9567	0.002069	0.015829	0.012731	0.076400	0.059124	0.069022	0.072039	0.045144	0.018337	0.006168
0.046308	14.9557	1.9494	0.002481	0.018449	0.015201	0.077623	0.060771	0.070945	0.073828	0.049901	0.021571	0.007600
0.050601	14.8344	1.9414	0.002931	0.021120	0.017826	0.076219	0.060647	0.070802	0.073306	0.053788	0.024891	0.009208
0.054961	14.7040	1.9327	0.003419	0.023800	0.020570	0.072448	0.058888	0.068748	0.070658	0.056647	0.028227	0.010990
0.059393	14.5650	1.9235	0.003944	0.026447	0.023390	0.066743	0.055721	0.065053	0.066204	0.058372	0.031504	0.012940
0.063905	14.4173	1.9135	0.004506	0.029041	0.026263	0.059667	0.051456	0.060075	0.060390	0.058920	0.034673	0.015060
0.068501	14.2614	1.9029	0.005106	0.031528	0.029121	0.051769	0.046398	0.054171	0.053651	0.058302	0.037636	0.017324
0.073187	14.0973	1.8917	0.005744	0.033838	0.031877	0.043597	0.040865	0.047712	0.046434	0.056603	0.040281	0.019689
0.077968	13.9252	1.8798	0.006419	0.035949	0.034491	0.035656	0.035170	0.041065	0.039174	0.053944	0.042559	0.022137
0.082850	13.7454	1.8673	0.007131	0.037819	0.036899	0.028317	0.029583	0.034544	0.032220	0.050486	0.044404	0.024634
0.087781	13.5601	1.8543	0.007692	0.038493	0.038128	0.021407	0.023817	0.027814	0.025313	0.045402	0.044701	0.026491
0.092547	13.3782	1.8413	0.007692	0.036286	0.036410	0.014958	0.017765	0.020748	0.018410	0.037788	0.041595	0.026296
0.097020	13.2053	1.8288	0.007692	0.034240	0.034727	0.010548	0.013367	0.015615	0.013513	0.031599	0.038698	0.026014
0.101255	13.0402	1.8168	0.007692	0.032332	0.033088	0.007497	0.010132	0.011838	0.009994	0.026531	0.035997	0.025663
0.105291	12.8817	1.8050	0.007692	0.030546	0.031499	0.005364	0.007727	0.009030	0.007440	0.022354	0.033479	0.025258
0.109159	12.7290	1.7936	0.007692	0.028869	0.029964	0.003860	0.005923	0.006924	0.005569	0.018892	0.031132	0.024812
0.112881	12.5815	1.7825	0.007692	0.027289	0.028483	0.002791	0.004559	0.005332	0.004188	0.016010	0.028945	0.024332
0.116478	12.4386	1.7715	0.007692	0.025799	0.027058	0.002028	0.003523	0.004122	0.003162	0.013600	0.026907	0.023825
0.119964	12.2999	1.7608	0.007692	0.024392	0.025690	0.001479	0.002731	0.003197	0.002396	0.011579	0.025008	0.023299
0.123353	12.1651	1.7502	0.007692	0.023062	0.024378	0.001082	0.002127	0.002487	0.001822	0.009877	0.023238	0.022758
0.126654	12.0337	1.7398	0.007692	0.021803	0.023121	0.000794	0.001673	0.001939	0.001389	0.008441	0.021589	0.022206
0.129878	11.9056	1.7295	0.007692	0.020612	0.021918	0.000585	0.001355	0.001516	0.001061	0.007226	0.020053	0.021647
0.133032	11.7806	1.7193	0.007692	0.019483	0.020769	0.000432	0.001185	0.001187	0.000813	0.006195	0.018622	0.021083
0.135789	11.6715	1.7103	0.006000	0.014453	0.015435	0.000257	0.000928	0.000745	0.000501	0.004217	0.013595	0.016052
0.138164	11.5778	1.7025	0.006000	0.013830	0.014792	0.000204	0.001061	0.000616	0.000408	0.003747	0.012828	0.015708
0.140507	11.4856	1.6947	0.006000	0.013235	0.014171	0.000161	0.001341	0.000510	0.000332	0.003332	0.012102	0.015365
0.142820	11.3949	1.6869	0.006000	0.012665	0.013574	0.000128	0.001789	0.000421	0.000271	0.002965	0.011416	0.015024
0.145104	11.3055	1.6792	0.006000	0.012120	0.012999	0.000102	0.002404	0.000347	0.000221	0.002640	0.010767	0.014684
0.147362	11.2176	1.6716	0.006000	0.011598	0.012445	0.000081	0.003168	0.000285	0.000181	0.002352	0.010153	0.014347
0.149596	11.1310	1.6639	0.006000	0.011099	0.011913	0.000064	0.004035	0.000233	0.000148	0.002097	0.009572	0.014013
0.151808	11.0457	1.6563	0.006000	0.010622	0.011401	0.000051	0.004942	0.000190	0.000121	0.001870	0.009024	0.013682
0.153998	10.9618	1.6486	0.006000	0.010164	0.010910	0.000041	0.005820	0.000154	0.000099	0.001669	0.008505	0.013355
0.156168	10.8791	1.6410	0.006000	0.009725	0.010438	0.000033	0.006602	0.000124	0.000081	0.001491	0.008015	0.013032
0.158320	10.7977	1.6334	0.006000	0.009304	0.009985	0.000026	0.007234	0.000099	0.000067	0.001333	0.007552	0.012713
0.160455	10.7175	1.6258	0.006000	0.008900	0.009550	0.000021	0.007683	0.000079	0.000055	0.001192	0.007115	0.012398
0.162574	10.6386	1.6182	0.006000	0.008511	0.009133	0.000017	0.007934	0.000062	0.000045	0.001066	0.006702	0.012089
0.164679	10.5607	1.6105	0.006000	0.008137	0.008733	0.000013	0.007992	0.000049	0.000037	0.000955	0.006312	0.011784
0.166769	10.4840	1.6029	0.006000	0.007777	0.008349	0.000011	0.007875	0.000038	0.000030	0.000855	0.005943	0.011484
0.168847	10.4082	1.5952	0.006000	0.007432	0.007980	0.000009	0.007611	0.000030	0.000025	0.000766	0.005595	0.011188
0.170916	10.3365	1.5876	0.006000	0.007109	0.007636	0.000007	0.007263	0.000024	0.000021	0.000689	0.005272	0.010903
0.172973	10.2658	1.5799	0.006000	0.006798	0.007306	0.000006	0.006834	0.000018	0.000017	0.000620	0.004967	0.010623
0.175019	10.1931	1.5722	0.006000	0.006492	0.006981	0.000005	0.006323	0.000014	0.000014	0.000556	0.004674	0.010343
0.177055	10.1212	1.5645	0.006000	0.006198	0.006669	0.000004	0.005786	0.000011	0.000012	0.000499	0.004397	0.010068
0.179084	10.0501	1.5567	0.006000	0.005916	0.006370	0.000003	0.005243	0.000009	0.000010	0.000448	0.004135	0.009797
0.181104	9.9799	1.5490	0.006000	0.005646	0.006083	0.000002	0.004712	0.000007	0.000008	0.000403	0.003888	0.009532
0.183118	9.9105	1.5412	0.006000	0.005387	0.005807	0.000002	0.004203	0.000005	0.000007	0.000362	0.003654	0.009273
0.185125	9.8418	1.5334	0.006000	0.005140	0.005544	0.000002	0.003727	0.000004	0.000005	0.000325	0.003434	0.009018
0.187127	9.7739	1.5256	0.006000	0.004903	0.005291	0.000001	0.003286	0.000003	0.000005	0.000292	0.003227	0.008768
0.189788	9.6845	1.5151	0.010000	0.007671	0.008284	0.000002	0.004596	0.000004	0.000006	0.000422	0.004947	0.014072
0.193106	9.5743	1.5019	0.010000	0.007085	0.007657	0.000001	0.003658	0.000003	0.000004	0.000353	0.004453	0.013416
0.196415	9.4658	1.4886	0.010000	0.006541	0.007073	0.000001	0.002886	0.000002	0.000003	0.000296	0.004005	0.012783
0.199718	9.3590	1.4752	0.010000	0.006036	0.006529	0.000001	0.002261	0.000001	0.000002	0.000247	0.003599	0.012173

TABLE XI. (*Continued*).

$R/R_\odot$	T_6	$\log(\rho)$	$d(Mass)$	$d(energy)$	$d\varphi$(pp)	$d\varphi(^8B)$	$d\varphi(^{13}N)$	$d\varphi(^{15}O)$	$d\varphi(^{17}F)$	$d\varphi(^7Be)$	$d\varphi$(pep)	$d\varphi$(hep)
0.203018	9.2537	1.4617	0.010000	0.005568	0.006024	0.000000	0.001761	0.000001	0.000002	0.000207	0.003231	0.011585
0.206317	9.1500	1.4480	0.010000	0.005133	0.005554	0.000000	0.001366	0.000001	0.000001	0.000173	0.002898	0.011019
0.209618	9.0477	1.4342	0.010000	0.004730	0.005117	0.000000	0.001055	0.000000	0.000001	0.000145	0.002597	0.010476
0.212923	8.9469	1.4203	0.010000	0.004356	0.004711	0.000000	0.000812	0.000000	0.000001	0.000121	0.002324	0.009954
0.216234	8.8473	1.4062	0.010000	0.004010	0.004335	0.000000	0.000624	0.000000	0.000000	0.000102	0.002078	0.009453
0.219555	8.7491	1.3920	0.010000	0.003690	0.003986	0.000000	0.000478	0.000000	0.000000	0.000085	0.001856	0.008973
0.222887	8.6520	1.3776	0.010000	0.003393	0.003661	0.000000	0.000365	0.000000	0.000000	0.000071	0.001656	0.008513
0.226232	8.5557	1.3630	0.010000	0.003118	0.003360	0.000000	0.000278	0.000000	0.000000	0.000059	0.001476	0.008073
0.229593	8.4602	1.3483	0.010000	0.002864	0.003081	0.000000	0.000211	0.000000	0.000000	0.000049	0.001313	0.007653
0.232972	8.3653	1.3333	0.010000	0.002629	0.002822	0.000000	0.000160	0.000000	0.000000	0.000041	0.001167	0.007251
0.236372	8.2712	1.3182	0.010000	0.002412	0.002582	0.000000	0.000121	0.000000	0.000000	0.000034	0.001035	0.006869
0.239794	8.1777	1.3029	0.010000	0.002211	0.002359	0.000000	0.000091	0.000000	0.000000	0.000029	0.000917	0.006504
0.243241	8.0848	1.2874	0.010000	0.002026	0.002154	0.000000	0.000068	0.000000	0.000000	0.000024	0.000811	0.006157
0.246716	7.9925	1.2716	0.010000	0.001856	0.001964	0.000000	0.000051	0.000000	0.000000	0.000020	0.000716	0.005827
0.250222	7.9008	1.2556	0.010000	0.001698	0.001788	0.000000	0.000038	0.000000	0.000000	0.000016	0.000631	0.005510
0.253760	7.8096	1.2394	0.010000	0.001551	0.001626	0.000000	0.000028	0.000000	0.000000	0.000013	0.000555	0.005203
0.257334	7.7189	1.2229	0.010000	0.001411	0.001477	0.000000	0.000021	0.000000	0.000000	0.000011	0.000487	0.004898
0.260946	7.6287	1.2061	0.010000	0.001277	0.001340	0.000000	0.000016	0.000000	0.000000	0.000009	0.000427	0.004585
0.264600	7.5389	1.1890	0.010000	0.001144	0.001213	0.000000	0.000011	0.000000	0.000000	0.000007	0.000374	0.004253
0.268298	7.4496	1.1716	0.010000	0.001011	0.001097	0.000000	0.000008	0.000000	0.000000	0.000006	0.000326	0.003895
0.272044	7.3607	1.1539	0.010000	0.000879	0.000991	0.000000	0.000006	0.000000	0.000000	0.000005	0.000284	0.003504
0.280751	7.1626	1.1135	0.035000	0.002080	0.002746	0.000000	0.000010	0.000000	0.000000	0.000008	0.000724	0.008788
0.294808	6.8550	1.0458	0.035000	0.001073	0.001869	0.000000	0.000003	0.000000	0.000000	0.000002	0.000429	0.004266
0.309802	6.5466	0.9729	0.035000	0.000598	0.001237	0.000000	0.000001	0.000000	0.000000	0.000001	0.000244	0.001665
0.325982	6.2360	0.8935	0.035000	0.000357	0.000791	0.000000	0.000000	0.000000	0.000000	0.000000	0.000133	0.000569
0.343676	5.9215	0.8062	0.035000	0.000210	0.000486	0.000000	0.000000	0.000000	0.000000	0.000000	0.000068	0.000176
0.363339	5.5994	0.7091	0.035000	0.000115	0.000283	0.000000	0.000000	0.000000	0.000000	0.000000	0.000032	0.000049
0.385619	5.2643	0.5998	0.035000	0.000054	0.000154	0.000000	0.000000	0.000000	0.000000	0.000000	0.000014	0.000012
0.411497	4.9113	0.4741	0.035000	0.000018	0.000076	0.000000	0.000000	0.000000	0.000000	0.000000	0.000005	0.000003
0.442571	4.5314	0.3262	0.035000	-0.000002	0.000033	0.000000	0.000000	0.000000	0.000000	0.000000	0.000002	0.000001
0.481707	4.1077	0.1459	0.035000	-0.000012	0.000012	0.000000	0.000000	0.000000	0.000000	0.000000	0.000000	0.000000
0.523422	3.7037	-0.0483	0.023730	-0.000010	0.000003	0.000000	0.000000	0.000000	0.000000	0.000000	0.000000	0.000000
0.562430	3.3650	-0.2219	0.018099	-0.000009	0.000001	0.000000	0.000000	0.000000	0.000000	0.000000	0.000000	0.000000
0.600638	3.0595	-0.3867	0.013804	-0.000007	0.000000	0.000000	0.000000	0.000000	0.000000	0.000000	0.000000	0.000000
0.637722	2.7785	-0.5420	0.010528	-0.000006	0.000000	0.000000	0.000000	0.000000	0.000000	0.000000	0.000000	0.000000
0.673285	2.5126	-0.6863	0.008030	-0.000005	0.000000	0.000000	0.000000	0.000000	0.000000	0.000000	0.000000	0.000000
0.706835	2.2482	-0.8173	0.006124	-0.000004	0.0	0.0	0.0	0.0	0.0	0.0	0.0	0.000000
0.737676	1.9661	-0.9300	0.004671	-0.000001	0.0	0.0	0.0	0.0	0.0	0.0	0.0	0.000000
0.765309	1.6944	-1.0287	0.003563	0.0	0.0	0.0	0.0	0.0	0.0	0.0	0.0	0.000000
0.789883	1.4664	-1.1237	0.002717	0.0	0.0	0.0	0.0	0.0	0.0	0.0	0.0	0.000000
0.811795	1.2740	-1.2160	0.002072	0.0	0.0	0.0	0.0	0.0	0.0	0.0	0.0	0.000000
0.831385	1.1102	-1.3064	0.001581	0.0	0.0	0.0	0.0	0.0	0.0	0.0	0.0	0.000000
0.848946	0.9695	-1.3955	0.001206	0.0	0.0	0.0	0.0	0.0	0.0	0.0	0.0	0.000000
0.864737	0.8476	-1.4838	0.000919	0.0	0.0	0.0	0.0	0.0	0.0	0.0	0.0	0.000000
0.878987	0.7412	-1.5721	0.000701	0.0	0.0	0.0	0.0	0.0	0.0	0.0	0.0	0.000000
0.891906	0.6476	-1.6610	0.000535	0.0	0.0	0.0	0.0	0.0	0.0	0.0	0.0	0.000000
0.903687	0.5644	-1.7515	0.000408	0.0	0.0	0.0	0.0	0.0	0.0	0.0	0.0	0.000000
0.914518	0.4898	-1.8451	0.000311	0.0	0.0	0.0	0.0	0.0	0.0	0.0	0.0	0.000000

Tables X and XI differ in that the quantities in Table X refer to the end points of each zone, whereas the temperature, radius, and electron density in Table XI refer to the zone center. The remaining quantities in Table XI are all integrals over the individual zones. The quantities in Table XI can be summed to yield the total fluxes from the neutrino producing reactions. The constraint on the total luminosity for the converged solar model has been enforced through the trapezoidal rule and the reported total neutrino fluxes have also been calculated with this algorithm. Consequently, Table XI is the appropriate source to obtain local neutrino fluxes for studying the MSW effect.

Figure 6 illustrates some of the most interesting physical characteristics of the standard solar model. In Fig. 6(a) we show the fraction of the energy generation that is produced at each solar radius. [The numerical values used in plotting Figs. 6(a) and 8, see below, were obtained

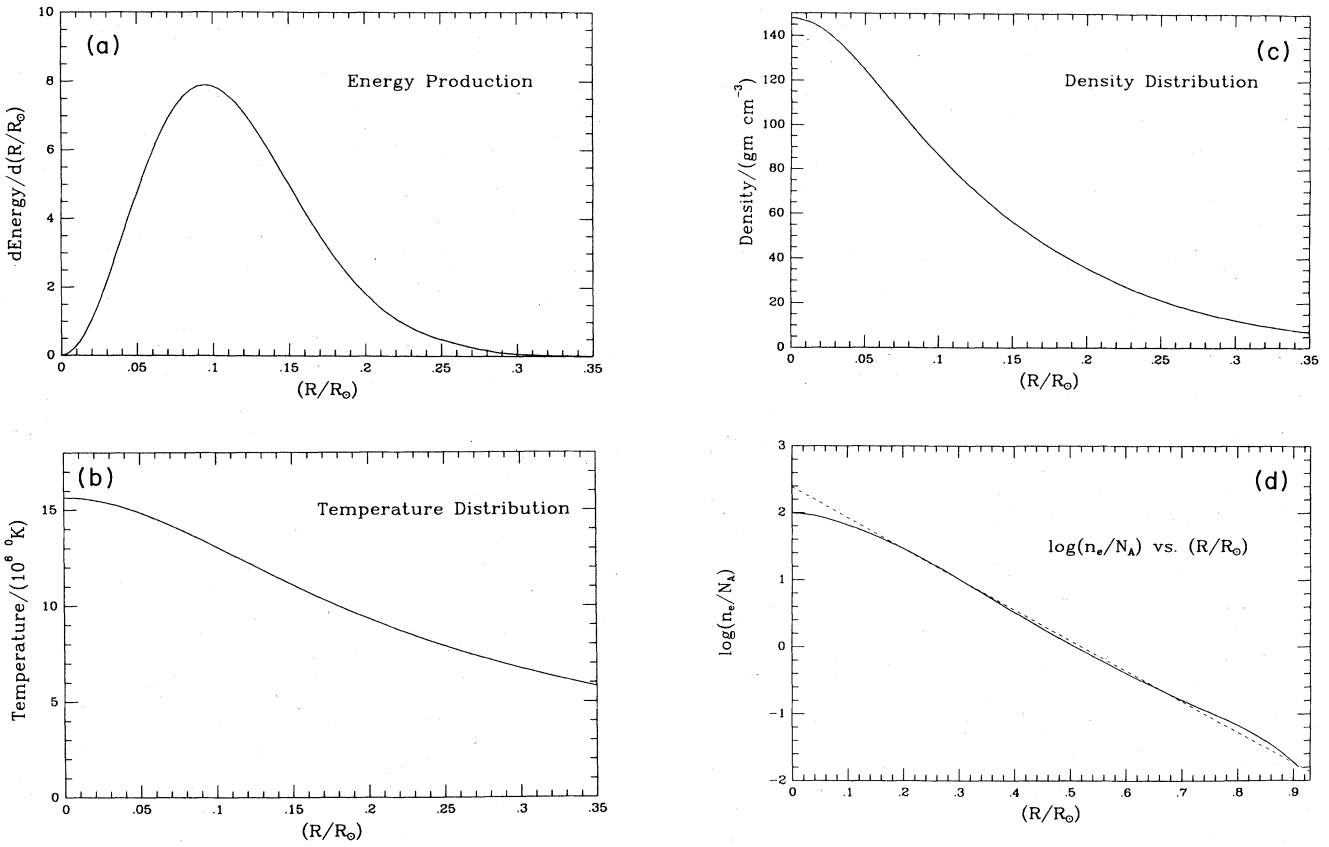

FIG. 6. Energy production, temperature, density, and electron density: (a) the fraction of the energy generation that originates in a given fraction of the solar radius as a function of position in the sun; (b) temperature distribution in the sun; (c) density distributions in the sun; (d) solid line, the logarithm of the electron number density N_e, divided by Avogadro's number N_A, as a function of solar radius; dotted line, exponential fit to the density distribution, the parameters of which are given in the text. These results are obtained from the standard solar model described in Sec. V.B and Tables X and XI.

directly from the computer code. If the numbers given in Table XI were used to compute these derivatives by dividing by the inner and outer radii of the zone, the resulting figures would show some numerical noise associated with the finite zone size.] The energy generation peaks at a radius of $0.09R_\odot$, which corresponds to about $0.06M_\odot$; the half-peak values of the energy generation extend from $0.04R_\odot$ to $0.16R_\odot$, i.e., from the inner $0.007M_\odot$ to $0.23M_\odot$. Figures 6(b) and 6(c) illustrate the distribution of the density and temperature; the central values are, respectively, 148 g cm^{-3} and 15.6×10^6 K. The density decreases much more rapidly than the temperature [see Eq. (12)]; the half-peak value for the density occurs at $0.12R_\odot$, whereas the half-peak value for the temperature occurs much further out, at $0.25R_\odot$. The peak of the energy generation occurs at a temperature of about 14×10^6 K and a density of about 95 g cm^{-3}.

The way that the electron density depends upon radius is crucial for the MSW effect. Using the values given in Table XI, we find that the logarithm of the electron density divided by Avogadro's number can be approximated by the expression

$$\log(n_e/N_A)=2.32-4.17x-0.000\,125/[x^2+(0.5)^2]\ , \tag{13}$$

where $x=R/R_\odot<0.25$. This expression reproduces the values given in Table XI to a root-mean-square accuracy of 3%.

Figure 6(d) shows the dependence of the electron number density upon solar radius. Many authors have represented the logarithm of the electron density by a linear function of the solar radius. The dotted line in Fig. 6(d) shows the fit of a linear function to the electron density of the standard solar model. The equation for the straight line in Fig. 6(d) is $\log(n_e/N_A)=2.39-4.58x$ or $n_e/N_A=245\exp(-10.54x)$ cm^{-3}, where as before $x=R/R_\odot$. Note that the linear fit is not exact and the parameters depend upon where the fitting is done. In particular, the formula given here is in error by about a factor of 2 at the solar center. The reader should be aware that some published analytic representations of the electron density in the sun are incorrect by factors of order unity and that the domains of validity of the ex-

ponential formulas are sometimes not specified properly.

Figure 7 shows the dependence of the mass fractions upon position in the sun. Figure 7(a) shows how helium is increased in abundance with respect to hydrogen by nuclear burning in the solar interior. The most remarkable distribution is shown in Fig. 7(b), which illustrates the strongly peaked abundance (on a linear scale) of ^{3}He. In the innermost region, the ^{3}He abundance is small because ^{3}He is burned rapidly by reactions 5 and 6 in Table I. In the outer region, no ^{3}He is produced by proton burning. There is a sharp peak in the ^{3}He abundance near $0.28R_\odot$. In this region, ^{3}He is produced by the first proton burning reactions (numbers 1 and 3 in Table I), but is mostly not burned because reactions 4 and 5 in Table I require higher temperatures.

Table XII presents the computed solar luminosity and radius as a function of time. The model of the present sun has a luminosity that has increased by 41% from the nominal (cf. paper I, Sec. III.B) zero-age model, and the effective temperature has increased by 3%.

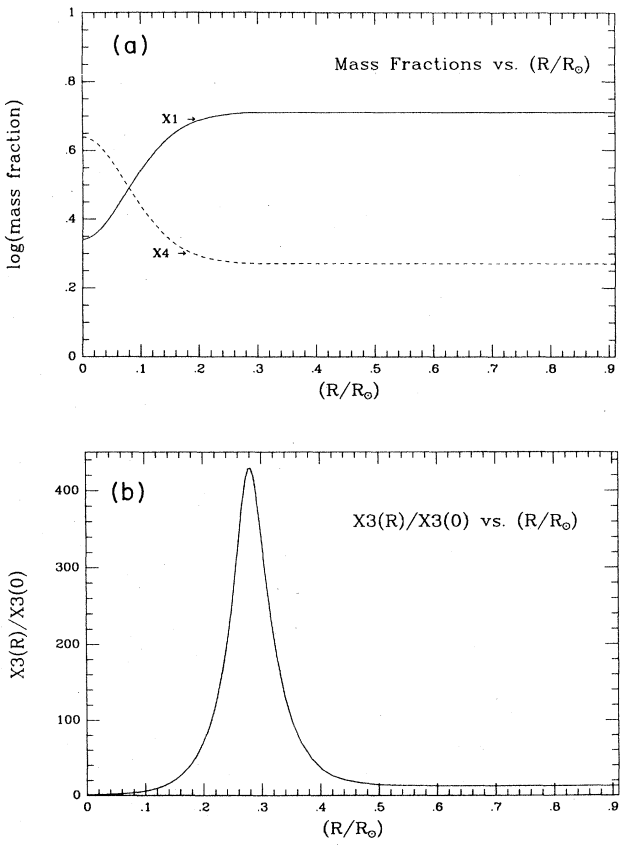

FIG. 7. Mass fractions as a function of radius: (a) logarithm of the hydrogen and helium mass fractions as a function of positon in the sun; (b) dependence of the ^{3}He abundance upon position. The figures shown here illustrate the values obtained for the standard solar model described in Sec. V.B and Table X.

TABLE XII. Surface properties of the standard solar model as a function of time.

Time (10^9 yr)	Radius ($R_\odot$)	Luminosity ($L_\odot$)	T_e (^0K)
0.00	0.87321	0.70687	5665
0.04	0.88918	0.71408	5627
0.27	0.89293	0.73446	5655
0.50	0.89934	0.74542	5656
1.50	0.91971	0.79552	5683
2.50	0.94228	0.85142	5712
3.50	0.96744	0.91644	5743
4.60	1.00000	1.00000	5773

C. Neutrino fluxes from standard models

Our best estimates for each of the neutrino fluxes, together with the theoretical uncertainties, are given in Table XIII. The fluxes were computed for the standard solar model. The total theoretical range for each flux was evaluated using the parameter uncertainties discussed in Sec. II and the partial derivatives with respect to input parameters that are given in Sec. VI [see Table XV and Eqs. (15) and (16) below]. The second column in Table XIII gives the fluxes and the total uncertainties. Columns 3–9 give the fractional uncertainties from each of the indicated parameters.

What information about the solar interior do the individual neutrino fluxes carry? Figure 8 shows where in the sun the *p-p*, ^{8}B, ^{7}Be, and hep neutrinos originate. By comparison with Figs. 6(a)–6(c) (and Table XI), which give the physical conditions as a function of solar radius this figure allows one to determine what information is imprinted on the neutrinos of each nuclear source. The region in which the *p-p* flux is produced is very similar to that of the total energy generation [cf. Fig. 6(a)]; the peak occurs in both distributions at essentially the same position, $0.09R_\odot$ and $T=14\times10^6$ K. The half-peak positions for the *p-p* production are shifted outward with respect to the energy generation by about $0.01R_\odot$.

Because of its strong temperature dependence, the ^{8}B production is peaked at much smaller radii, $0.05R_\odot$ and $T=15\times10^6$ K, and is generated in a narrower region, $0.02R_\odot$ to $0.07R_\odot$. The region of ^{7}Be production is intermediate between the ^{8}B and *p-p* regions, peaking at $0.06R_\odot$ and spreading (half-peak range) from $0.03R_\odot$ to $0.10R_\odot$.

The hep distribution is the most extended, ranging (half-peak points) from $0.06R_\odot$ to $0.21R_\odot$ with a peak at $0.13R_\odot$ and $T=12\times10^6$ K. The reason that the hep neutrinos are produced at relatively large radii in the solar core is that the ^{3}He abundance increases as one goes outward from the center, peaking at $0.27R_\odot$. At the lower temperatures in the outer solar core, the *p-p* chain

TABLE XIII. Neutrino fluxes and theoretical uncertainties for the standard solar model. The unit of flux is 10^{10} cm^{-2} s^{-1}. We also show the fractional uncertainties associated with each important parameter (e.g., *p-p* reaction rate, heavy-element-to-hydrogen ratio *Z/X*, or opacity).

Source	Flux (10^{10}cm^{-2}sec^{-1})	pp	^{3}He-^{3}He	^{3}He-^{4}He	p-^{7}Be	p-^{14}N	Z/X	Opacity
pp	$6.0(1 \pm 0.02)$	0.01	0.00	0.00	0.00	0.01	0.01	0.00
pep	$1.4 \times 10^{-2}(1 \pm 0.05)$	0.01	0.00	0.01	0.00	0.01	0.03	0.02
hep	7.6×10^{-7}	0.00	0.07	0.00	0.00	0.00	0.03	0.00
^{7}Be	$4.7 \times 10^{-1}(1 \pm 0.15)$	0.05	0.07	0.05	0.00	0.00	0.11	0.04
^{8}B	$5.8 \times 10^{-4}(1 \pm 0.37)$	0.12	0.06	0.05	0.22	0.00	0.25	0.08
^{13}N	$6.1 \times 10^{-2}(1 \pm 0.50)$	0.12	0.00	0.00	0.00	0.30	0.38	0.03
^{15}O	$5.2 \times 10^{-2}(1 \pm 0.58)$	0.14	0.00	0.00	0.00	0.36	0.42	0.06
^{17}F	$5.2 \times 10^{-4}(1 \pm 0.46)$	0.14	0.00	0.0	0.00	0.00	0.44	0.06

produces ^{3}He (by reactions 1 and 3 in Table I), but the rate for burning ^{3}He (by reactions 5 and 6 in Table I) lags behind the production rate, creating a relatively large nonequilibrium abundance of ^{3}He.

The solar neutrino experiments that measure individual recoil electrons of higher energy, like the natural water electron scattering detectors and the ^{2}H and ^{40}Ar experiments (see Sec. VIII.B), sample neutrinos from two different parts of the solar interior. These detectors are sensitive to both the ^{8}B neutrinos, produced at relatively small radii and high temperatures, and the hep neutrinos, which are generated at larger radii and lower temperatures. Fortunately, it is possible to distinguish on the basis of the energy of the recoil electrons between events that originate from hep neutrinos and those that are caused by ^{8}B neutrinos (see Sec. VIII.B), allowing one experiment to probe regions of the solar interior that are both inside and outside the main energy-producing region (see Fig. 8).

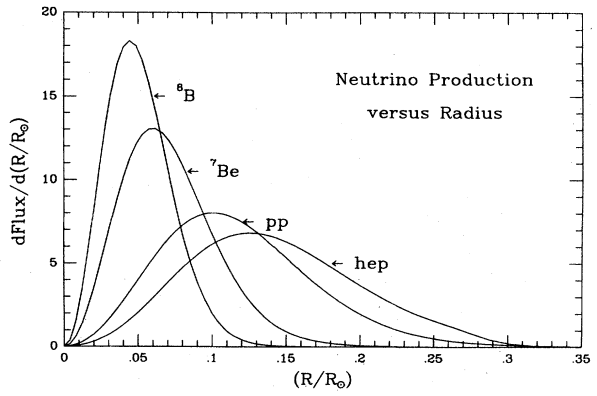

FIG. 8. Neutrino production as a function of radius. The fraction of neutrinos that originate in each fraction of the solar radius is $[d\,\mathrm{Flux}/d(R/R_\odot)][d(R/R_\odot)]$. The figure illustrates the production fraction for ^{8}B, ^{7}Be, *p-p*, and hep neutrinos for the standard solar model described in Sec. V.B and Table XI.

The flux of neutrinos from the proton-proton reaction is the most accurately known; the estimated uncertainty in this flux is only 2%. It is often mistakenly said in the literature that the flux of this reaction is fixed by the observed solar luminosity. *In fact, the computed flux of p-p solar neutrinos would be about one-half as large as we have calculated if ^{3}He were burned primarily by interactions with an alpha particle rather than (as in the standard model) by interactions with other ^{3}He nuclei.* Two *p-p* reactions are required to terminate the chain via reaction 5 in Table I (which predominates in the standard solar model), whereas only one *p-p* reaction is necessary if reaction 6 dominates. Fortunately, the cross-section factors for reactions 5 and 6 are relatively well known (see Table I); they indicate that reaction 5 occurs about 6 times as often as reaction 6 under average solar conditions.

The uncertainty in the flux of ^{7}Be neutrinos is also moderately small, of order 14%.

The uncertainty in the crucial ^{8}B neutrinos is large, 34%. The largest single uncertainty in the calculation of this flux derives from the measurement of the low-energy nuclear cross-section factor for the production of ^{8}B, although there is a comparable uncertainty due to the heavy-element abundance.

The uncertainties are about 40% to 50% for the CNO neutrinos. The largest contributors to their uncertainties are the heavy-element abundance and the rate at which ^{14}N is burned.

We are unable to estimate an overall uncertainty for the hep neutrinos because of the need for further measurement of the thermal neutron capture cross section (see Sec. II.A). All of the other uncertainties are small.

Table XIV, rows 1–6, give the neutrino fluxes that were computed for a sequence of six standard solar models that take account of successive stages of improvement to the input parameters and physics. For comparison, the first model we list in Table XIV represents the results we obtained with the standard solar model that was presented in paper I. The physical characteristics described in the previous subsection (V.B) and the neutrino fluxes given in Table XIII were derived from the sixth model, the one designated "Best" in Table XIV.

The principal changes that we have made since paper I are represented by the models NewS, NewESc, AllNew, and CNO Cor, whose characteristics are given in the second through fifth rows of Table XIV. The principal changes that we have made are described below. NewS was constructed using improved nuclear reaction cross sections and Q values (see Sec. II.A). NewESc utilizes the Los Alamos treatment of the corrections to electron scattering due to correlations among the electrons (see Sec. II.C). AllNew uses the new determinations of the surface abundances due to Grevesse and Aller (see Sec. II.B). CNO Cor incorporates the change in the radiative opacity that is caused by the conversion of carbon and oxygen to nitrogen. Each model in the sequence described above includes the improvements made in the preceding models.

Our "Best" model (row 6 in Table XIV) includes all of the above changes, as well as the most recent reevaluation of the rate of the ^3He-^3He reaction (see Sec. II.A, row 5 in Table I, and Krauss *et al.*, 1987). This reevaluation reduced the calculated flux of ^8B neutrinos by 4%.

The most important changes in the nuclear cross sections are (cf. Sec. II.A) the lower value for the S factor for the $^7Be(p,\gamma)^8B$ reaction and the increased S factor for the p-p reaction. These two changes, together with the other much smaller variations caused by refinements in other parameters, reduce the ^8B neutrino flux by 29% with respect to the value computed in paper I. The ^7Be and pep neutrino fluxes are changed by only a few per-

TABLE XIV. Neutrino fluxes for standard and nonstandard solar models. The unit of flux is $cm^{-2}\ s^{-1}$ at the Earth's surface. The first six rows refer to a sequence of progressively more complete "standard" solar models that are described in Sec. V.C. The next seven models, rows 7–13, refer to nonstandard models with either a low primordial heavy-element abundance or a high primordial helium abundance, in the solar interior; these models are described in Sec. IX.A. The models in rows 14 and 15 were constructed to illustrate the sensitivity of the results to changes in nuclear parameters; they are described in Sec. IX.B. The model CATMOS was constructed using the computer code developed to calculate helioseismological frequencies and is described in Sec. X.D and Appendix C. The entry under WIMP's was not computed in detail, but instead was scaled from the results of Gilliland *et al.* (1986) in the manner described in Sec. IX.C.

Model	Y	Z	p-p (E10)	pep (E8)	hep (E3)	^7Be (E9)	^8B (E6)	^{13}N (E8)	^{15}O (E8)	^{17}F (E6)
Paper I	0.252	0.0167	6.07	1.50		4.3	5.6	5.0	4.0	3.5
NewS	0.248	0.0168	6.10	1.46	8.39	4.25	3.98	4.02	3.26	3.08
NewESc	0.250	0.0167	6.08	1.44	8.30	4.24	4.39	4.29	3.53	3.35
AllNew	0.270	0.0197	6.00	1.41	7.97	4.75	5.52	5.77	4.89	4.82
CNO Cor	0.271	0.0196	5.98	1.39	7.90	4.88	5.97	6.08	5.21	5.15
Best	0.271	0.0196	6.00	1.40	7.58	4.69	5.76	6.09	5.22	5.16
Z1	0.127	0.0023	6.38	1.66	10.42	1.83	0.80	0.22	0.12	0.10
Z2	0.116	0.0024	6.40	1.64	10.60	1.67	0.67	0.21	0.10	0.09
Z3	0.114	0.0024	6.41	1.64	10.65	1.63	0.65	0.20	0.10	0.09
$Y1$	0.268	0.0196	6.32	1.40	7.91	4.99	6.03	6.26	5.38	5.26
$Y2$	0.266	0.0196	6.04	1.40	7.87	5.15	6.45	6.56	5.70	5.66
$Y3$	0.263	0.0196	6.02	1.40	7.79	5.30	6.88	6.90	6.04	5.91
$Y4$	0.258	0.0196	6.02	1.40	7.76	5.24	6.76	6.78	5.92	5.79
No ^8B	0.271	0.0196	5.98	1.39	7.90	4.88	0.0	6.08	5.21	5.15
$S_{3,4} = 0$	0.250	0.0168	6.49	1.62	8.70	0.0	0.0	3.98	3.14	2.99
CATMOS	0.271	0.0196	6.06	1.45		4.86	5.41	4.99	4.23	4.04
WIMP's			6.15	1.5		3.3	1.4	2.2	1.9	1.9

cent; the CNO neutrino fluxes are changed by about 20%.

The Los Alamos implementation of the correlation correction to electron scattering (cf. Sec. II.B) increases the calculated ^{8}B neutrino flux by about 10% (cf. rows 2 and 3 in Table XIV) and changes the other fluxes by less than 10%.

The improved determination of surface abundances (cf. Sec. II.C) increases the ^{8}B neutrino flux by about 26% (cf. rows 3 and 4 in Table XIV), almost canceling the net effect of all the other changes. The flux of ^{7}Be neutrinos is also increased significantly, by about 12%. The ^{13}N and ^{15}O fluxes are increased by about 35%.

The changes in the radiative opacity due to CNO conversion (cf. Sec. II.C) are reflected in the differences between rows 4 and 5. This correction is mainly important for the flux of ^{8}B neutrinos, which it increases by 8%.

In all of the further discussions in this paper, we use as our "standard model" the model labeled "Best," whose fluxes are shown in the sixth row in Table XIV.

In all of the models, we have incorporated a number of minor improvements to the computer code. The sensitivity of the fluxes to each of these improvements is indicated by changes produced in the flux of ^{8}B neutrinos. These minor improvements are (with associated percentage changes in the ^{8}B neutrino flux in parentheses): use of the finer opacity grid ($+1.3\%$; cf. Sec. II.C); tripling the number of time steps (-2.4%; cf. Table XII); use of a finer mass zoning ($+1.9\%$; see Tables X and XI); and use of more accurate nuclear Q values ($+0.3\%$; see Appendix A).

The net changes in calculated neutrino fluxes in the 5 years that have elapsed from paper I to the present discussion can be evaluated by comparing rows of Table XIV.

For accidental reasons, the net change in the calculated ^{8}B neutrino flux is small, $\approx 3\%$. The *uncertainty* in this flux is more than 10 times larger than the difference between the presently calculated value and the value we obtained in 1982. The change in the pep neutrino flux (from reaction 2 in Table I), which is closely related to the *p-p* reaction, is, ironically, rather larger, $\approx 8\%$. The net changes in the ^{7}Be, ^{13}N, and ^{15}O neutrino fluxes are also larger, about 9%, 21%, and 30%, respectively. The flux from the basic *p-p* reaction has changed by only about 1%.

D. The primordial helium abundance

The primordial helium abundance is determined automatically by the iteration of the standard solar model to agree with the observed (present-day) solar luminosity. One can understand how this comes about by the following simplified argument. Suppose all of the noncomposition parameters and physics (such as nuclear reaction rates, the equation of state in the solar interior, or the solar luminosity) are held fixed and also keep constant the *relative* abundance of all of the elements heavier than helium. Then the solar model depends only on the mass fractions of hydrogen, X, of helium, Y, and of heavy elements, Z. There are three conditions on these three quantities: (1) their sum is unity; (2) Z/X is given by the surface observations of the relative element abundances; and (3) the model luminosity must equal the observed luminosity. Thus these conditions determine the mass fractions, and, in particular, the cosmologically important quantity Y. Of course, if one changes either the physics or the parameters used in calculating the standard solar model, then the inferred value for Y will be altered. An extensive discussion of the sensitivity of the primordial helium abundance to various input parameters and physics has been given in Sec. III.C and Table X in paper I.

The helium abundance of the standard model discussed here is $Y=0.271$. This value is significantly larger, as anticipated by Cassé, Cahen, and Doom (1986), than the helium abundance, 0.252, given in paper I. The primary reason is that the best value for the observed ratio of Z/X has increased from the Ross-Aller value used in paper I, 0.0228, to the Grevesse value of 0.027 65 that is adopted here (see Sec. II.B). By iterating models with different assumed values of Z/X, we obtained in paper I the relation[4]

$$\frac{\partial \ln Y}{\partial \ln(Z/X)} = +0.30 \ . \tag{14}$$

Using the Ross-Aller value of Z/X, the Grevesse value of Z/X, and the paper I value of Y, Eq. (14) predicts a new value of $Y=0.267$, in good agreement with the result of 0.271 that is obtained by detailed modeling, which includes other input parameter changes.

However, our result is 5% lower than the value of $Y=0.285$ that is obtained by Cassé *et al.* (1986) also for the Grevesse heavy-element-to-hydrogen ratio. In addition, our value, given in paper I, of $Y=0.244$ for the standard solar model with Ross-Aller abundances (and without the Ulrich, 1982, equation of state is 9% less than the value of $Y=0.265$ that the Cassé *et al.* calculation implies for the same case.[5]

In an effort to help clarify this discrepancy, Cassé (1986) generously made available to us the computer code used to calculate their standard solar models. We have

[4]The plus sign in Eq. (14) was incorrectly printed as a minus sign in paper I, a fact that was pointed out by Cassé, Cahen, and Doom (1986).

[5]Cassé *et al.* (1986) quote a value for $Y=0.273$ but for $Z=0.0179$. This implies that their effective value of $Z/X=0.0252$. We have corrected for the difference in Z/X's with the aid of Eq. (14). In a recent private communication (July, 1987), M. Cassé has informed us that their latest calculation gives a result for Y that is in good agreement with the value we obtain.

examined this code and have found a number of reasons why the Cassé *et al.* (1986) result for the primordial helium abundance should differ from ours. (1) Cassé *et al.* scaled the opacity computed for the Ross-Aller (1976) mixture of heavy elements to the Grevesse value of Z/X. However, the increase in heavy-element abundance between the Ross-Aller mixture and the Grevesse abundance comes largely from the new neon abundance, rather than a uniform rescaling of all of the elements. We have used a Los Alamos opacity computed for the Grevesse mixture (see Table II) that correctly represents the increased neon contribution. (2) The Cassé *et al.* model contains a small convective core whose size varies in an unexpectedly nonmonotonic fashion with solar age. Most modern solar models, including ours, do not have a convective core, although at early times our model is close to having a central convective core. It seems likely that the numerical procedures that lead to the convective core in the Cassé *et al.* model are related to the difference between our standard models and theirs in primordial helium abundance. (3) The numerical procedures used by Cassé *et al.* are coarser than we have found desirable in solar neutrino calculations. The number of integration zones is significantly smaller (by about a factor of 2) in their program than in our standard calculations, which typically have ~ 100 zones in the region in which the opacity and temperature change rapidly. More extensive numerical investigations would be required to determine if their integration of the time dependence of the nuclear abundance equations is properly combined with the composition relations so as to give the elements' abundances at the new integration time (see Appendix B of paper I for a discussion of some of the pitfalls and problems in this calculation).

The differences in helium abundance between our program and that of Cassé *et al.* (1986) are significant and require further investigation. We have calculated helium abundances by varying a number of parameters and input physics, but have been unable to produce differences as large as the 5–9 % discrepancies cited above. Nevertheless, the neutrino fluxes computed with the two models are in agreement to the accuracy (better than 10%) that is required to interpret contemporary solar neutrino experiments.

E. The lithium abundance

The observed lithium abundance on the surface of the sun is much less than is expected on the basis of the most straightforward application of the standard solar model. The observed surface abundance of lithium in the sun is (Muller *et al.*, 1975) $\log[N(\mathrm{Li})]=0.95\pm0.1$ on a scale on which $\log[N(\mathrm{H})]=12.0$. The maximum, and presumed primordial, abundance of lithium for population I objects is 3.0 ± 0.01 on the same scale, as shown by measurements on meteorites (Nichiporuk and Moore, 1974; Reeves and Meyer, 1978), young T Tauri stars, F and G dwarfs in galactic clusters, and in the field (see Duncan, 1981, Boesgaard, 1976, and Boesgaard, Budge, and Burck, 1988, for a summary of the evidence). It is generally assumed that the sun originally contained the maximum population I lithium abundance quoted above and that the observed surface abundance is the result of depletion by a factor of order 100 due to nuclear burning near the solar surface by the $^7\mathrm{Li}(p,\alpha)^4\mathrm{He}$ reaction (number 8 in Table I).

Why should we discuss lithium depletion in the context of the solar neutrino question? Any comparison between solar models and observational data potentially could provide us with additional information about the structure and evolution of the sun. Because the lithium discrepancy is large, we might hope that solution to the lithium problem would shed some light on the solar neutrino problem. We shall see below that lithium burning is efficient even in the outer layers of the sun, so that there is no necessary link between the two problems. Nevertheless, some of the mechanisms proposed to explain the lithium depletion involve diffusion or mixing of solar material in regions in which, according to the standard model, this should not occur. For example, in a series of papers Schatzman and collaborators (Schatzman, 1969; Schatzman and Maeder, 1981; Baglin, Morel, and Schatzman, 1985; Lebreton and Maeder, 1987) have argued that mild turbulence could cause diffusion of lithium to higher temperatures, explaining the observed depletion. The paper by Lebreton and Maeder (1987) contains a clear discussion of the possible mechanisms for producing the required mild turbulence and discusses the relationship between the solar neutrino problem, helioseismology, and lithium depletion. On the other hand, standard solar models have a temperature of about 2×10^6 K near the base of the convective envelope and, as has been realized for a long time, this temperature is not large enough to cause the observed depletion of lithium.

Previous calculations of the amount of depletion expected in standard solar models have been done with less accurate input parameters than are now available. In particular, the cross-section factor for the most important burning reaction, $^7\mathrm{Li}(p,\alpha)^4\mathrm{He}$, has recently been shown to be smaller by a factor of 2 than was used in previous estimates (see Rolfs and Kavanagh, 1986). Using more modern values of the input parameters, we confirm (see below) the earlier determinations of the magnitude of the required depletion.

In what follows, we discuss lithium depletion in terms of the derived parameter $\tau=-\ln[N(\mathrm{Li})/N_0(\mathrm{Li})]$, where $N_0(\mathrm{Li})$ is the initial lithium abundance and τ represents the integrated exposure of the lithium nucleus to the $^7\mathrm{Li}(p,\alpha)^4\mathrm{He}$ reaction. The observed value is $\tau_{\mathrm{obs}}=4.7$. The value obtained from our SUNEV standard model code (see Appendix B) is $\tau_{\mathrm{calc}}=0.0037$, which confirms the conclusion of previous authors regarding the magnitude of the difference (a factor of 10^2) between the calculated and observed depletion. We have also varied the input parameters within the uncertainties discussed in Sec. II; none of the variations reduces significantly the

discrepancy between τ_{obs} and τ_{calc}. For example, the logarithmic derivatives of τ with respect to both Z/X and the cross-section factor for the p-p reaction are only 0.02.[6]

Bodenheimer (1964) showed many years ago that somewhat higher temperatures in the convective zone during pre-main-sequence evolution would be consistent with the observed depletion. Unfortunately, the observed dependence of lithium depletion upon stellar mass is not well explained by the original Bodenheimer calculations. D'Antona and Mazzitelli (1984) have postulated instead that pre-main-sequence evolution includes more extensive mixing than is generally assumed. On the other hand, Boesgaard, Budge, and Ramsey (1987) have found one young main sequence star, HD23386, in the Pleiades cluster with a mass near $1M_{\odot}$ (spectral type G1 V) that has a surface abundance of lithium equal to the maximum observed lithium abundance. Pre-main-sequence lithium depletion has evidently not occurred in this star. If this proxy evidence applies to all stars of about one solar mass (and lithium depletion does not depend upon rotation or some other intrinsic parameter), then lithium must be depleted during main sequence solar evolution.

In order to provide a simple way of thinking about the amount of mixing required in the convective envelope, we have computed a sequence of solar models in which matter is artificially homogenized within a region that extends to different specified fractions of a solar mass below the convection zone. Since any realistic mixing will be less thorough than our assumed complete homogenization, our calculations provide a minimum depth to which the mixing must extend. We find that in the homogeneous models, the mixing must extend to a mass of $0.046M_{\odot}$ in order to explain the observed depletion. The temperature at this depth is 3×10^6 K and the radius is $0.62R_{\odot}$. The temperature that we find required to deplete lithium to the observed solar abundance is about a factor of 0.4×10^6 K higher than has been estimated previously by some authors (see, for example, Duncan, 1981). The depletion parameter τ depends strongly upon the mass fraction that is assumed to be mixed; τ varies from 7.9 to 2.1 as the mass fraction varies from 0.050 to 0.041, and the temperature at the base of the mixed region decreases from 3.0×10^6 K to 2.8×10^6 K.

VI. FRACTIONAL UNCERTAINTIES IN THE PREDICTED NEUTRINO FLUXES: GAUSSIAN ESTIMATES

In this section, we estimate the uncertanties in the calculated neutrino fluxes by assuming that all of the input parameters are normally distributed with the previously specified best estimates and standard deviations (see Sec. II) and that the probability distribution of each neutrino flux is also Gaussian. In the following section, we shall investigate by Monte Carlo simulations the *shape* of the probability distribution for the neutrino fluxes.

A. Logarithmic derivatives

In order to estimate the uncertainties in the predictions for individual experiments that are caused by the imprecisely known values of different input parameters, we have calculated the logarithmic derivatives of each of the neutrino fluxes with respect to each of the most significant input parameters. These derivatives can also be used to exhibit the dependence of the predicted counting rate upon different parameters [cf. Eq. (8) of Bahcall, Bahcall, and Ulrich, 1969] and to evaluate the effect, without constructing a new sequence of standard solar models, of small changes in the best estimates for parameters.

The derivatives were determined by changing a single parameter by a small amount (typically by of order 10%) (e.g., the cross-section factor for the p-p reaction or the solar age) and then recalculating a series of standard solar models until they converged accurately to the assumed present-day luminosity and radius. The differences in neutrino fluxes between the model constructed with the perturbed parameter and the standard solar model were used to form the logarithmic derivatives,

$$\alpha_{i,j}=\frac{\partial \ln\phi_i}{\partial \ln\chi_j} . \tag{15}$$

Table XV contains the logarithmic derivatives of the neutrino fluxes with respect to each of the significant parameters. The results shown in Table XV are in good agreement with the derivatives given in paper I and Eq. (8) of Bahcall, Bahcall, and Ulrich (1969), although the values given here are calculated with respect to the new standard solar model. We have not listed in Table XV the derivatives with respect to S_{17}, since the rarity of this reaction guarantees that the only derivative significantly different from zero is $\partial \ln\phi(^8\mathrm{B})/\partial \ln S_{17}=1.00$.

B. Neutrino flux uncertainties

There are two sources of uncertainty, in the production and in the detection, that enter the predictions for the counting rate in any solar neutrino experiment. In order to make maximum use of solar neutrinos to reveal new things about the sun or about weak interactions, we need to separate the production uncertainties from the unknown aspects of the detector sensitivity. In this section, we determine the uncertainties in the calculated production rates of solar neutrino fluxes. In Sec. VIII we present the predicted capture rates and their total uncer-

[6]The SUNEV code does not represent the theoretical structure of the convective envelope as precisely as does the CATMOS code (see Appendix B). We were forced to use SUNEV because we cannot calculate nuclear burning with CATMOS. Fortunately, the uncertainties introduced by using SUNEV for this application are not significant compared to the large difference between the observed and calculated values of τ.

TABLE XV. Calculated partial derivatives of neutrino fluxes. Each column contains the logarithmic partial derivatives of the neutrino fluxes with respect to the parameter shown at the top of the column. For example, $\partial \ln \phi_{pp} / \partial \ln S_{11} = +0.138$.

Source	S_{11}	S_{33}	S_{34}	$S_{1,14}$	$L_\odot$	$R_\odot$	Z/X	Age
p-p	+0.14	+0.03	−0.06	−0.02	+0.73	+0.01	−0.08	−0.07
pep	−0.17	+0.05	−0.09	−0.02	+0.87	+0.21	−0.17	+0.00
hep	−0.08	−0.45	−0.08	−0.01	+0.12	−0.09	−0.22	−0.11
^{7}Be	−0.97	−0.43	+0.86	−0.00	+3.40	+0.22	+0.58	+0.69
^{8}B	−2.59	−0.40	+0.81	+0.01	+6.76	+0.48	+1.27	+1.28
^{13}N	−2.53	+0.02	−0.05	+0.85	+5.16	+0.28	+1.86	+1.01
^{15}O	−2.93	+0.02	−0.05	+1.00	+5.94	+0.49	+2.03	+1.27
^{17}F	−2.94	+0.02	−0.05	+0.01	+6.25	+0.37	+2.09	+1.29

tainties (production and detection) for specific experiments.

The results of this section are especially relevant for experiments that are designed to detect neutrinos from individual solar nuclear reactions. For the reader's convenience, we list briefly below some of the experiments that detect primarily one neutrino flux. For example, the ^{115}In detector (Raghavan, 1976) is primarily sensitive to *p-p* neutrinos. The scintillator proposed by Mann (1986) could detect ^{7}Be neutrinos. The natural-water (Bakich and Peak, 1985; Beier, 1986; Suzuki, 1986; Hirata *et al.*, 1987a), heavy-water (Chen, 1985; Sinclair *et al.*, 1986; Aardsma *et al.*, 1987), liquid-argon (Bahcall, Baldo-Ceolin, Cline, and Rubbia, 1986), and liquid-scintillator (Badino *et al.*, 1984) experiments are sensitive primarily to ^{8}B neutrinos.

The total fractional uncertainty in individual neutrino fluxes, φ_i, can be computed from the following expression:

$$\frac{\delta\varphi_i}{\varphi_i} = \left[\sum_j [(1+\delta\chi_j/\chi_j)^{\alpha_{i,j}} - 1]^2 \right]^{1/2} . \quad (16)$$

Here the ratios $\delta\chi_j/\chi_j$ are the fractional uncertainties in each of the parameters χ_j discussed in Sec. II in this paper and, where not given explicitly here, in Sec. II in paper I. The logarithmic derivatives used in the calculations are given in Table XV.

Table XIII lists the computed total theoretical uncertainties in the individual neutrino fluxes that result from uncertainties in nuclear reaction rates, assumed primordial heavy-element abundances, the Rosseland mean opacity, and the solar constant. These results do not include the (sometimes large) uncertainties in the neutrino absorption cross sections, which are discussed in Secs. IV and VIII. The uncertainty from the opacity is calculated as described in Sec. III.E in paper I (see especially Table XIV in paper I). We have assumed that the fractional total theoretical range is equal to the difference between the Los Alamos and Livermore opacities, divided by their average value. The uncertainty in the equation of state does not affect significantly the calculated neutrino fluxes (see Sec. III.F in paper I).

The neutrinos from the *p-p* and pep reactions have the smallest calculated uncertainties, of order a few percent. This uncertainty is small because the flux of *p-p* (and related pep) neutrinos is determined mainly by the solar constant and the fact that, with current models and accepted reaction rates (see Table I), the ^{3}He-^{3}He reaction occurs much more frequently than the ^{3}He-^{4}He reaction.

The crucial flux of ^{8}B neutrinos is uncertain by 34%. About half of this large uncertainty is caused by the relatively poorly known low-energy nuclear cross-section factor for producing ^{8}B (cf. reaction 10 in Table I and the discussion in Sec. II.A).

The fluxes from CNO neutrino sources are all uncertain by about 50%, primarily because of the large uncertainty in the primordial heavy-element abundance and the rate at which ^{14}N is burned. None of the experiments so far proposed is sensitive to the neutrinos from the CNO cycle, since these neutrinos are relatively rare and do not have high energies.

We have not listed an uncertainty for the flux of hep neutrinos because their estimated production rate depends upon the thermal neutron capture cross section for ^{3}He, which should be measured more accurately (see discussion in Sec. II.A). Note, however, that apart from the nuclear physics uncertainties this flux is almost as model independent as the pep flux.

VII. MONTE CARLO SIMULATIONS OF THE UNCERTAINTIES

Are the error estimates described in Sec. VI reliable? Could enough measured parameters be in error, all in the right direction, to reduce the correct standard capture rate to the rate observed in the ^{37}Cl experiment? In the

previous section, we have assumed that the errors in the calculated neutrino fluxes are normally distributed and can be obtained by calculating partial derivatives of fluxes with respect to the standard model, extrapolating small changes to large uncertainties. In principle, the assumption of an extrapolated Gaussian could be vitiated by the nonlinear relations imposed by the partial differential equations of stellar structure, which are combined with the boundary conditions of matching the observed solar luminosity, effective temperature, and heavy-element-to-hydrogen ratio (cf. Rood, 1978). We did address partially the question of large changes in paper I, where we showed by an explicit calculation that the effects of a simultaneous change of four nuclear parameters, each by its estimated 3σ limit and each in the direction to reduce the flux of ^{8}B neutrinos, could be well approximated by the results obtained with the partial derivatives. Table XII in paper I shows that the *large* change in each of the neutrino fluxes for this specific quadrupole 3σ variation is given to an accuracy of better than 10% for all of the solar neutrino fluxes of interest. Nevertheless, the nagging question remains: is the *distribution* of uncertainties for a given flux or capture rate sufficiently well approximated by a Gaussian with the standard deviation calculated as described in Sec. VI?

We have answered this question by brute force. We have constructed 1000 accurate solar models with five input parameters that were chosen each from a normal distribution with the mean and standard deviation specified in Sec. II. The calculations were carried out in background mode on four microvaxes at the Institute for Advanced Study using an automated version of the SUNEV code described in Appendix C. The five quantities that were allowed to vary randomly were the primordial heavy-element-to-hydrogen ratio Z/X and the cross-section factors for the p-p, ^{3}He-^{3}He, ^{3}He-^{4}He, and p-^{7}Be reactions (reactions 1, 5, 6, and 9 in Table I). These quantities represent five of the dominant uncertainties in predicting the rate of the ^{37}Cl experiment (see Sec. VIII.A.1 and Table XVI). The inclusion of additional parameters (with the uncertainties given in Sec. II) in the simulations would have changed by a small amount the total range of fluxes and capture rates found in the simulations, but would not have affected our general conclusions.

The Monte Carlo simulations are in remarkable agreement with the results obtained in Sec. VI using partial derivatives of fluxes with respect to each of the parameters and the assumption that the uncertainties are normally distributed. The fractional standard deviations that are calculated from the Monte Carlo simulations (and in parentheses the value obtained using partial derivatives) are for the p-p, pep, hep, ^{7}Be, ^{8}B, ^{13}N, ^{15}O, and ^{17}F fluxes, respectively; 0.006 (0.006), 0.011 (0.011), 0.029 (0.027), 0.050 (0.048), 0.120 (0.120), 0.124 (0.133), 0.137 (0.148), and 0.141 (0.153). The numbers in parentheses were of course calculated using just the partial derivatives for the five parameters that were allowed to vary in the simulations. *In all cases, the standard deviations calculated by the two different methods agree to better than 10%.*[7]

What about the very large variations? What is the probability that a random variation of the input parameters would yield a neutrino flux that differs from the best estimate (average of the simulations) by more than some specified number of standard deviations?

Figure 9 compares the distribution of fluxes obtained from the simulation with that calculated using the assumption of a Gaussian distribution with a standard deviation evaluated using the partial derivatives given in Table XV. We show three separate curves in Fig. 9: (1) the normal distribution (solid curve); (2) simulations above the average value (short dashes); and (3) simulations below the average value (long dashes).

Figure 9(a) compares the three distributions between zero and four standard deviations. The probability distributions for all three cases are very similar, so much so that it is hard to see on this scale how the other two curves deviate from the normal distribution.

For clarity, Fig. 9(b) displays the three distributions in the limit of large deviations more than 2σ differences from the mean. We see from this comparison that the number of very small values of the ^{8}B flux in the simulated distribution is somewhat lower than for the normal distribution. For the 1000 simulated cases, we would have expected 6.2 cases that are 2.5σ below the mean and

[7]Filippone and Schramm (1982) simulated the uncertainties in the ^{37}Cl and ^{71}Ga experiments by calculating 100 solar models. Our results differ from theirs primarily because Filippone and Schramm assumed a large and asymmetric 1σ standard deviation for the cross-section factor for the ^{3}He-^{4}He reaction (number 6 in Table I), which was plus 17% in the direction of increasing cross-section factor and minus 44% in the direction of decreasing cross-section factor. Their adopted plus uncertainty is 3 times as large as ours (see Table I in this paper or Sec. II in paper I), and their minus uncertainty is more than 7 times as large as ours. With such a large adopted uncertainty, Filippone and Schramm must have made some (unspecified) assumption in their simulations to prevent negative nuclear cross sections from occurring. The reason that Filippone and Schramm used a large asymmetric error is that they decided to define their 1σ range so as to include a discrepant experimental value reported by the Münster group. Subsequent experiments have shown that the Münster result was in error (see Parker, 1986, and Table I of this paper). We are unable to make specific comparisons with the neutrino flux calculations of Filippone and Schramm, since the details of their solar model are not specified in their paper. There may have been convergence problems with some of their models, since they apparently only converged the models to an accuracy of a few percent in luminosity (Filippone, 1982), instead of the typical value we use of either 0.01% or 0.001%. Some additional questions concerning the Filippone and Schramm calculations are discussed in comment 7 in Sec. VI of paper I.

TABLE XVI. Individual uncertainties in predicted capture rates. Each column contains the uncertainty in SNU of the total capture rate caused by the uncertainty in the parameter at the top of the column.

Uncertainty from Parameter / Detector	p-p (SNU)	^{3}He $-^3$ He (SNU)	^{3}He $-^4$ He (SNU)	$p-^7$ Be (SNU)	Z/X (SNU)	Opacity (SNU)	σ_{abs} (SNU)	Total (SNU)
^{2}H	0.7	0.4	0.3	1.3	1.5	0.5	0.6	2.3
^{7}Li	5.1	1.6	1.2	4.9	12.2	2.5	4.2	16
^{37}Cl	0.9	0.5	0.4	1.3	1.8	0.5	0.6	2.6
^{40}Ar	0.2	0.1	0.1	0.4	0.4	0.1	0.1	0.6
^{71}Ga	4.1	2.8	2.2	3.1	10.1	2.8	16	20
^{81}Br	2.6	1.5	1.2	3.4	5.8	1.6	16	17
^{98}Mo	2.1	1.1	0.8	3.8	4.3	1.4	17	18.5
^{115}In	8.2	6.3	4.9	3.2	22.3	6.9	639	640

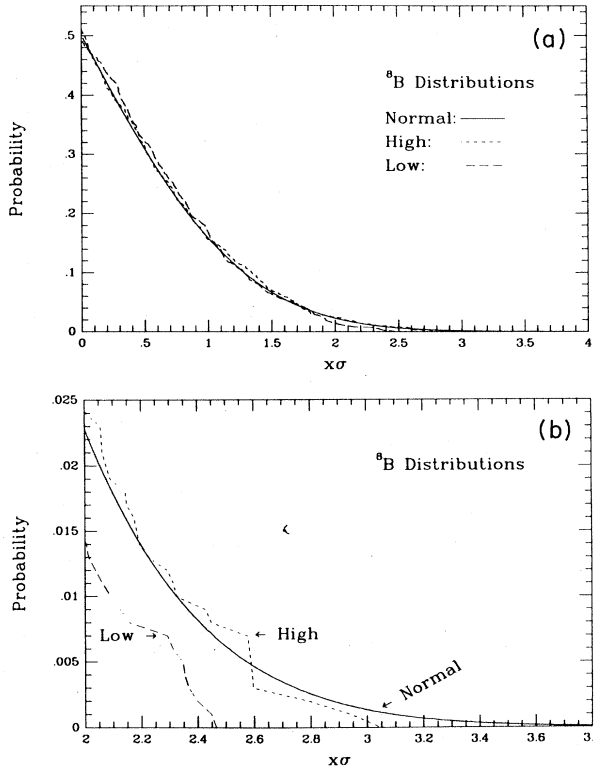

FIG. 9. Distribution of ^{8}B neutrino fluxes in 1000 solar models. This figure compares the distribution of ^{8}B neutrino fluxes calculated from 1000 accurate solar models with what is expected from a Gaussian distribution whose mean and standard deviation are calculated as described in Sec. VI. The parameters of the 1000 solar models were selected randomly from normal distributions for each of five important parameters, listed in the text, whose means and standard deviations are given in Sec. II. Solid curves; normal distribution; short-dashed curves, simulations that have ^{8}B fluxes above the average value; long-dashed curves, simulations that have ^{8}B fluxes below the average value. (a) The three distributions between zero and four standard deviations; (b) the three distributions at large deviations, on an expanded scale.

we found none. The high values are in good agreement with the normal distribution.

The smallest ^{8}B flux found in our simulations was 4.0×10^6 cm^{-2}s^{-1} and the largest value was 7.9×10^6 cm^{-2}s^{-1}. The corresponding 3σ limits that we calculated with the Gaussian partial-derivative method are 3.6×10^6 cm^{-2}s^{-1} and 7.7×10^6 cm^{-2}s^{-1}.

The agreement between the Monte Carlo simulations and the Gaussian extrapolation is similarly excellent for the total capture rates predicted for the ^{37}Cl and ^{71}Ga experiments. The 1000 simulations have capture rates varying between 5.8 SNU and 10.5 SNU; the corresponding 3σ limits calculated as described in Sec. VI are 5.4 SNU and 10.3 SNU. For the ^{71}Ga detector, the 1000 simulations range from 119 SNU to 144 SNU, while the range calculated via the Gaussian extrapolation is 120 SNU to 143 SNU.

We could have run more simulations to determine if the slight differences from a normal distribution are really significant or not. We decided, however, that more simulations would not tell us anything of value. We do not know the error distributions of the input parameters sufficiently well to justify studying in detail the tail of the combined uncertainty distribution.

The question of greatest importance is does one expect variations of the input parameters with the *assumed* best values and standard deviations given in Sec. II to lead, with a significant probability, to the existing discrepancy between observation and calculation for the ^{37}Cl experiment? The answer given in Fig. 9 and the above-cited range of capture rates is "no."

VIII. PREDICTED EVENT RATES IN SOLAR NEUTRINO EXPERIMENTS

In this section we present the total theoretical range in the predicted event rate, as well as a best-estimate rate, for each of the detectors whose neutrino cross sections

are discussed in Sec. IV. We combine incoherently the uncertainties in the predicted event rates due to each of the factors discussed previously, including nuclear reaction cross sections, solar constant, primordial composition, radiative opacity, equation of state, and solar age. We denote each of the neutrino fluxes by φ_i and each of the input parameters by χ_j. The neutrino fluxes are taken from the model "Best" in Table XIV, which gives the values computed with the standard solar model for each of the sources. The best-estimate event rate is $R=\sum_i \varphi_i \sigma_i$. Here 1 SNU $=10^{-36}$ event (target atom)$^{-1}$ (s)$^{-1}$ (Bahcall, 1969b).

The total incoherent uncertainty in the predicted rate, δR, for a particular experiment is obtained from the relation.

$$\delta R=\left[\sum_j\left[\sum_i(\varphi\sigma)_i[(1+\delta\chi_j/\chi_j)^{\alpha_{i,j}}-1]\right]^2\right]^{1/2}. \tag{17}$$

For each parameter j, the sum is carried out coherently over each of the neutrino sources i.

The neutrino cross sections we use here are given in Tables VII and VIII. The other input parameters and the logarithmic derivatives [defined in Eq. (15)] that were used in the calculations are described in Secs. II, VI, and VII in this paper and Secs. II and IV in paper I.

For nonstandard solar models, also assuming nothing significant happens to the neutrinos after they are produced, the predicted rates and uncertainties can be calculated in the same way, using the appropriate neutrino fluxes. The procedure is parallel to that used for the standard solar models because the shapes of the individual neutrino spectra are unchanged and therefore the cross sections given in Tables VII and VIII still apply. If the shapes of the individual neutrino spectra are changed by processes such as the MSW effect, one must integrate over energy the appropriate spectral shape times the cross section as a function of energy (given in Table IX or Bahcall, 1987). The MSW effect in the Earth can cause, for certain values of the neutrino mixing angles and mass differences, large time-dependent effects in the observed event rates in radiochemical detectors (see, for example, Carlson, 1986; Baltz and Weneser, 1987; Cribier, Rich, Spiro, Vignaud, Hampel, and Cleveland, 1987; Dar and Mann, 1987; Kuo and Pantaleone, 1987). If we are lucky and the parameters nature has chosen are the ones for which the time-dependent effects are large, then the radiochemical experiments could directly demonstrate the existence of the MSW effect.

We follow historical precedent and begin with radiochemical detectors and then discuss direct counting detectors.

A. Radiochemical detectors

We consider first the three experiments that are in progress, involving ^{37}Cl, ^{71}Ga, and ^{98}Mo detectors, and then give the predictions for two other often discussed potential detectors ^{7}Li and ^{81}Br.

1. ^{37}Cl

The predicted capture rate for a ^{37}Cl detector is

$$\sum_i \phi_i\sigma_i = 7.9(1\pm0.33)\ \text{SNU}\ . \tag{18}$$

This detector is sensitive to neutrinos with energies above 0.814 MeV, which excludes the abundant p-p neutrinos.

The principal uncertainties in the calculated capture rate are shown in the third row in Table XVI. The contributions of different neutrino sources to the total capture rate are shown in Table XVII.

TABLE XVII. Capture rates predicted by the standard solar model. The capture rates predicted by the standard solar model, row 5 in Table XIV (CNO Cor), are given for each target (first column) and for each neutrino source (columns 2–9). The total rate is given in the last column. All event rates are in SNU.

Target	p-p	pep	hep	^{7}Be	^{8}B	^{13}N	^{15}O	^{17}F	Total
^{2}H	0.0	0.0	0.02	0.0	6.0	0.0	0.0	0.0	6.0
^{7}Li	0.0	9.2	0.06	4.5	22.5	2.6	12.8	0.1	51.8
^{37}Cl	0.0	0.2	0.03	1.1	6.1	0.1	0.3	0.004	7.9
^{40}Ar	0.0	0.0	0.02	0.0	1.7	0.0	0.0	0.0	1.7
^{71}Ga	70.8	3.0	0.06	34.3	14.0	3.8	6.1	0.06	132
^{81}Br	0.0	1.1	0.07	8.6	15.3	0.9	1.9	0.02	27.8
^{98}Mo	0.0	0.0	0.08	0.0	17.3	0.0	0.0	0.0	17.4
^{115}In	468	8.1	0.05	116	14.4	13.6	18.5	0.2	639

How reliable is the theoretical prediction? Figure 10 illustrates one way of answering this question. We plot in Fig. 10, as a function of the date of publication, all of the predicted capture rates, and their quoted errors, for each paper in this series. All of the 14 values published since 1968 are consistent with the range given in Eq. (18). The first calculation in 1963 was made before the realization (Bahcall, 1964) that the capture rate for ^{8}B neutrinos is enhanced by a factor of about 17 by transitions to excited states, especially to the analog state.

The best-estimate capture rate is 4% larger than the value of 7.6 SNU that was determined in paper I. The total theoretical uncertainty has decreased from 43%, or 3.3 SNU, in paper I to 33%, or 2.6 SNU, in Eq. (18) above.

The total uncertainty is made up of contributions of comparable size from several different input parameters (see row 3 of Table XVI): 1.8 SNU from the primordial heavy-element-to-hydrogen ratio [cf. Eq. (1)]; 1.3 SNU from the S factor for the ^{7}Be-p reaction; 0.9 SNU from the p-p reaction; and 0.6 SNU from the neutrino absorption cross sections. Since several different parameters contribute appreciably to the total uncertainty, it seems unlikely that the total theoretical uncertainty will be reduced much below 2 SNU, or of order 25% of the predicted capture rate, in the foreseeable future.

The ^{37}Cl experiment is primarily sensitive to neutrinos from ^{8}B decay. Approximately 77% (6.1 SNU) of the predicted event rate is contributed by ^{8}B neutrinos; the next largest contribution is the 14% (1.1 SNU) from ^{7}Be

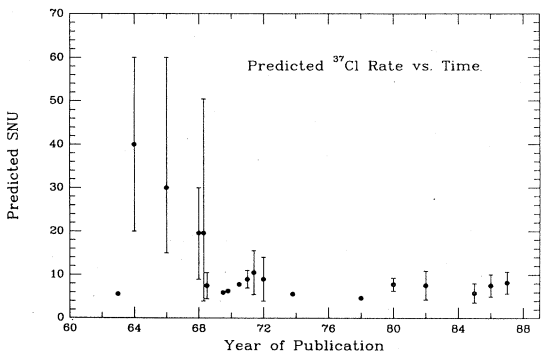

FIG. 10. Predicted capture rates as a function of time. The published predictions of neutrino capture rates in the ^{37}Cl experiment are shown as a function of the date of publication. The values and their error bars are from Bahcall. Fowler, Iben, and Sears (1963), Bahcall (1964), Bahcall (1966), Bahcall and Shaviv (1968), Bahcall, Bahcall, Fowler, and Shaviv (1968), Bahcall, Bahcall, and Shaviv (1968), Bahcall (1969a), Bahcall and Ulrich (1970), Bahcall and Ulrich (1971), Bahcall, Heubener, Magee, Merts, and Ulrich (1973), Bahcall (1977), Bahcall, Heubner, Lubow, Magee, Merts, Argo, Parker, Rozsnyai, and Ulrich (1980), Bahcall, Heubner, Lubow, Parker, and Ulrich (1982), Bahcall, Cleveland, Davis, and Rowley (1985), Bahcall (1986), and the present paper (1987). Similar results have been obtained by many other authors.

neutrinos. Most of the calculated uncertainty is caused by the ^{8}B neutrino flux. About 87%, or 2.3 SNU out of the total estimated uncertainty of 2.6 SNU, is associated with the ^{8}B flux.

We can use the ^{37}Cl experiment to set an upper limit on the flux of electron neutrinos with a ^{8}B spectrum that reaches the Earth from the sun. The ratio of the observed to the calculated flux is the crucial quantity that must be compared with models of weak interactions to determine if neutrinos oscillate or decay on the way to the Earth from the sun. However, the conversion of the experimental limit to the desired ratio of observed to predicted fluxes depends upon what one is willing to assume. We illustrate this dependence in the following discussion.

The observed event rate is (Davis, 1964; Davis, 1978; Rowley, Cleveland, and Davis, 1985; Davis, 1986)

$$\sum_i (\varphi\sigma)_i = 2.0 \pm 0.3 \text{ SNU} . \tag{19}$$

We can convert this experimental constraint into a limit on the ^{8}B neutrino flux by dividing the event rate in SNU's by the absorption cross section given in Table VII. Ignoring for the moment all of the estimated uncertainties, we find

$$\varphi(^8\text{B})_{\text{no errors}} \leq 2\times 10^6 \text{ cm}^{-2}\text{s}^{-1} , \tag{20}$$

which is about a factor of 3 times smaller than the best-estimate value of 5.8×10^6 cm^{-2}s^{-1} obtained from the standard model.

If we assume instead that the 3σ upper limit to the *entire* observed capture rate, i.e., 2.9 SNU, is due to ^{8}B neutrinos, then we can obtain a *conservative* upper limit to the observed flux. We obtain

$$\varphi(^8\text{B})_{\text{observed}} \leq 2.7\times 10^6 \text{ cm}^{-2}\text{s}^{-1} . \tag{21}$$

The limit given in Eq. (21) is about a factor of 2.15 times smaller than the best-estimate flux given in Tables XIII and XIV.

Since the theoretical uncertainties are much larger than the observational errors, we can obtain a conservative limit to the decrease in flux by using, instead of the best estimate provided by the standard solar model, the smaller value that is decreased by the estimated total theoretical uncertainty given in Table XIII. The "theoretical lower limit" is

$$\varphi_{\text{theoretical}} \geq 3.7\times 10^6 \text{ cm}^{-2}\text{s}^{-1} , \tag{22}$$

which is about 1.9 times larger than the experimental upper limit given in Eq. (20).

We note that there is another extreme possibility. The experimental result cited in Eq. (19) is consistent with *no* observed ^{8}B neutrino flux. The contribution of all but ^{8}B neutrinos is 1.8 SNU (see Table XVIII below, next to last column), which is consistent with the observed capture rate. We note in addition that the observed event rate could, in principle, be due partly or wholly to interactions caused by something other than neutrinos from the solar interior. In this case also, we would have no evi-

dence yet available that a finite ^{8}B neutrino flux has been detected.

We conclude that the experimental limit on the ratio of observed to predicted ^{8}B neutrino flux is in the range

$$0 \leq \left[\frac{\varphi(^8\mathrm{B})_{\mathrm{observed}}}{\varphi(^8\mathrm{B})_{\mathrm{predicted}}} \right] \leq 0.5 \ . \tag{23}$$

Measurements with the ^{37}Cl detector are continuing in order to build up statistics on the possible time dependence of the capture rate, to provide overlap with observations using other neutrino detectors (see below), and to search for evidence of a day-night effect caused by regeneration of electron neutrinos as neutrinos of different type pass through the Earth (see Davis, 1986).

Is the rate of neutrino events observed in the ^{37}Cl experiment consistent with statistical fluctuations? Or is there some significant dependence upon time, perhaps correlated with the season of the year or the intensity of solar cosmic radiation? Does the time dependence of the observed capture rate suggest that the neutrino has a finite magnetic moment and that what we observe is influenced by the solar magnetic field configuration along the line of sight (see Voloshin, Vysotskii, and Okun, 1986)? Answers to these questions are important but controversial and can only be settled by obtaining more data to check the time dependences that have been claimed. For two opposing viewpoints,[8] with references to the previous literature, see Davis (1986) and Bahcall, Field, and Press (1987). Davis has described an apparently remarkable correlation between sunspot number and the event rate observed in his solar neutrino experiment. On the other hand, Bahcall *et al.* have shown that while the correlation is significant at the 5% level, it depends sensitively upon how the errors are estimated and on a small number (four) of experimental runs. Moreover, they have argued that a correlation, if real, would be puzzling on energetic grounds. It is important to settle this question observationally. If a correlation were to be established unequivocably between event rate in the ^{37}Cl experiment and sunspot activity, it would have fundamental implications suggesting either that we do not understand the order of magnitude of energy generation in sunspots or that new physics is occurring that is outside of the standard electroweak theory (Voloshin and Vysotskii, 1986, Okun, 1986).

[8]The intensity of the controversy surrounding this question can be gauged from the fact that at the Solar Neutrino Workshop held at the Institute of Theoretical Physics in Santa Barbara in April, 1987 the two co-organizers (Bahcall and Davis) publicly wagered a bottle of "good" French champagne on whether or not SNU's are correlated with sunspots. The observations, the most crucial of which will occur in 1990 and 1991, will be collaboratively interpreted and the wager consumed jointly.

2. ^{71}Ga

The predicted capture rate for a ^{71}Ga detector is

$$\sum_i \varphi_i \sigma_i = 132^{+20}_{-17} \ \mathrm{SNU} \ . \tag{24}$$

All electron neutrinos with energies above 0.233 MeV can be absorbed by ^{71}Ga. This low threshold energy makes ^{71}Ga sensitive to the fundamental *p-p* neutrinos.

The contributions of different neutrino sources to the total capture rate are shown in Table XVII. Neutrinos from the basic *p-p* reaction produce approximately half, 54% or 71 SNU, of the computed total capture rate. The other main contributors are ^{7}Be neutrinos, 26% or 34 SNU, and ^{8}B neutrinos, 11% or 14.0 SNU.

The principal uncertainties in the calculated rate are shown in the fifth row in Table XVI. The dominant uncertainty is caused by the transitions to excited states whose matrix elements must be inferred from (p,n) measurements (see discussion in Sec. V.D of paper I and in Sec. IV of this paper). According to the prescription for calculating errors that is described in Sec. IV.B.1, the maximum increase that could be caused by excited-state transitions is +16 SNU, and the corresponding extreme decrease is −8 SNU. Excited-state transitions contribute 88%, or 12 SNU, of the total ^{8}B contribution. The curve of absorption cross sections versus excitation energy has a broad peak in the range 3–5 MeV, which contains about one-third of the total calculated strength. If we were to ignore all of the uncertainties associated with the excited-state transitions, then the remaining total calculated uncertainty would be only 12 SNU (or 9% of the total capture rate).

The transition from the ground state of ^{71}Ga to the isobaric-analog state in ^{71}Ge does not contribute significantly to the expected capture rate because the analog state decays mostly by particle emission. The cross section for absorption of ^{8}B neutrino is large, 3.14×10^{-43} cm^{-2}, but the upper limit for the γ decay of this state is less than 10% (Champagne *et al.*, 1987). Thus transitions to the isobaric-analog state account for less than 0.2 SNU.

The largest change in the predicted capture rate for the ^{71}Ga experiment since the calculations in paper I were performed is caused by transitions to excited states in ^{71}Ge. The rate given in paper I was 106.4 SNU if excited states were ignored completely and 119 SNU if transitions to low-lying excited levels (up to 0.71-MeV excitation energy) were included with a maximum plausible estimate based upon systematics of measured laboratory β decays involving similar transitions. No estimate was made in paper I of transitions to highly excited levels in ^{71}Ge since (see Bahcall, 1978) no measurements were available for analogous β-decay transitions. The (p,n) measurements of Rapaport *et al.* (1985) and Krofcheck (1987) yield a predicted capture rate of 3 SNU to the low-lying levels in ^{71}Ga, consistent with the guessed range of 0 to 13 SNU given in paper I. In addition, how-

ever, the (p,n) measurements suggest that there is a large contribution from transitions to highly excited states. We estimate that the total contribution of transitions to excited states is 16.8 SNU, slightly larger than the upper limit for low-lying levels that was suggested in Bahcall (1978).

Transitions to *highly excited* states account for about 12 SNU; this estimate is based entirely upon (p,n) measurements. The theoretical ^{51}Cr cross section given in Eq. (5) has only a small ($\simeq 6\%$) contribution from excited states, none of which are above 0.5 MeV. Therefore the calibration of the ^{71}Ga detector with a ^{51}Cr source cannot remove the significant uncertainty in the sensitivity caused by transitions to highly excited states.

Excited-state transitions cause a significant uncertainty—of order 10% in the total capture rate—for the standard solar model predictions, an uncertainty which seems unavoidable unless an unanticipated major improvement is achieved in the accuracy with which GT matrix elements to excited states can be determined (cf. the discussion of p,n measurements in Sec. IV.B.1 and of calibrations with a muon beam in Sec. IV.D).

How large are the uncertainties if, as appears likely, the standard predictions are incorrect? The answer depends upon what is wrong with the standard predictions. The fractional uncertainties would be increased if, as is possible for one MSW solution, lower-energy neutrinos are preferentially affected by resonant matter oscillations and only the higher-energy electron neutrinos reach the Earth without having their flavor changed. In this case, nearly all of the small expected event rate (~ 10 SNU) could come from transitions whose strength is determined entirely by (p,n) interactions and is therefore very uncertain (see Sec. IV.B.1). On the other hand, most nonstandard solar models would give rise to smaller uncertainties in the predicted event rate, since they primarily suppress the higher-energy neutrinos that populate excited states. The most extreme of these nonstandard models is the so-called "No ^{8}B" model (see Tables XIV and XVIII), in which all of the higher-energy neutrinos are artificially removed. This "model" predicts a capture rate of 1.8 SNU for the ^{37}Cl experiment and is therefore in satisfactory agreement with the neutrino observations (although it is inconsistent with a number of excellent laboratory experiments on the nuclear reaction cross section; see Sec. II.A). The "No ^{8}B" hypothesis effectively minimizes the uncertainty in the predicted event rate, since the capture rates for high-energy neutrinos are less well known, due to uncertainties in both the production rates and the absorption cross sections. For this particularly favorable case (with regard to uncertainties), we find $\sum_i \varphi_i \sigma_i = 118^{+13}_{-12}$ SNU. The total theoretical uncertainty is approximately 10%.

Two major solar neutrino experiments using ^{71}Ga are under way, one by a primarily European collaboration (GALLEX) and the second by a group in the Soviet Union (see Hampel, 1985; Barabanov *et al.*, 1985; Kirsten, 1986; see also Kuzmin and Zatsepin, 1966; Kuzmin, 1966; Bahcall *et al.*, 1978). The GALLEX collaboration will use 30 tons of gallium in an aqueous solution of gallium chloride and hydrochloric acid; the detector will be located in the Gran Sasso Laboratory in Italy. Measurements are not expected to begin until 1990. The Soviet experiment will use 60 tons of gallium metal as a detector in a solar neutrino laboratory constructed in the Baksan valley. The Soviet experimentalists expect to have a detector that is operating in 1988 or 1989. The initial chemical extraction is different in the GALLEX and the Soviet experiments, but the final chemical procedures and the methods of low-level counting will be similar for both collaborations. The comparison of the results from the two experiments will be a valuable check on any possible systematic errors.

3. ^{98}Mo

The ^{98}Mo detector is sensitive only to ^{8}B (and hep) neutrinos (see Table VII). The ground-state-to-ground-state transition, which has a threshold energy of 1.68 MeV, is forbidden. All of the transitions of interest are to excited states of ^{98}Tc.

The predicted capture rate is

$$\sum_i \varphi_i \sigma_i = 17.4^{+18.5}_{-11} \text{ SNU} , \tag{25}$$

of which all but 0.08 SNU comes from ^{8}B neutrinos. The dominant uncertainty in the predicted capture rate is from the neutrino capture cross sections; the total uncertainty from all other sources is only 6 SNU (see Table XVI).

Since the half-life of ^{98}Tc is 4×10^6 yr, this detector provides information about the ^{8}B neutrino flux averaged over the past several million years (see Cowan and Haxton, 1982).

A geochemical experiment has been developed at Los Alamos National Laboratory to extract ^{98}Tc produced by solar neutrino capture on ^{98}Mo. The experiment will make use of about 13 tons of molybdenite obtained from 2600 tons of ore that was buried deeply in the Henderson Mine in Colorado, operated by the AMAX corporation. An ultrasensitive mass spectrometer will be used to detect the predicted 10^7 atoms of ^{98}Tc. Wolfsberg *et al.* (1985) have described the sophistical experimental procedures that they are using. The first results of this experiment are expected in 1988.

4. ^{7}Li

The predicted capture rate for a ^{7}Li detector is

$$\sum_i \varphi_i \sigma_i = 51.8(1\pm 0.31) \text{ SNU} . \tag{26}$$

The ^{7}Li experiment is also mostly sensitive to neutrinos from ^{8}B decay, although much less so than the ^{37}Cl or ^{98}Mo experiments. The threshold energy for neutrino ab-

sorption is 0.862 MeV, which means that only the *p-p* neutrinos are undetectable with this target. Approximately 43% (22.5 SNU) of the predicted event rate is contributed by ^{8}B neutrinos; the next largest contributions are the 25% (13 SNU) from ^{15}O neutrinos and the 18% (9 SNU) from pep neutrinos. About half of the total calculated uncertainty is related to the ^{8}B neutrino flux.

The principal uncertainties in the calculated capture rate are shown in the second row in Table XVI. The contributions of different neutrino sources to the total capture rate are shown in the second row in Table XVII for standard solar models and in Table XVIII for nonstandard models.

This detector provides the best available opportunity for detecting the CNO neutrinos. For the illustrative case in which no ^{8}B neutrinos reach the Earth (see next to last column in Table XVIII), the predicted capture rate is 29.3±8.5 SNU, of which 12.8 SNU is from ^{15}O and 2.6 SNU is from ^{13}N. Thus for this extreme (but conceptually possible) case, the CNO neutrinos contribute more than half (53%) of the counting rate. The neutrino absorption cross sections for this case are all well determined (to an accuracy of about 6%; see Sec. IV.B).

The theoretical advantages of using ^{7}Li to detect solar neutrinos have been recognized for a long time (Bahcall, 1969b). Moreover, Rowley (1978) has stressed that a lithium detector would be relatively cheap, the chemical procedures straightforward, and the backgrounds manageable; the difficult part is detecting the ^{7}Be that is produced by neutrino capture. Various schemes have been proposed to count ^{7}Be atoms (see Rowley, 1978), but none of the methods has as yet been demonstrated in the laboratory.

5. ^{81}Br

The predicted capture rate for a ^{81}Br detector is

$$\sum_i \varphi_i \sigma_i = 27.8^{+17}_{-11} \text{ SNU} . \quad (27)$$

The effective threshold energy for neutrino absorption by ^{81}Br is 0.471 MeV (cf. Sec. IV.B), which excludes the important *p-p* neutrinos.

The contributions of different neutrino sources to the total capture rate are shown in the sixth row in Table XVII. Neutrinos from ^{8}B decay constitute about 55% of the expected capture rate. The next most important source is ^{7}Be, whose neutrinos contribute 31% of the total capture rate.

All previous discussions of this experiment have supposed that it would be primarily sensitive to ^{7}Be neutrinos (e.g., Scott, 1976; Bahcall, 1981; Haxton, 1981; Itoh and Kohyama, 1981; Hurst *et al.* 1984, 1985; Davis, 1986). The reason for this important change in the predicted nature of the detector sensitivity is the large measured Gamow-Teller strength to highly excited levels of ^{81}Kr that was found in the (p,n) measurements of Krofcheck *et al.* (1987).

The principal uncertainties in the calculated rate are shown in the second row of Table XVI. The dominant uncertainty is caused by the transitions to excited states whose matrix elements must be inferred from (p,n) measurements (cf. discussion in Sec. V.D of paper I and in Sec. IV of this paper). According to the prescription for calculating errors that is described in Sec. IV.B.1, the total uncertainty due to neutrino absorption cross sections is +16 SNU or −8 SNU. If we ignore all of the uncer-

TABLE XVIII. Capture rates predicted by some nonstandard solar models. The total capture rates predicted by some nonstandard solar models are given in columns 3–11. For comparison, the rates for the standard solar model are given in column 2. The nonstandard models are described in Sec. IX and the standard model is described in Sec. V. All rates are in SNU.

Target	Stnd.	Z1	Z2	Z3	Y1	Y2	Y3	Y4	No ^{8}B	$S_{3,4}=0$	WIMP's
^{2}H	6.0	0.9	0.7	0.7	6.3	6.7	7.2	7.1	0.02	0.0	1.5
^{7}Li	51.8	16.2	15.4	15.3	53.6	56.3	59.1	58.2	29.3	20.2	24
^{37}Cl	7.9	1.6	1.4	1.4	8.3	8.8	9.3	9.2	1.8	0.6	2.7
^{40}Ar	1.7	0.3	0.2	0.2	1.8	1.9	2.0	2.0	0.02	0.0	0.4
^{71}Ga	132	94.5	93.2	93.0	139	138	141	140	118	86	107
^{81}Br	28	6.9	6.2	6.1	29	31	32	32	12.5	3	12
^{98}Mo	17	2.5	2.1	2.1	18	19	21	20	0.1	0.1	4.3
^{115}In	639	556	553	552	673	658	663	661	624	536	585

tainties associated with absorption cross sections, then the remaining total theoretical uncertainty is only 7 SNU (or 25% of the total capture rate).

A bromine detector experiment would be a natural successor to the ^{37}Cl experiment since it could be performed inexpensively using the same tank and would involve similar chemical procedures (Hurst *et al.*, 1984, 1985; Davis, 1986). Resonance ionization spectroscopy could be used to detect the atoms of ^{81}Kr that are produced by neutrino capture (Hurst *et al.*, 1985). The relatively large uncertainty in the theoretical predictions [see Eq. (27)], resulting from inaccurately known neutrino cross sections, limits the inferences that would be possible from a bromine experiment. However, a ^{81}Br detector could provide valuable constraints on both the ^{8}B and the ^{7}Be neutrino fluxes.

6. ^{205}Tl

A ^{205}Tl detector would provide especially interesting information, since (see Freedman *et al.*, 1976; Freedman, 1978; Henning *et al.*, 1985) it is sensitive to neutrinos emitted over the past 10^7 yr. However, the neutrino absorption cross sections for the most obvious transitions between low-lying states cannot be calculated accurately (see Bahcall, 1978, Sec. IV.1), and it is difficult to give a rigorous upper limit to the uncertainties (see Braun and Talmi, 1987). This situation is particularly distressing because ^{205}Tl could potentially furnish unique information about the time dependence of the fundamental *p-p* neutrinos. Freedman (1986) has suggested that it may be possible to measure the Gamow-Teller strength of the most important low-lying transition by a very clever laboratory technique.

We have estimated the rate of the transitions to higher-energy excited states of ^{205}Pb using preliminary (p,n) data obtained by Krofcheck (1987) and his collaborators and generously made available to us. These data cannot be used in the traditional way to obtain the cross sections for the previously considered dominant transition to the low-lying 0.0023-MeV excited state of ^{205}Pb because this transition is first forbidden. Nevertheless, we can perform an illustrative calculation of the cross section for absorption of ^{8}B neutrinos because allowed transitions to higher-energy states of ^{205}Pb presumably dominate this process, and the usual calibration procedure may be appropriate. The result is of interest even though it is very preliminary, since it shows that the capture rate may not be completely dominated by *p-p* neutrinos, as has been assumed in all previous discussions.

We find a total absorption cross section for ^{8}B neutrinos incident on ^{205}Tl of $\sigma \approx 8\times 10^{-42}$ cm^2. Given the preliminary nature of the data, this cross section must be considered to be uncertain by at least a factor of 2 and probably more; we do not consider the result sufficiently reliable to merit inclusion in Table VII. We have also reestimated the cross sections for all the other sources using the log ft value of 5.7 that was suggested by Braun and Talmi (1986) as possibly appropriate for the transitions to the lowest-lying $1/2^-$ state in ^{205}Pb (0.0023-MeV excitation). The log ft value of Braun and Talmi implies that all of the "nominal" cross sections of Bahcall (1978) should be reduced by a factor of about 2.5. The threshold energy for neutrino absorption via this lowest first-forbidden transition is only 0.062 MeV. This low threshold causes ^{205}Tl to be sensitive to the basic *p-p* neutrinos.

With the above cross sections, we find a total rate of

$$\sum_i \varphi_i \sigma_i = 263 \text{ SNU} . \tag{28}$$

We refrain from quoting a formal uncertainty on the above rate because all of the neutrino absorption cross sections are very uncertain. Nevertheless, it is of interest to note here that the nominal contributions of *p-p*, ^{7}Be, and ^{8}B neutrinos to the total rate are, respectively, 173 SNU, 34 SNU, and 46 SNU. Within the large uncertainties that apply for this case, we note that the ^{7}Be and ^{8}B neutrinos contribute an amount comparable to the *p-p* neutrinos.

B. Direct counting experiments

We consider in this section experiments in which individual recoil electrons are detected. The recoil energy of the electrons can be produced either by neutrino-electron scattering or by neutrino absorption. In both cases, the angular distribution of the electrons with respect to the Earth-sun axis is an important measurable quantity (not observable for radiochemical experiments). For neutrino-electron scattering, the angular distribution is strongly forward peaked for relativistic electrons [see Eqs. (20) and (21) of Bahcall, 1987]. For neutrino absorption, the angular distribution is much less concentrated and is given by the simple formula (Bahcall, 1964)

$$P(\theta) = \left[1 + \left[\frac{v_e}{c}\right]\alpha \cos\theta\right] , \tag{29a}$$

where v_e is the recoil velocity of the electron, and the asymmetry parameter α is given by

$$\alpha = \frac{\langle 1\rangle^2 - \frac{1}{3}(G_A/G_V)^2\langle\sigma\rangle^2}{\langle 1\rangle^2 + (G_A/G_V)^2\langle\sigma\rangle^2} . \tag{29b}$$

Here, $(G_A/G_V)^2 \approx 1.54$ and $\langle 1\rangle^2$, $\langle\sigma\rangle^2$ are, respectively, the usual reduced matrix elements for the Fermi and Gamow-Teller interactions. (For example, for neutron decay, $\langle 1\rangle^2 = 1, \langle\sigma\rangle^2 = 3$.) For the ^{2}H detector, $\alpha = -\frac{1}{3}$ and for ^{40}Ar, $\alpha = +1$.

The absorption experiments discussed here (^{2}H and ^{40}Ar detectors) will provide a direct measurement of the incident spectrum of high-energy neutrinos. The measured spectrum can be compared with the calculated spectra shown in Figs. 2–5, which assume nothing happens to the neutrinos from the time they are produced until they are detected. For absorption experiments, the

energy of the produced electron is essentially equal to the energy of the incident neutrino minus a constant, which makes the comparison between observed and calculated spectra particularly simple and unambiguous.

For neutrino-electron scattering, the comparison is less direct because a neutrino with a given energy can produce a broad range of recoil electrons. Since there will be significant uncertainties in both the measured energy and the scattering angle of the recoil electron, it will be much more difficult (than is the case for absorption experiments) to reconstruct the incident neutrino spectrum from the measured electron recoil energies and scattering angles. Nevertheless, important information about the incident neutrino energy spectrum can be obtained from neutrino-electron scattering experiments (see especially Sec. VI.6 and Fig. 15 of Bahcall, 1987).

1. Neutrino-electron scattering (general)

Neutrino-electron scattering experiments can be used to study the flavor content, spectrum shape, intensity, time dependence, and angular distribution of solar neutrino sources. Assuming that the energy spectra of the various neutrino sources are identical to the spectral distributions when the neutrinos are produced, Bahcall (1987) gives the predicted energy and angular dependence of the recoil electrons, as well as the total cross sections, for all of the sources considered in this paper. The modifications implied by the MSW effect are described by Bahcall, Gelb, and Rosen (1987). The results depend strongly upon the assumed threshold for the minimum electron recoil energy that is accepted. However, the *minimum* reduction that can be caused by the complete conversion of electron neutrinos to muon or tau neutrinos via the MSW effect is almost constant, about 0.15 for a 5-MeV threshold and 0.14 for a 10-MeV threshold (see Table II of Bahcall, 1987).

Table XIII displays the calculated total neutrino fluxes and their fractional uncertainties for each of the solar neutrino sources. Several solar neutrino experiments involving neutrino-electron scattering are either under way or in an advanced stage of planning. They include detectors composed of a liquid scintillator that could detect ^{7}Be neutrinos (see Mann, 1986), and ^{8}B detectors that use natural water (Bakich and Peak, 1985; Beier, 1986; Suzuki, 1986; Hirata *et al.*, 1987), heavy water (Chen, 1985; Sinclair *et al.*, 1986; Aardsma *et al.*, 1987), liquid argon (Bahcall, Baldo-Ceolin, Cline, and Rubbia, 1986), or liquid scintillators (Badino *et al.*, 1984). These experiments could, if we are lucky, reveal directly the existence of an MSW effect by showing evidence for resonance effects in the Earth (see Bahcall, Gelb, and Rosen, 1987; Hiroi, Sakuma, Yanagida, and Yoshimura, 1988).

Work has begun on two promising proposals that could ultimately lead to the direct detection of the basic *p-p* neutrinos and a test of whether the observed low-energy neutrinos have the fundamental spectrum shown in Fig. 3 and Table IV. These exceptionally interesting but difficult experiments involve the use of crystalline silicon as a low-temperature bolometer (see Cabrera, Krauss, and Wilczek, 1985; Marthoff, 1987) or superfluid helium (Lanou, Maris, and Seidel, 1987).

2. Kamiokande II

The first electron scattering experiment to yield definitive results is the Kamiokande II natural-water Cherenkov detector (see Beier, 1986; Suzuki, 1986; Hirata *et al.*, 1987a, 1987b; Totsuka, 1987). Hirata *et al.* (1987b) give an upper limit at the 90% confidence level for the flux of ^{8}B neutrinos of

$$\varphi(^{8}\mathrm{B}) \leq 3.2 \times 10^{6}\ \mathrm{cm}^{-1}\mathrm{s}^{-1}\ .$$

This upper limit is about 55% of the value calculated with the best standard solar model and is inconsistent, at the 90% confidence level, with the range of values allowed by the recognized uncertainties in the calculation of the flux (see Table XIII). The Kamiokande II result is of great importance, since up to the present time all of the observational results on solar neutrinos have come from a single experiment, the ^{37}Cl detector of Davis and his collaborators.

If the MSW effect is the correct explanation of the solar neutrino problem, then a moderate increase in sensitivity in the Kamiokande II detector should reveal a solar neutrino signal. The minimum rate expected from complete conversion of electron neutrinos to muon or tau neutrinos (see Table II of Bahcall 1987; Bahcall, Gelb, and Rosen, 1987; Hiroi, Sakuma, Yanagida, and Yoshimura, 1987) is 14% of the standard model prediction. Thus Kamiokande II should see a definite solar neutrino signal with an increase in sensitivity of no more than a factor of 3.8 of the already obtained sensitivity, provided the MSW effect is the correct explanation.

The Kamiokande experiment was originally designed as a 3-kt water Cherenkov detector in order to study proton decay. In late 1984, improvements were begun to make possible the detection of the relatively low-energy events that are expected to be produced by solar neutrinos. The upper limit quoted above results from 128 d of low-background data accumulated from December 1986 to May 1987. This detector also provided the first-ever observation of neutrinos from a supernova (Hirata *et al.*, 1987a); the supernova neutrinos happen to have energies in about the same range as those expected from solar ^{8}B neutrinos. Fortunately, Kamiokande II had been converted to a solar neutrino detector some months before the blast of neutrinos from the Large Magellanic Cloud reached the Earth. Reductions in the background rate that are in progress should lead to a much improved limit, or a detection, of the solar neutrino ^{8}B flux, perhaps in 1988.

How many electron scattering events should have occurred in the Kamiokande detector if the standard solar model were correct? The standard model predicts a few hundred per year, sufficient to obtain good statistics.

From ^{8}B neutrinos, one expects 325 events per yr for a minimum accepted recoil electron kinetic energy of 7 MeV (fiducial volume of 680 ton); for an 8-MeV threshold, one expects 190 events from ^{8}B neutrinos per yr. The number of events that would be observed in the detector must be calculated by convolving the expected spectrum of electron recoil energies (given in Table VI of Bahcall, 1987) with the detection efficiency as a function of energy. The above numbers should provide a crude approximation to the actual expected numbers, since canceling effects occur in the energy convolution. (Lower-energy electrons that can be produced by more abundant lower-energy neutrinos are mistaken for higher-energy electrons because of the finite energy resolution, and a significant fraction of all of the events near threshold are not detected.)

Unfortunately, the size of the Kamiokande II detector is not large enough to permit a robust detection of the hep neutrinos if the standard solar model is correct. The expected number of events from hep neutrinos is only 1.5 per yr for a 7-MeV threshold and 1.1 per yr for an 8-MeV threshold. In order to have, on the basis of the standard solar model, the expected event rate from hep neutrinos exceed by a factor of 3 or more, the expected event rate from ^{8}B neutrinos, the minimum value for the recoil kinetic energy of the electrons must be 14 MeV (cf. Tables II and III of Bahcall, 1987). For Kamiokande II, one expects above 14 MeV only 0.08 hep events per year.

3. ^{2}H

The ^{2}H detector is sensitive only to ^{8}B and hep neutrinos. The predicted capture rate depends upon the adopted minimum recoil energy of the electrons that are produced, although not very strongly (see Table VIII). For the plausible (Aardsma *et al.*, 1987) threshold of 5-MeV kinetic energy,

$$\sum_i \varphi_i \sigma_i = 6.01(1\pm 0.38)\ \text{SNU}\ , \tag{30}$$

of which all but 0.02 SNU comes from ^{8}B neutrinos. The calculated rate increases only by 11% when the threshold is lowered to 3 MeV.

The cross section for neutrino absorption on ^{2}H can be calculated accurately (see Sec. IV). Therefore almost all of the uncertainty in the predicted capture rate is from the 34% uncertainty in the estimated ^{8}B neutrino flux (see Tables XIII and XVI).

How many events are expected to occur in the 1-kt detector of heavy water proposed as a solar neutrino experiment by Aardsma *et al.* (1987)? Assuming nothing happens to the neutrinos on the way to the Earth from the sun and a threshold of 5 MeV, the expected rate of absorption events from ^{8}B neutrinos is

$$(\text{Rate})_{^8\text{B}}(>5\ \text{MeV}) = 1.2\times 10^4[\varphi(^8\text{B})/6\times 10^6\ \text{cm}^2\text{s}^{-1}]\ \text{events kt}^{-1}\text{yr}^{-1}\ . \tag{31}$$

For the same threshold, the number of neutrino electron scattering events is (see Bahcall, 1987) about 8.65% as large as the absorption rate, i.e., with the same assumptions approximately 1.0×10^3 scattering events should occur in the 1-kt detector per yr for the standard model flux. If a significant fraction of the higher-energy ^{8}B neutrinos reach the Earth, one could measure well with this proposed experiment the shape of the ^{8}B neutrino spectrum.

If the MSW effect converts most of the higher-energy electron neutrinos into neutrinos of a different flavor, then the main process that is observed will be neutrino-electron scattering. Assuming complete flavor conversion of all of the ^{8}B neutrinos, the expected rate is reduced to 1.5×10^2 scattering events per kt per yr (see row 4 in Table II of Bahcall, 1987, for the appropriate scattering cross section). This rate can be considered as a plausible lower limit to be expected in the proposed (Aardsma *et al.*, 1987) deuterium experiment, provided only that the standard solar model is not disastrously incorrect.

The proposed heavy-water detector can also observe neutrons from the neutral-current neutrino disintegration of the deuteron (Aardsma *et al.*, 1987): $\nu + {}^2\text{H} \rightarrow \nu + p + n$ (threshold 2.2 MeV). The cross section for this neutral-current process is independent of neutrino type. The reaction will therefore be sensitive to the total ^{8}B neutrino flux, independent of MSW or vacuum oscillation effects. The ratio of event rates for the charged-current (absorption) process and the neutral-current (disintegration) process can be a sensitive indicator of possible weak-interaction effects (Bahcall, Kubodera, and Nozawa, 1988).

Will one be able to detect unambiguously the hep neutrinos? For the standard model predictions, the answer is "yes" provided that a significant fraction of the higher-energy solar neutrinos do not change their flavor on the way to the Earth and that the measurement of the thermal neutron cross section on ^{3}He does not lead (see Sec. II.A) to a much reduced cross section for the production of these highest-energy neutrinos. Consider a threshold electron recoil energy that is sufficiently large that the expected number of events from hep neutrinos exceeds by a big factor the expected number of events from ^{8}B neutrinos. One can find such a threshold because the absorption cross sections depend sensitively, for a given neutrino energy spectrum, on the difference between the minimum accepted recoil energy and the maximum energy of the neutrino spectrum (see Table VIII); the hep neutrinos have a larger end-point energy than do the ^{8}B neutrinos (see Sec. III). For a minimum electron recoil kinetic energy of 13.5 MeV, hep neutrinos are expected to cause many more events than do ^{8}B neutrinos, assuming the thermal neutron cross section on ^{3}He shown in Table I, the neutrino fluxes from the standard model given in Table XIII, and the neutrino absorption cross sections given in Table VIII. In this relatively clean region of the recoil spectrum, we expect 10 events per kt per yr from absorption of hep neutrinos and only 2

events from the absorption of ^{8}B neutrinos.[9] Given the above assumptions, neutrino-electron scattering is expected to be too rare to be detectable in this energy range.

Suppose the standard solar model is disastrously wrong and that the flux of neutrinos from ^{8}B decay that is produced in the sun is less than the calculated value by orders of magnitude. Will one still be able to observe the hep neutrinos? Yes, if the diminution is not caused by something happening to the ^{8}B neutrinos after they are produced. About 43 absorption events and 9 scattering events with electron recoil energies above 5 MeV are calculated to occur per kt per yr in a heavy-water detector exposed to the flux of hep neutrinos given by the standard solar model. Since the hep flux is relatively insensitive to changes in the solar model (except for some nonstandard models in which the flux is much *larger*; see discussions in Secs. V, IX, and XI.H), one can be confident that a total of about 50 hep events should occur per kt per yr with electron recoil energies about 5 MeV unless MSW effects or some other weak-interaction process removes the high-energy neutrinos of electron flavor.

A Canadian-American-English collaboration has been established to carry out a solar neutrino experiment with 1 kt of D_2O that is to be placed in an INCO nickel mine near Sudbury, Ontario (see Aardsma *et al.*, 1987). Canada is the only country in the world that has sufficient surplus deuterium (due to the presently depressed market in heavy-water reactors) to make possible this experiment. The nominal 1987 cost of the deuterium is 250 million Canadian dollars. The event rates, detection efficiencies, and backgrounds in the proposed 1-kt detector have all been extensively studied and show that the proposed experiment is feasible and will provide crucial information about the energy spectrum, the distribution of flavors, and the time dependence of incident solar neutrinos. If funded promptly, this experiment could begin providing data by 1991.

4. ^{40}Ar

The ^{40}Ar detector is sensitive only to ^{8}B and hep neutrinos. The threshold energy T_{thresh} for exciting the superallowed transition that dominates the capture rate is $T_{\text{thresh}}=5.885$ MeV. For typical values of the minimum counted recoil electron energy T_{min}, the sum of $T_{\text{thresh}}+T_{\text{min}}$ is well beyond the peak, 6.4 MeV (see Table V and Fig. 4), of the energy spectrum of the ^{8}B neutrinos. The predicted capture rate therefore depends sensitively (see Table VIII) upon the adopted threshold T_{min}. For the plausible (Bahcall, Baldo-Ceolin, Cline, and Rubbia, 1986) threshold of 5-MeV kinetic energy,

$$\sum_i \varphi_i \sigma_i = 1.70(1\pm 0.38)\ \text{SNU}\ , \tag{32}$$

of which all but 0.02 SNU comes from ^{8}B neutrinos. The cross section for neutrino absorption on ^{40}Ar can be calculated accurately (see Sec. IV). Therefore almost all of the uncertainty in the predicted capture rate is from the 34% uncertainty in the estimated neutrino flux (see Tables XIII and XVI).

The predicted standard rate of absorption events from ^{8}B neutrinos is

$$(\varphi\sigma)_{^8\text{B}}(>5\ \text{MeV}) = 831[\varphi(^8\text{B})/6\times 10^6\ \text{cm}^2\,\text{s}^{-1}]\ \text{events}\,\text{kt}^{-1}\text{yr}^{-1}\ . \tag{33}$$

The absorption events will be relatively easy to distinguish from background events, since neutrino absorption will be accompanied by characteristic γ-ray deexcitation of the isobaric-analog excited state that is excited by neutrino capture (see Bahcall, Baldo-Ceolin, Cline, and Rubbia, 1986; Raghavan, 1986).

Approval has been obtained (Cline and Rubbia, 1987) for placing a 3-kt detector of liquid argon in the Gran Sasso underground laboratory in Italy. The detector is expected to begin operating sometime around 1990. If a significant fraction of the standard model flux of the higher-energy ^{8}B neutrinos reach the Earth, one could measure well with this experiment the shape of the ^{8}B neutrino spectrum.

Because of the large value of T_{thresh} for absorption events, the number of neutrino-electron scattering events exceeds the number of absorption events for most reasonable values of the minimum accepted electron recoil energy T_{min} (see Tables II and III of Bahcall, 1987, for the relevant scattering cross sections). For $T_{\text{min}}=5$ MeV, the rate of neutrino-electron scattering events is about 11% larger than the absorption rate, i.e., approximately 3×10^3 scattering events should occur in a 3-kt detector per yr. The ratio of scattering to absorption events increases rapidly with increasing T_{min}; the ratio is about 13.5 for the relatively moderate value of $T_{\text{min}}=8$ MeV.

If the MSW effect converts most of the higher-energy electron neutrinos into neutrinos of a different flavor, then the main process that is observed will be neutrino-electron scattering. Assuming complete flavor conversion of all of the ^{8}B neutrinos, the expected rate is reduced, for $T_{\text{min}}=5$ MeV, by a factor of 6.64 (see Table II of Bahcall, 1987) to about 140 scattering events per kt per yr. This value may be regarded as a plausible lower limit for the expected event rate provided that the standard solar model is not disastrously in error.

hep neutrinos will produce a unique signature in this detector. For a minimum electron recoil energy of 9 MeV, the expected number of absorptions per kt per yr is

[9]The ^{37}Cl and Kamiokande experiments show that the actual contamination by ^{8}B neutrinos will be at least a factor of 2 less than the above estimate, which is based on fluxes from the standard solar model.

3.4 from hep neutrinos and only 0.8 from ^{8}B neutrinos. Thus, one expects an observable, although not large, signal from hep neutrinos in a large liquid-argon detector provided that the highest-energy solar neutrinos do not change their flavor on the way to the Earth and that the thermal neutron cross section on ^{3}He has approximately the value assumed in Sec. II.A. Much larger event rates would be expected from nonstandard solar models in which ^{3}He is mixed into the core (cf. Bahcall, Bahcall, and Ulrich, 1968; Ezer and Cameron, 1968; Shaviv and Salpeter, 1968).

Even if the standard solar model is off by an order of magnitude or more in the flux of the rare ^{8}B neutrinos, one may still expect to observe the much less model-sensitive flux of hep neutrinos. The standard model predicts about 7 hep absorption events per kt per yr with electron recoil kinetic energies above 5 MeV.

5. ^{11}B

A ^{11}B target would provide the opportunity (see Raghavan, Pakvasa, and Brown, 1986) to perform several simultaneous experiments with ^{8}B solar neutrinos. In the same detector, one can study: neutral-current excitations to three excited nuclear states in ^{11}B; charged-current transitions to four nuclear levels in the mirror nucleus ^{11}C; and neutrino-electron scattering. The neutral-current transitions were estimated (Raghavan *et al.*, 1986) from shell-model calculations and electromagnetic excitation experiments. The charged-current transitions can determine the energy spectrum of the electron-flavor ^{8}B neutrinos. The ratios of corresponding neutral-current and charged-current transitions should indicate the relation between the spectrum of electron-flavor neutrinos and the spectrum of all neutrinos (which contribute to the neutral-current excitations). The threshold for charged-current reactions range from 2 to 7 MeV, thereby providing different samplings of the electron-flavor ^{8}B neutrino spectrum. Raghavan (1987) is studying the most likely background sources and is developing a detailed experimental design.

6. ^{115}In

The predicted capture rate for an ^{115}In detector is

$$\sum_i \varphi_i \sigma_i = 639^{+640}_{-321} \text{ SNU} . \quad (34)$$

The effective threshold energy for allowed neutrino capture is 0.119 MeV. This low threshold is reflected in the great sensitivity of ^{115}In to the *p-p* neutrinos.

The basic proton-proton reaction supplies about 73% of the capture rate predicted by the standard solar model, the largest percentage for any of the targets we have discussed in this paper. Unfortunately, the detection of *p-p* neutrinos is especially difficult for this nucleus because of an intense low-energy background (see discussion by Raghavan, 1976). However, there is a large expected signal (116 SNU), from ^{7}Be neutrinos, which produce a recoil electron with a higher energy than the most intense background. The contributions of different neutrino sources to the total capture rate are shown in the last row in Table XVII.

All of the usual astrophysical and reaction uncertainties are relatively small for an ^{115}In detector. The uncertainties from all sources other than neutrino absorption cross sections amount to only 28 SNU. The total uncertainty in the predictions is therefore dominated by the uncertainty in the neutrino absorption cross sections, which at present must be estimated with the aid of (p,n) reactions.

From a theoretical point of view, this experiment has many attractions *provided* that the absorption cross section can be accurately determined. A calibration experiment with ^{51}Cr is the most direct and potentially accurate method of determining the cross section [see Sec. IV.C and especially Eq. (7)].

Two projects are under way to develop an ^{115}In solar neutrino experiment (see Booth, Salmon, and Hukin, 1985; de Bellefon, Espigat, and Waysand, 1985; Booth, 1987).

IX. NONSTANDARD MODELS

What do measurements of the solar neutrino fluxes tell us about stellar evolution? What is really being tested by these experiments?

The best way to determine what is at stake for the theory of stellar evolution is to calculate nonstandard solar models, using different assumptions regarding the underlying astrophysical context, or to vary arbitrarily important physical quantities such as the equation of state, opacity, or nuclear reaction rates. Many of the nonstandard models have been systematically investigated and reviewed (Bahcall, Bahcall, and Ulrich, 1969; Rood, 1978; Roxburgh, 1985a, 1985b; Schatzman, 1985; Newman, 1986). Unfortunately, relatively few of the nonstandard models have been calculated with a precision equal to that used for standard models; hence, it is often difficult to determine exactly what they predict for the different solar neutrino experiments that are discussed in Sec. VIII.

We discuss in this section two classes of models for which we have calculated accurate neutrino fluxes and oscillation frequencies. We discuss first models with *ad hoc* inhomogeneities in their chemical compositions (i.e., inhomogeneities that are not due to nuclear fusion) and then describe two models with nonstandard nuclear physics.

A. *ad hoc* inhomogeneous models

In this section we consider models with specially concocted inhomogeneities in their primordial abundance distribution. We hypothesize that segregation of the elements took place while the sun formed out of the solar

nebula or as a result of diffusion during the sun's early history. The variation of chemical composition from planet to planet shows that at least some elemental segregation was possible early in the sun's life. The roles of agents and processes such as magnetic fields, cosmic-ray ionization, ambipolar diffusion, grain formation, molecule freeze-out onto grains, gravitational settling, grain coagulation, radiation pressure, and the dynamics of accretion disks in the formation of the sun are sufficiently poorly understood that we feel justified in at least calculating the effects of possible inhomogeneities.

We consider two qualitatively different types of variable composition models. In the first set of models, the heavy-element abundance Z, which is assumed to be the same at all points and at all times in the standard model, is assumed to have a smaller value in the interior than in the outer regions. In the second set of models, the primordial helium abundance is assumed to be nonuniform, larger in the interior than in the outer regions. The first set of models (variable Z) was developed as a possible solution of the solar neutrino problem (Bahcall and Ulrich, 1971), and the second set of models (variable primordial Y) was considered by Ulrich *et al.* (1983) as a possible solution of a problem in helioseismology (see Sec. X).

Models with variable Z are nonstandard because their opacities are different from those in the standard model, while models with variable primordial Y alter directly the mean molecular weight and sound speed. Although both types of variation could be present simultaneously, we consider them separately in order to isolate their principal effects. Also, in order to limit the number of free parameters, we have assumed that the abundance changes occur as step functions, which eliminates the necessity of specifying a mass increment over which the variation occurs. The discontinuity is treated numerically by inserting a pair of mass points at the same mass and by assigning the appropriate (but different) compositions to the inner and outer members of the pair. The equations of energy transport and hydrostatic equilibrium then require that the temperature and pressure be continuous across the discontinuity, while the density and entropy are different across the boundary. Dynamical stability requires that the outer density be less than or equal to the inner density.

We have evolved seven *ad hoc* inhomogeneous models, three with reduced heavy-element abundances in the interior and four with increased helium abundance in the interior. In both cases, we calculate models with the discontinuity occurring in different places in order to illustrate the sensitivity of the computed neutrino fluxes and oscillation frequencies to the location of the composition jump. The neutrino fluxes from each of these models, as well as the primordial composition parameters, are given in rows 6–12 in Table XIV. In order to maximize the differences from the standard solar model, we have assumed that the decrease in heavy elements occurs close to the base of the convective envelope and that the enhancement of helium occurs near the solar core.

Rows 6–8 in Table XIV describe the three so-called "low-Z" models for which we have artificially reduced the heavy-element abundance in the interior region of the sun. The values of Y and Z given in Table XIV are the assumed primordial values in the solar interior, we have continued to use the Grevesse value (see Sec. II.B) for Z/X in the outer regions. For the model labeled $Z1$, the discontinuity in composition was introduced at $0.559R_\odot$; the discontinuities for $Z2$ and $Z3$ were introduced at $0.664R_\odot$ and $0.682R_\odot$, respectively. The reduction of heavy elements alters the model structure primarily through the change in the heavy-element opacity. Hence the maximum effect on the central temperature and neutrino flux is achieved by placing the composition jump as near to the solar surface as possible so that the opacity is reduced throughout the radiative regions. In the following section, we shall present the oscillation frequencies computed from these models.

Rows 9–12 in Table XIV give the neutrino fluxes and composition parameters for four models that we have evolved with an inhomogeneous primordial helium and hydrogen composition. Each of the models had an initial helium abundance that was enhanced by 0.025 (and a hydrogen abundance that was decreased by the corresponding amount) for a specified fraction of the interior mass of the sun. For the models labeled $Y1$ through $Y4$ in Table XIV, the fraction of the mass in which the initial helium abundance was enhanced was, respectively, $0.05M_\odot$, $0.10M_\odot$, $0.20M_\odot$, and $0.40M_\odot$.

Table XVIII presents, for all seven of the inhomogeneous models discussed above, the expected capture rates in each of the experiments discussed in the previous section. The low-Z models reduce the calculated capture rate in the ^{37}Cl experiment to a value that is approximately consistent with observation, i.e., ~ 1.5 SNU. The "high-Y" models increase the capture rate for the ^{37}Cl experiment by 0.1 to 1 SNU, giving a calculated rate between 8.3 SNU and 9.2 SNU.

B. Models with different nuclear physics

If the rare reaction that produces ^{8}B neutrinos, number 9 in Table I, did not occur for some unknown reason, the predicted capture rate for the ^{37}Cl experiment would be 1.8 SNU (see next to last column in Table XVIII), in agreement with observation. It is of interest therefore to record what this "very nonstandard" nuclear physics hypothesis would yield for other detectors; the results are shown in the next to last column in Table XVIII. Unfortunately, the calculated capture rates for this nonstandard nuclear physics hypothesis are degenerate, within the expected experimental uncertainties, with the rates predicted using some of the possible MSW parameters.

What happens to the calculated p-mode oscillation frequencies if we artificially change the overall energy generation significantly? We have answered this question by

constructing a solar model in which the rate of the important $^3He + {}^4He$ reaction (number 6 in Table I) is set equal to zero ($S_{3,4}=0$). For the standard solar model, about 15% of the terminations of the *p-p* chain proceed through this reaction. Therefore the calculated solar structure is significantly altered from what is obtained with the standard parameters, unlike the previously considered "No ^8B model." The result calculated for $S_{3,4}=0$ is a significantly different temperature and density profile for this nonstandard model.

Table XIV, next to last row, gives the calculated neutrino fluxes for the $S_{3,4}=0$ model, and the last column in Table XVIII gives the calculated event rates in different detectors. For five of the seven detectors listed in Table XVIII, the predicted event rate is reduced by more than an order of magnitude; solar neutrino astronomy would be very much more difficult were this nonphysical hypothesis correct. However, we show in Sec. X.F that the *p*-mode frequencies calculated for this model are not significantly different from those evaluated for the standard solar model.

C. WIMP's

Weakly interacting massive particles (WIMP's) have been proposed as a simultaneous solution to the missing mass problem and to the solar neutrino problem (see, for example, Press and Spergel, 1985; Faulkner and Gilliland, 1985; Spergel and Press, 1985). If exotic weakly interacting particles make up the galactic missing mass, then they can modify the energy transport in the solar core in just such a way as to reduce the calculated capture rate to the value observed for ^{37}Cl, provided that the scattering cross section and the mass for the WIMP's are chosen to lie in an appropriate range (see Faulkner and Gilliland, 1985; Spergel and Press, 1985; Gould, 1987). There are difficulties in making this scenario consistent with any already discovered particle, but various authors have discussed new particles that might satisfy the required conditions (e.g., Gelmini, Hall, and Lin, 1987; Raby and West, 1987; Griest and Seckel, 1987).

There is not yet available a definitive calculation of the predicted neutrino fluxes if WIMP's are the correct solution of the solar neutrino problem. However, Gilliland, Faulker, Press, and Spergel (1986) have estimated the expected neutrino fluxes using reaction rates from Fowler, Caughlan, and Zimmerman (1975), the equation of state of Eggleton, Faulkner, and Flannery (1973), and opacities from Cox and Steward (1970). Without performing a detailed *ab initio* calculation, we cannot rigorously correct the calculated fluxes of Gilliland *et al.* (1986) to take account of all the improvements since the 1970s in reaction rates, opacities, and equation of state.

However, we have estimated the neutrino fluxes to be expected on the WIMP hypothesis by assuming that, for each neutrino source, the ratio of the flux on the WIMP hypothesis to our best estimate for the flux on the standard model is the same as the ratio of WIMP to standard fluxes calculated by Gilliland *et al.* (1986). Explicitly, we assume $\varphi_{\rm WIMP}(i)/\varphi_{\rm Best}(i)=\varphi_{{\rm WIMP},G}(i)/\varphi_{{\rm standard},G}$, where the subscript G stands for Gilliland *et al.* (1986).

The neutrino fluxes determined by scaling in the above-described fashion are listed in the last row in Table XIV. The important flux of ^8B neutrinos should be given reasonably accurately by this procedure, since it depends most strongly upon the cross section for the rare (p,γ) reaction on ^7Be, which does not affect the structure of the sun. The fluxes of *p-p* and pep neutrinos are also probably well determined since they differ by only 2% and 7%, respectively, in the WIMP and standard models. The flux of ^7Be neutrinos is probably not very well determined; it is about 20% higher in the standard model than in the WIMP model. The CNO fluxes cannot be reliably evaluated by the scaling procedure we have used; their neutrino fluxes are about a factor of 2 larger for the standard model than for the WIMP model. Fortunately, the CNO neutrinos are not crucial for any of the experiments we discuss here.

The calculated capture rates for different solar neutrino experiments are given in the last column in Table XVIII. They illustrate the expected trends. The main result is that the flux of ^8B neutrinos is reduced by about a factor of 4 relative to the standard model; this reduction decreases by about the same factor the calculated capture rate for electron-neutrino scattering and for ^2H, ^{40}Ar, ^{81}Br, and ^{98}Mo detectors. The reduction is about a factor of 2 for a ^7Li detector and almost a factor of 3 for ^{37}Cl. For ^{71}Ga the reduction is only about 25% and is even smaller for an ^{115}In detector.

The WIMP hypothesis can be tuned so that it reduces the ^8B neutrino flux by a factor of 4 or by almost any desired reduction factor that may be indicated by the observations. Unfortunately, Gilliland *et al.* gave individual neutrino fluxes for only one set of WIMP parameters. The basic results that are likely to be relatively invariant to future improvements in the solar model and in the choice of WIMP parameters are the relative lack of change in the *p-p* flux from the standard to the WIMP model (only 2.5%; cf. columns 2 and 12 in Table XVIII) and, to within a factor of order 2, the ratio of ^7Be to ^8B flux (about 2.4×10^3 with the assumed input nuclear physics parameters).

D. Temperature dependence of the ^8B and *p-p* neutrino fluxes

The local rate of production of ^8B neutrinos is a sensitive function of temperature; Flux $\propto T^{\alpha}$, where $\alpha\simeq 13$ at the center of the sun. The total flux of neutrinos from the sun is an integral over the entire temperature and density profile and depends also upon the nuclear reaction cross sections. Very approximately, the ^8B neutrino flux is proportional to $(S_{pp}\times S_{34}^2\times S_{17}^2/S_{33}\times S_{e,7}^2)^{1/2}$. The S factors in the above expression correspond, in order of appearance, to reactions 1, 6, 9, 5, and 7 in Table I. Since the temperature dependence is strong, one may

write the total rate of ^{8}B neutrino production in the following suggestive form:

$$\varphi(^8\mathrm{B}) \approx \mathrm{const} \times T^{\beta} . \tag{35a}$$

Figure 11(a) shows the relation between ^{8}B neutrino flux and central temperature for the 1000 solar models that are described in Sec. VII. With $\beta \sim 18$, Eq. (35a) describes well the relation between temperature and ^{8}B neutrino flux for the models we have calculated. *If one assumes that nothing happens to the neutrinos from the time they are produced until they are observed on Earth and that the nuclear cross sections are reasonably well known, then a measurement of the ^{8}B neutrino flux will determine the central temperature of the sun to an accuracy of about a percent or better.*

The *p-p* neutrino flux is much less sensitive to temperature. Figure 11(b) shows the relation between the *p-p* neutrino flux and the central temperature for the 1000 solar models in Sec. VII. The band of points in Fig. 11(b) is well described by the equation

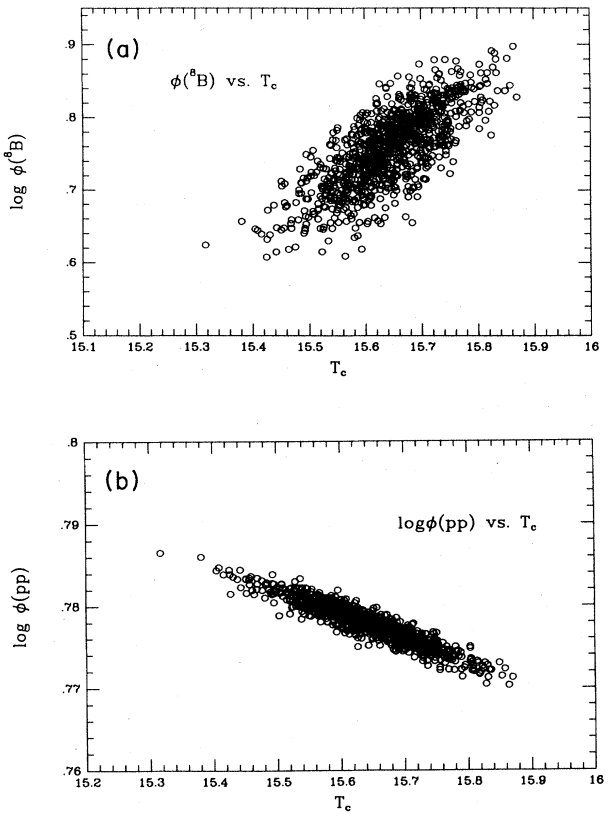

FIG. 11. Temperature dependence of the ^{8}B and *p-p* neutrino fluxes. (a) Logarithm of the calculated ^{8}B neutrino flux shown as a function of central temperature for the 1000 solar models that are discussed in Sec. VII; for this figure, the temperature is given in units of 10^6 K and the flux in units of 10^6 cm^{-2} s^{-1}. (b) Logarithm of the *p-p* neutrino flux displayed as a function of central temperature for the same 1000 solar models; for this figure, the flux is expressed in units of 10^{10} cm^{-2} s^{-1}; the unit of temperature is the same as for (a).

$$\varphi(p\text{-}p) \approx \mathrm{const} \times T^{\alpha} , \tag{35b}$$

where $\alpha \simeq -1.2$. Note that the *p-p* neutrino flux decreases with increasing temperature, contrary to naive expectation. The reason for this nonintuitive behavior is that as the temperature increases a greater fraction of the terminations of the *p-p* chain occurs via the ^{3}He-^{4}He reaction (which produces only one *p-p* neutrino) and a smaller fraction occurs via the ^{3}He-^{3}He reaction (which requires two *p-p* neutrinos).

The reader should keep in mind that each of the models used in constructing Fig. 11 is the end result of solving a complicated set of coupled differential equations with boundary conditions in space and in time that describe the physical evolution of the sun (see Sec. V.A), together with many input parameters. The iterated solar model that satisfies the boundary conditions and the initial physical assumptions yields a complete temperature and density profile of the solar interior. The central temperature is *not* an adjustable parameter; it is a by-product. We have used the central temperature in plotting Fig. 11 only for simplicity. We could have plotted the ^{8}B neutrino flux versus, for example, the average temperature in the inner 10% of the solar mass or versus the temperature at $0.05R_{\odot}$, where the rate of generation of ^{8}B neutrinos peaks (see Sec. V.C).

X. HELIOSEISMOLOGY

Helioseismology, like terrestrial seismology, provides information about the interior of the body under study by using observations of very slight motions on the surface. The method is analogous to striking a bell and using the frequencies of the emitted sound to make inferences about the bell's constitution. Leighton, Noyes, and Simon (1962) first discovered solar oscillations by studying the velocity shifts in absorption lines formed in the solar surface. To their surprise, they found—instead of the anticipated purely chaotic motions—that the surface of the sun is filled with patches that oscillate intermittently with periods of the order of 5 min and velocity amplitudes of order 0.5 km s^{-1}. The oscillatory motion was subsequently detected in measurements of the solar intensity. The oscillations typically persist for several periods with a spatial coherence of order a few percent of the solar diameter.

The correct explanation for the observed solar motions was a long time in coming. We now know (Ulrich, 1970; Leibacher and Stein, 1971) that the sun acts as a resonant cavity. Sound waves that are excited in its interior are largely trapped between the solar surface and the lower boundary of the convection zone. The observed motions result from the superposition of several million resonant modes with different periods and horizontal wave lengths. Individual modes may have velocity amplitudes of as much as 20 cm s^{-1} and vertical excursions of as large as 1 or 2 m.

In order for a mode to resonate in the solar acoustic

cavity, an integral number of waves must fit along the path leading from the solar surface to the base of the cavity. The depth of the cavity is fixed by the condition that horizontal wave number equal the total wave number (i.e., the vertical wave number becomes equal to zero), at which point the wave is refracted back towards the surface. The vertical wave number decreases with increasing depth in the sun because the temperature rises in the inner regions. For many of the waves that have been most intensively studied, the base of the resonant cavity is close to the base of the convective zone.

For a given horizontal wavelength only certain periods will correspond to a resonance in the solar cavity. It was therefore predicted (Ulrich, 1970) and subsequently observed (Deubner, 1975; Rhodes, Ulrich, and Simon, 1977) that the strongest solar oscillations fall in a series of narrow bands when the results are displayed in a two-dimensional power spectrum that shows amplitude as a function of both period and horizontal wavelength. Just as in a musical instrument, the largest amplitudes correspond to standing waves that experience constructive interference at the boundaries of the cavity. The simplest example is an oscillating organ pipe. The information about the conditions in the cavity (in the sun or in the organ pipe) is contained in the observed frequency spectrum, since the rate of propagation depends upon the physical conditions of the medium in which the wave travels. However, unlike most musical instruments with which we are familiar, the sun oscillates in three dimensions, giving rise to an especially rich spectrum of tones or frequencies. These frequencies provide information about the temperature and density distribution within the sun and its chemical composition. Solar rotation breaks the symmetry between otherwise degenerate modes and enables observers and theorists working together to make important inferences about the rate at which interior regions of the sun are rotating.

Observations by Claverie *et al.* (1979) and by Grec, Fossat, and Pomerantz (1980), which utilized the integrated light from the entire solar disk, showed that the oscillations are globally coherent. The modes observed by these techniques provide the most important information currently available for the study of the deep solar interior, since they penetrate most deeply toward the solar center (see discussion below).

What causes the excitation and the damping of solar oscillations? This question is difficult to answer both theoretically and observationally. Fortunately for us, the growth and decay of the modes is not particularly important for the purposes of this paper. We need only to assume that frequencies are not significantly influenced by the damping or excitation processes. The stability of the oscillations sets a limit on the precision of the helioseismological constraints that we can impose on solar models. Present observations indicate that the frequencies of the oscillations can be measured to an accuracy of about two parts in ten thousand, which provides very strong constraints. Indeed, some of the earliest detailed observational results led to the conclusion that the depth of the solar convection zone was deeper than previously believed (Gough, 1977; Rhodes, Ulrich, and Simon, 1977). We show in this paper (see especially Sec. X.E and Fig. 20) that the available observations require still further revisions in the calculations.

In this paper, *we focus on the relation between the oscillation frequencies and the neutrino fluxes.*

We describe in this section the state of the art of helioseismological calculations and observations. We begin in Sec. X.A with a general review of the method: theory and observation. More detailed reviews of the method have been given by Deubner and Gough (1984), Leibacher *et al.* (1985), Christensen-Dalsgaard, Gough, and Toomre (1985), and Toomre (1986). We pay particular attention to the form of the equation used to represent the dependence of the p-mode frequencies upon the principal quantum numbers, n and l [see especially Eq. (40)] and derive expressions relating the parameters we use to the parameters that appear in the asymptotic expressions. In our calculations, we avoid many of the uncertainties, present in some other treatments, by calculating the eigenfrequencies directly from solar models that include a full treatment of the atmospheric zones and without invoking asymptotic approximations. In order to focus on information about the solar interior, we discuss the technique of differential helioseismology and apply the method to the frequency separation between the $l=0$ and the $l=2$ modes in Secs. X.B and X.C. Section X.B describes the physical reasons why the frequency separation between the $l=0$ and the $l=2$ modes [δ_{02}; see Eq. (41), note also that δ_{02} is unrelated to the Kronecker delta] is expected to be relatively insensitive to surface uncertainties and summarizes briefly the observational results. We use in Sec. X.C the kernel-function approach of Backus and Gilbert (1967) to illustrate semiquantitatively the sensitivity of the computed eigenfrequencies to variations in the solar model. This study provides added justification for the expectation that the separation δ_{02} should not be strongly influenced by surface uncertainties. We describe in Sec. X.D the two separate codes that we have developed: SUNEV (primarily for solar interior calculations) and CATMOS (primarily for helioseismological calculations). Table XIX shows a quantitative comparison of the two models. The neutrino fluxes calculated from the two codes are in excellent agreement. In Sec. X.E, we compare with the observational results the eigenfrequencies that are calculated from different standard models. Table XX summarizes the comparisons. The calculations represent well the general features of the measured frequency spectrum; the observed and predicted frequencies agree to an accuracy of order 0.5%. However, there are small but persistent discrepancies; the most serious pertains to the frequency splitting δ_{02}, for which the observations yield 9.45 ± 0.25 μHz and the calculations give about 10.6 μHz (out of a total of about 3×10^3 μHz). We discuss in Sec. X.F models with nonstandard physics. We show that even a dras-

tic modification of the nuclear energy generation will not lead to measurable changes in the predicted p-mode eigenfrequencies [see row 8 in Table XX below and Eq. (54)]. This result illustrates the complementarity of solar neutrino experiments and helioseismology. Finally, we show in Sec. X.G that models with an inhomogeneous helium abundance are potentially capable of resolving the discrepancies between the measured and computed values of δ_{02} without significantly affecting the predicted neutrino fluxes.

A. The method

Helioseismology consists in the comparison of the observed frequencies of oscillation of the solar surface with the frequencies computed using a model of the solar interior and surface. Progress in determining the solar conditions is achieved by refining the model in order to match more closely the observed frequencies. The modes that have been unambiguously detected are confined to the range of periods near 5 minutes. The restoring force in this frequency range is the compressibility of the gas. The observed p modes correspond to standing acoustic oscillations.

The sensitivity of a given eigenmode to the properties of the solar interior depends upon the amplitude of the mode at the position of interest. For the 5-min (pressure) modes, this amplitude is much larger in the surface layers than in the interior. Therefore the information that these oscillations contain about the interior layers where the neutrinos are produced is contaminated by effects from the surface.

For simplicity, we shall concentrate on perturbations with a high degree of symmetry; however, we recognize that some observed properties of the sun do not have a high degree of symmetry. For example, the density of magnetic fibrils of the type discussed by Bogdan and Zweibel (1985) could be concentrated in regions of solar activity that have a preferred latitude and possibly even a preferred longitude. Significant asymmetries of this type could cause the overlap integral between the perturbation and the modes of different angular dependences to yield a larger frequency shift for the mode that has a greater fraction of its amplitude in the region of the perturbation. Our limited knowledge of the character of such asymmetric effects makes it difficult to set rigorous upper limits to the potential size of the resulting frequency shifts.

Important constraints on the magnitude of asymmetric perturbations can be obtained from the fact that such perturbations break the degeneracy in the azimuthal quantum number. The resulting multiple frequencies are potentially observable, and their absence could be used to set upper limits on the size of the perturbations. Gough (1982) has discussed inhomogeneities of this kind and has applied constraints derived from the absence of observed splittings to the question of a large internal dipole magnetic field. A similar discussion is needed for the inhomogeneities that result from convection, fibrils, and other complicated phenomena that are observed near the solar surface.

The modes in the 5-min band that provide the most information about the central regions of the sun are those which propagate closest to the solar core, and those in turn are most nearly spherically symmetric [see Eq. (49) and the following discussion]. These central-peaking modes correspond to the lowest-degree spherical harmonics and have been observed by full, and nearly full, solar disk techniques by Claverie *et al.* (1979, 1981). Grec, Fossat, and Pomerantz (1980), and Henning and Scherrer (1986). Because the global acoustic modes are propagating in a nearly vertical direction at the solar surface, and because the vertical wavelength is small compared to the solar radius, near the solar surface the amplitude as a function of depth is primarily a function of frequency rather than spherical harmonic degree. Consequently surface effects can be partially canceled, and properties of the deep interior can be deduced in principle by studying differences between modes of similar frequencies.

There are two related fundamental questions that we have to address. What are the frequencies, or frequency differences, that are least affected by poorly understood surface physics like convection or turbulence? How big are the surface effects in the optimal cases? In what follows, we suggest reasons why the frequency difference δ_{02} given in Eq. (41) below may be a particularly useful quantity to study in order to obtain information about the solar interior.

The gravity modes could provide more direct information about the regions of nuclear energy generation, since they are confined below the convection zone and in fact have amplitudes that reach their maxima in the inner 10% of the solar radius. Unfortunately, observations of these modes are not yet in a state that would allow us to infer reliably the properties of the solar interior.

There has been an emphasis in the published literature on parameters that have their basis in analytic approximations: The asymptotic expressions derived by Tassoul (1980) and Vandakurov (1967), and popularized by Christensen-Dalsgaard and Gough, have been the focus of many discussions. We start, following Gough (1984), from the following result:

$$\nu_{n,l}=\nu_0\left[n+\frac{l}{2}+\varepsilon\right]-\nu_0\left[\frac{\alpha l(l+1)-\beta}{n+\frac{l}{2}+\varepsilon}\right], \qquad (36)$$

where $\nu_{n,l}$ is the frequency of the nth eigenmode that is described by the spherical harmonic $Y_l^m(\theta,\varphi)$, and the various quantities on the right-hand side of Eq. (36) are adjustable parameters, except for the quantum numbers l and n. The form of Eq. (36) constrains the dependence of the frequencies upon the quantum numbers, but permits, for all of the modes, the adjustment of the zero point, slope, and curvature of the relationship between $\nu_{n,l}$ and n. Once the overall parameters are specified, the l depen-

dence of the zero point, slope, and curvature are determined. The use of Eq. (36) may therefore discard valuable information contained in the observations about the l dependence. This information is potentially valuable since, for the high-n, low-l modes, the value of l strongly influences the depth of penetration into the solar core. We have developed a fitting procedure [see Eq. (40) below] that retains a significant amount of the observational information regarding the l dependence.

Scherrer *et al.* (1983) have used the following fitting formula:

$$\nu_{n,l}=\nu_{00}-l(l+1)D_0 +[\Delta\nu_0+l(l+1)d_0]\left[n+\frac{l}{2}-n_0\right] . \quad (37)$$

Equation (37) can be obtained by expanding Eq. (36) about an arbitrary fiducial point for n (denoted by n_0) and retaining only those terms that are linear in n. The quantity ν_{00} in Eq. (37) and below is an offset frequency that is close to $\nu_{n_0,0}$. The l dependence of the slope of $\nu_{n,l}$ with n is also retained from Eq. (36). Equation (37) has the advantage that the differences between pairs of frequencies are closely related to the fitting parameters. For example, frequencies for successive values of n at fixed l are separated by approximately $\Delta\nu_0$. An often used approximate relation between the structural characteristics of the solar model and ν_0 is

$$\nu_0=\left[2\int_0^{R_\odot}\frac{dr}{c}\right]^{-1} , \quad (38)$$

where c is the sound speed. Note that ν_0 and $\Delta\nu_0$ are close numerically but differ as is described below [see Eq. (42)]. The fitting parameter D_0 is related approximately to the differences between nearly degenerate frequencies at l and $l+2$ by

$$D_0\simeq(\nu_{n,l}-\nu_{n-1,l+2})/(4l+6) . \quad (39)$$

Although the asymptotic expressions and various fitting parameters are useful for understanding what is being measured and in explaining the major features of the solar spectrum, there are four significant problems with this approach.

First, the formulas are not exact and the values of the fitting parameters depend on the way they are derived from the data. For example, the curvature in the ν vs n relationship at fixed l implies that the values of ν_0 and $\Delta\nu_0$ depend on the range of n used to make the determination. An inaccurate representation of the l dependence can cause similar problems. Second, when the form of the n or l dependence deviates from the observed dependence, the systematic mismatch increases the formal rms error in the derived fitting parameters and obscures the estimate of the errors of measurement. Consequently one loses the possibility of estimating objectively the errors of measurement from the size of the rms deviation. Third, the higher-order terms contain information about the solar interior that is unavailable if these terms are neglected. Fourth, the integral formula in Eq. (38) is difficult to cut off at the solar surface. The solar atmosphere and chromosphere is 2000 km thick and has a sound speed of roughly 7 km s^{-1}. Consequently this region contributes about 8% to the integral in the denominator. If the integral is cut off at the temperature minimum, the contribution between $\tau=\frac{2}{3}$ and $\tau=0.001$ is only 1.5%, but the resulting value of ν_0 is larger than the exact value obtained by the eigenfrequency calculation by about 2%. Consequently, *quantitative use of Eq. (38) is ambiguous.*

In order to base our conclusions on comparisons that are only weakly dependent on the choice of mode frequencies, we fit the frequencies *at each* l to a polynomial in n. If the lower-order frequencies are not included in the fit (i.e., we retain only $n>15$), a parabolic fit of ν vs n is adequate to represent the data to within the observational uncertainty quoted by Pallé *et al.* (1987). We use the form

$$\nu_{n,l}=\nu_{0l}+\Delta\nu_l(n-n_0)+a_l(n-n_0)^2 , \quad (40)$$

where n_0 is a reference value of n that we have taken to be $18-l/2$ with $l/2$ truncated to the next lowest integer. The formula given in Eq. (40) includes the quadratic dependence of $\nu_{n,l}$ on n from Eq. (36) and *permits the fitting coefficients to be determined independently for each* l. The quantities ν_{0l} and $\Delta\nu_l$ depend on the choice of n_0 in a way that can be calculated explicitly from Eq. (40). If the fit is good, the exact range of n values included in the fit will not influence the derived coefficients. This expectation has been verified by numerical tests with both simulated and actual observational data.

The parameter ν_{0l} plays a role similar to the frequency itself but, because it depends on several individual frequencies, it has a smaller rms error than any single measurement or calculation. The difference of two offset values ν_{0l} for $l=0$ and 2 is

$$\delta_{02}=\nu_{00}-\nu_{02} , \quad (41)$$

which is essentially 6 times D_0.

For any particular value of l, the relationship between the fitting coefficients and the parameters in Eq. (36) can be derived by a straightforward expansion of Eq. (36). Note that ν_0 and ν_{0l} are distinct quantities: ν_0 is the fitting parameter from Eq. (36), which is similar to a frequency spacing interval. In contrast ν_{0l} is the zero-point frequency in Eq. (40) and $\Delta\nu_l$ is similar to ν_0. As long as $|a_l|<\Delta\nu_l^2/\nu_{0l}$ then it can be shown that ν_0, $\delta\nu_l$, ν_{0l}, and a_l are related by the following quadratic equation:

$$\nu_0^2-\Delta\nu_l\nu_0-a_l\nu_{0l}=0 , \quad (42)$$

and a_l is given by

$$\nu_{0l}^3 a_l=-\nu_{0l}^4[\alpha l(l+1)-\beta] . \quad (43)$$

Equation (43) can be used to derive β from the fit to $l=0$, and Eq. (42) gives ν_0 from $\Delta\nu_l$, ν_{0l}, and a_l. The value of

ε is found from

$$\varepsilon=\frac{\nu_{0l}}{\nu_0}-n_0 \ , \tag{44}$$

and the value of α can be calculated from

$$\alpha=(\nu_{n-1,l+2}-\nu_{n,l})\frac{n+\frac{l}{2}+\varepsilon}{(4l+6)\nu_0} \ . \tag{45}$$

The parameter D_0 is related to α by

$$D_0=\frac{\alpha\nu_{n,l}}{n+\frac{l}{2}+\varepsilon} \ . \tag{46}$$

These expressions exhibit the l dependence of the fitting parameters of Eq. (36), and it will be seen in the discussion of both the observational and theoretical results below that the actual l dependence deviates from that expected according to Eq. (36) by amounts that are large compared to the uncertainties. The particular predictions we examine are

$$\Delta\nu_2-\Delta\nu_0=-\delta_{02}/(n_0+\varepsilon) \tag{47}$$

and

$$a_2-a_0=\delta_{02}/(n_0+\varepsilon)^2 \ . \tag{48}$$

In our calculations, we avoid the uncertain influence of the surface region on the *integral* expression for ν_0 that is given in Eq. (37) because we calculate the eigenfrequencies directly from the model, without making use of the approximate integral. However, the chromospheric layer does introduce a second resonant cavity, which makes possible an independent set of eigenfrequencies. When there is an accidental degeneracy between the frequencies of these two cavities, the interior frequencies are altered by observable amounts. The frequency pulling that results in the numerical calculations can be large. We use an automated procedure, based on the deviation from the fitting curves described above, to detect and delete these greatly perturbed frequencies.

How can we extract the significant parameters from the large number of frequency measurements? This is a major problem. Without a careful analysis, it is not clear which quantities contain significant information about the solar interior and which are only redundant or reflect primarily surface conditions.

Because of the large number of observed frequencies, there are many possible combinations in addition to those represented by the asymptotic expressions and in addition to the coefficients in Eq. (40). Some linear combinations of the frequencies are redundant with other linear combinations. Our object is to select the largest possible set of linearly independent combinations of frequencies and to evaluate the significance of the resulting quantities. The spectral analysis method of seismology as described by Parker (1977) provides a mechanism for carrying out this task. The significance of such trends in the data should be evaluated in an objective manner based on the errors in the frequency measurements and a comparison to theoretically derived trends. A complete global analysis of the solar frequencies will be discussed by Korzennik and Ulrich (1988).

Differential helioseismology, i.e., examining frequency differences rather than individual frequencies, is an important method for trying to isolate the effects of structure in the solar interior from the influence of the solar surface. Although the individual frequencies of two modes are usually difficult or impossible to calculate to the accuracy with which they are measured, for some pairs of modes the frequencies of each mode are expected to respond in similar ways to uncertain conditions near the solar surface. For such pairs, the frequency differences will contain relatively clear information about the solar interior. The following sections focus on the frequency differences between the $l=0$ and $l=2$ modes because the differential technique seems to be particularly illuminating for this case. The success of the argument depends on establishing three points: (1) the sensitivity of each frequency to local changes in the properties of the solar interior is proportional to the mode amplitude at that point; (2) appropriately selected pairs of modes have nearly identical amplitudes as a function of depth in the outer regions, so that the frequency difference is insensitive to surface phenomena; and (3) the predicted low sensitivity of the frequency differences to surface phenomena is exhibited by direct numerical calculations of standard solar models. The first of these points has been made plausible by Backus and Gilbert (1967), with rather general approximations, and will not be discussed further here. The second point is discussed for the case of δ_{02} in the next two sections; the results given in Sec. X.D. provide the numerical justification of the third point.

B. The separation between the $l=0$ and $l=2$ mode frequencies

The parameter D_0 [of Eq. (39)] represents the separations between the $l=0$ and $l=2$ mode frequencies [of Eq. (40)] and is sensitive to the gradients at the solar core. The observed frequency difference corresponding to D_0 is often quoted as 9.3 μ Hz and the theoretical value as 10.4 μ Hz. In fact, the observations from the Tenerife-Hawaii network reported by Pallé *et al.* (1987) show that this separation varies from 9.9 μ Hz for $n=15$ to 8.9 μ Hz for $n=28$. We discuss in this section the significance of this discrepancy and its trend with n.

The frequency separation δ_{02} [of Eq. (41), $\delta_{0,2}\approx 6D_0$] is relatively insensitive to surface uncertainties. Therefore the observed discrepancy between the results of the standard solar model and observations has often been taken to require some modification of the computed interior characteristics. This result is counter to what one might expect for modes in the 5-min band, since these modes spend the largest fraction of their travel time near the surface. Consequently the 5-min modes are more sensi-

tive to surface than to interior effects.

The local dispersion relation for the waves, in combination with the kernel-function theory of the next section, provides a framework for understanding why the δ_{02} combination is relatively independent of the solar outer structure. Each oscillation mode is described by an angular frequency ω and a vertical wave number k_v. The dispersion relationship between these quantities is

$$k_v^2=(\omega^2-\omega_0^2)c^{-2}-\frac{l(l+1)}{r^2}\left[\frac{N^2}{\omega^2}-1\right], \tag{49}$$

where r is the distance from the center of the sun, ω_0 is the acoustic cutoff frequency $c/2H$ (H is the density scale height), and N is the Brunt-Vaisala frequency. The turning point for the modes occurs at the depth for which $k_v=0$, which is at a radius $r\approx c[l(l+1)]^{1/2}/\omega$.

According to the variational analysis of Backus and Gilbert (1967), a change in a local quantity such as the sound speed alters the frequency of a mode by an amount proportional to the amplitude of the mode at that location. This proportionality is governed by the kernel functions, which are discussed in greater detail in the next subsection. The key result that is obtained from the kernel theory is that two modes will respond to localized perturbations of the model in the same way as long as their amplitude as a function of depth is similar. The modes obey the same outer boundary condition and remain in spatial phase as long as they have the same k_v. According to Eq. (49), the quantities that differ for the $l=0$ and the $l=2$ modes are the angular frequency ω and the horizontal structure, which is governed by $l(l+1)$. Near the solar surface, the vertical wave number is of order 2×10^{-8} cm^{-1}, while $[l(l+1)/r^2]^{1/2}$ is 3.5×10^{-11} cm^{-1} for $l=2$. Observationally, the difference in frequency between the $l=0$ and $l=2$ modes is only 10 μHz out of 3000 μHz. The combination of the differences from horizontal structure and angular frequency produces a spatial phase shift between the structure of the two sets of modes which is only a fraction of a percent per vertical wavelength. Less quantitatively, the angle of propagation between the mode that goes directly to the center of the sun ($l=0$) and the mode that misses the center ($l=2$) is small and, if we are fortunate, may not cause the mode structure to differ significantly near the solar surface.

It is plausible that the effect of the vertical spatial phase shift can be further reduced by combining several modes. Successive modes with a fixed l have an increasing number of nodes. Consequently the maxima of one mode tend to fall near the nodes of the next mode, and the average of several modes will depend on the model structure more smoothly than for any individual mode.

The effects described above reduce the sensitivity of δ_{02} to surface effects. On the other hand, p modes spend most of their travel time near the surface, which magnifies the importance of the outer regions. The combination of all these effects can be discussed quantitatively using the kernel-function theory. The key question is whether any of the many uncertainties in the modal analysis theory associated with the complicated physics of convection, magnetic fields, inhomogeneities, and surface activity can modify δ_{02} without making the agreement between theory and observation of ν_{00} substantially worse. In order to make progress at this stage, we are forced to assume that eigenmodes are described by linearly independent spherical harmonic eigenfunctions. We know observationally that inhomogeneities and anisotropies are present at the solar surface, but we cannot calculate how much they affect δ_{02}.

With the reservations described above, the frequency separation between the $l=0$ and the $l=2$ modes provides an important test of solar models (interior plus surface). The result is a strong hint that our present quantitative description requires improvement.

C. The kernel-function approach

We can understand semiquantitatively the sensitivity of the eigenfrequencies to solar model variations with the aid of the kernel functions derived by Backus and Gilbert (1967) using a variational analysis of the equations of motion. This approach does not provide an adequate tool by itself for the understanding of errors in the solar model because it does not incorporate the constraints from the equations of solar structure. In particular, the equations of energy transport and conservation are not included in the formalism. Some of the changes in the structure of the solar model that can be derived directly from the Backus and Gilbert approach will not be compatible with the energy equations. Nonetheless, the kernel functions are useful as a guide, and future extensions of the variational theory may make it possible to incorporate the energy constraints.

The dependence of the frequencies on the sound speed can be written in terms of the kernel functions as follows:

$$\frac{\delta\nu_{n,l}}{\nu_{n,l}}=\int_0^{R_\odot}K_{n,l}(r)\left[\frac{\delta c}{c}\right]dr\ . \tag{50}$$

The dimensionless kernel function $K_{n,l}$ is the logarithmic partial derivative of the frequency with respect to the fractional change in the sound velocity, $\delta c/c$ and is related to K^1 in Eq. (54) of Backus and Gilbert (1967), Appendix B by $K_{n,l}(r)=K^1/\rho r^2\omega^2$. A density term has been dropped from Eq. (50), since the present discussion is intended only to be illustrative. We can exhibit the sensitivity of the frequency separation δ_{02} to model variations by forming a difference of the kernel functions $K_{n,0}-K_{n,2}$. Since the coefficients ν_{00}, ν_{02}, and δ_{02} all depend on a range of n (in practice, typically between 15 and 30), we average the kernel difference over this same range of n and define $\langle K\rangle_0$ and $\Delta\langle K\rangle_{02}$ as

$$\langle K\rangle_0=(n_2-n_1+1)^{-1}\sum_{n=n_1}^{n_2}K_{n,0}\ , \tag{51}$$

$$\Delta\langle K\rangle_{02}=(n_2-n_1+1)^{-1}\sum_{n=n_1}^{n_2}(K_{n,0}-K_{n,2})\ , \qquad (52)$$

where n_1 and n_2 are the lower and upper limits on the n range.

Figures 12 and 13 display the dependencies of $\langle K\rangle_0$ and $\Delta\langle K\rangle_{02}$ on r. It is clear from these figures that the model values of δ_{02} are primarily dependent on gradients near the solar center, while ν_{00} depends mostly on the properties of the surface. However, even in the case of δ_{02}, there does appear to be some sensitivity to the structure in the outer layers.

Can δ_{02} be adjusted without at the same time introducing excessively large changes in ν_{00}? We examine the ratio $\langle K\rangle_0/\Delta\langle K\rangle_{02}$ in order to answer this question. The ratio gives the partial derivative $\partial\nu_{00}/\partial\delta_{02}$ that is caused by a local change in the sound speed when the model is held constant elsewhere. The smoothing effect of averaging over several modes has reduced but not eliminated the ripples in the two functions. Since $\Delta\langle K\rangle_{02}$ changes sign, the partial derivative would have many divergences if we were to look at sound speed changes in too small a zone of the sun. In order to avoid such divergences, which would only strengthen our argument, we first integrate $\langle K\rangle_0$ and $\Delta\langle K\rangle_{02}$ over a finite zone which we have taken as $0.1R_\odot$ and then calculate the ratio.

Figure 14 gives the resulting partial derivatives as a function of $r/R_\odot$. The kernel functions that relate $\nu_{n,l}$ to ρ yield qualitatively similar results.

We can now restrict the regions of the model that might be responsible for the discrepancy in δ_{02}. Since the discrepancy between calculation and observation in ν_{00} is approximately 10 μHz (or $\sim 0.5\%$), we can only permit changes in this quantity of the same order of magnitude before the agreement will be substantially worsened. If a model change is to produce a 1-μHz ($\sim 10\%$) change in δ_{02} subject to this restriction, then—according to Fig. 14—the zone involved must be inside of $r=0.3R_\odot$.

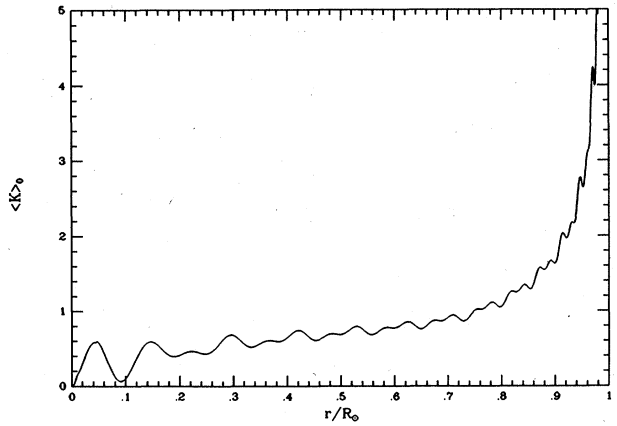

FIG. 12. The kernel-function average $\langle K\rangle_0$ vs radius. This kernel function illustrates the sensitivity of the zero-point frequency ν_{00} to localized changes in the sound speed.

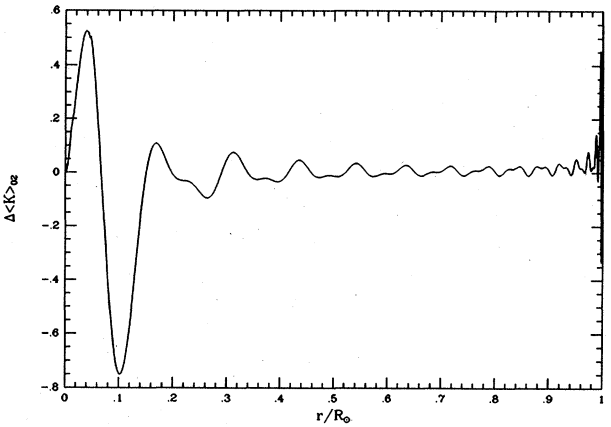

FIG. 13. The difference in kernel functions for $l=0$ and 2 as a function of radius. This kernel function difference illustrates the sensitivity of δ_{02} to localized changes in sound speed.

Since the neutrino fluxes are produced in the innermost part of this region, the resolution of the discrepancy may alter the predictions of the neutrino fluxes.

The hypothesis that WIMP's increase the conduction of energy near the solar core does alter the calculated neutrino fluxes, as has been discussed by Faulkner, Gough, and Vahia (1986) and by Däppen, Gilliland, and Christensen-Dalsgaard (1986). We show in Sec. X.F. below that an alternate hypothesis of inhomogeneous initial distribution of helium (see also Sec. IX.A) can also resolve the δ_{02} problem without significantly altering the predictions of ν_{00} or the neutrino fluxes.

D. Model computations

As outlined in a recent series of papers (Ulrich and Rhodes, 1983; Ulrich, 1986; Popper and Ulrich, 1986),

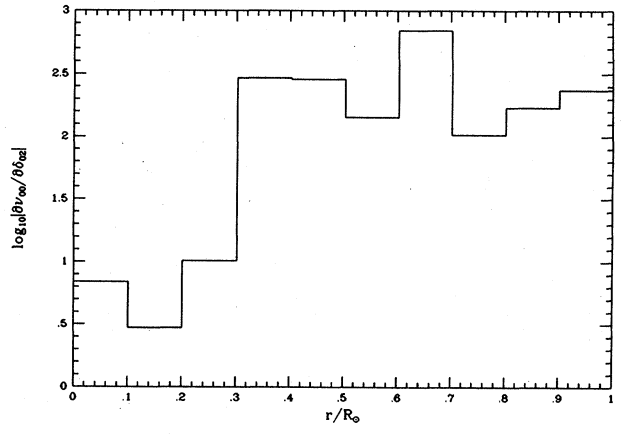

FIG. 14. Ratio of the averaged kernel function in Fig. 12 to the difference in kernel functions in Fig. 13 as a function of radius. This function illustrates the relative effect a change in the model will have on ν_{00} and δ_{02}.

the calculation of eigenfrequencies is based on a sequence of two models. The first model is constructed using a code, SUNEV, which treats the solar interior accurately and which yields the physical characteristics and neutrino fluxes given in Sec. V and Tables X–XII. This code describes the nuclear evolution in detail (see paper I) but replaces the surface zone with a grid of model atmospheres that is represented by an interpolation formula. The grid was computed in the early 1970s and is based on an earlier version of the present atmosphere code. Although this approach is inadequate for the calculation of seismological frequencies, it does provide a representation of the surface zone that is sufficiently accurate for the computation of solar neutrino fluxes.[10] The second model used a code, CATMOS, that takes the nuclear abundances and gravitational energy generation as a function of mass from SUNEV and calculates a detailed envelope structure. CATMOS carries the integration to the solar center and represents the innermost zone by fitting the lowest-order expansion of the central regular solution onto the numerical model.

The two codes are substantially independent of each other and share only the opacity lookup subroutine and parts of the nuclear energy production code. Thus, a comparison of their output illustrates the sensitivity of the calculated neutrino fluxes to the details of the numerical method. Unfortunately, the SUNEV models are inadequate for the purpose of computing seismological eigenfrequencies, so that we cannot carry out a similar exercise for the frequencies of the oscillations.

The basic physical functions, equation of state, opacity, and nuclear energy generation are similar but not identical in the two codes. The equation of state in CATMOS is more detailed than in SUNEV; the CATMOS equation of state includes partial ionization of 13 elements and molecule formation at low temperatures. SUNEV treats only the partial ionization of hydrogen and helium and enforces full ionization at high temperatures with the Planck-Larkin formalism. Both codes include the Debye-Huckel treatment of the electrostatic corrections, and both codes include the second Virial coefficient treatment of the collective effects according to Ebeling and Sandig (1973). The opacity tables at high temperature are identical for the two codes, while CATMOS includes low-temperature tables from Vardya (1964). The two sets of formulas for nuclear energy generation and cross-section factors are identical, but the abundance of ^{3}He in CATMOS is not carried over from SUNEV. In CATMOS, the ^{3}He reaction sequence is assumed to be in steady state. The CNO cycle approach to steady state is difficult to treat without a detailed time-dependent calculation but because of the need to apply the CNO correction to the opacity the time dependence cannot be ignored. We have adopted the following procedure: The ratios X_{12}/X_{14} and X_{16}/X_{14} are passed from SUNEV to CATMOS. The steady-state values of these ratios are calculated by CATMOS. If the SUNEV ratios differ from the CATMOS steady-state values by less than 10%, then the CATMOS value is adopted. If the SUNEV ratio exceeds the steady-state ratio by more than 50%, the SUNEV ratio is adopted. In between these fiducial values a linear interpolation is used.

The distribution of zoning is different in the two codes. CATMOS uses 250 points to represent the zone omitted from SUNEV, which encompases the outermost 8% of the sun. SUNEV uses a fourth-order accuracy integration scheme with 90 points for the inner 30% of the radius where the temperatures are above 5×10^6 K, while CATMOS has roughly the same number of points for the same region but uses a numerical scheme with second-order accuracy. In the section between the outermost zone of SUNEV and the beginning of the inner zone, SUNEV has only 15 points, while CATMOS uses 150. The interpolation formula used by SUNEV represents the physical parameters computed explicitly by CATMOS to within a few percent at the first point. Due to the different zoning in the two modes and the more detailed equation of state in CATMOS, the physical variables computed with SUNEV and CATMOS differ slightly and reach a maximum difference of 6% in density and pressure at a temperature of 2×10^6 K. The temperature as a function of radius agrees between the two models to within 0.5% for all points interior to 1×10^6 K. Quantitative comparisons of the models computed using the two codes are shown in Table XIX.

The most noticeable difference between the two models is in the central temperature, which is about 1.5% higher in CATMOS than in SUNEV. This difference is largely a reflection of the less obvious but equally important discrepancy between the two calculations of the mass as a function of the radius. CATMOS has a slightly higher included mass at each radius and, since the composition is assumed to be a function of $M(r)$, the abundance of hydrogen is systematically too large by a fraction of a percent. The iteration that is required to achieve the correct luminosity adjusts X by adding a constant increment to all mass points. The increment used by CATMOS to match the SUNEV model was $-0.003\,70$. The change in the central temperature goes in the direction to equalize the rate of nuclear energy production at the centers of the two models.

The rates of neutrino production for the CATMOS model are compared in Table XIV with the rates calculated using SUNEV (see rows 5 and 15 in Table XIV).

[10]Contrary to the comments of Cahen *et al.* (1986), it has been known for two decades that the solar neutrino fluxes are insensitive to variations of the solar surface parameters (see Sears, 1964; Bahcall and Shaviv, 1968). We present at the end of this section additional quantitative evidence that the calculated solar neutrino fluxes are insensitive to assumed properties of the solar surface; the fluxes calculated by two independent codes with different techniques agree to of order 2% (see rows 5 and 15 in Table XIV).

TABLE XIX. Comparison between two solar model codes. The characteristics of the SUNEV model are given on the top row of each entry and the characteristics of the CATMOS model are given on the bottom row of each entry.

r ($R_\odot$)	M ($M_\odot$)	T (10^6 °K)	ρ (gm cm^{-3})	P (dyn cm^{-2})
0.9204	0.9990	0.451	0.0151	8.95E 11
	0.9992	0.468	0.0149	9.09E 11
0.8420	0.9949	1.026	0.0525	7.16E 12
	0.9953	1.043	0.0497	6.88E 12
0.7254	0.9803	2.095	0.155	4.33E 13
	0.9816	2.101	0.145	4.08E 13
0.5054	0.9000	3.883	1.25	6.50E 14
	0.9004	3.861	1.22	6.29E 14
0.3349	0.6900	6.084	8.27	6.75E 15
	0.6967	6.072	8.22	6.70E 15
0.2212	0.4000	8.708	28.7	3.35E 16
	0.4054	8.724	28.9	3.38E 16
0.1145	0.1039	12.49	76.8	1.18E 17
	0.1055	12.57	77.9	1.21E 17
0.0000	0.0000	15.62	149	2.31E 17
	0.0000	15.85	150	2.37E 17

The neutrino fluxes calculated with SUNEV and CATMOS agree to within 2% or better for all of the fluxes except the CNO sources (for which nonequilibrium effects are important; see discussion above). *This excellent agreement, particularly for the difficult to calculate ^8B and ^7Be neutrino fluxes, gives us additional confidence that the answers are independent of the numerical procedures to the desired accuracy of a few percent.*

E. Standard models and comparison with observations

Table XX gives the principal results of our calculations of oscillation frequencies. The results given in the table for pressure oscillations have been limited to the $l=0$ and $l=2$ modes alone. The discussion of kernel functions given in Sec. X.B shows that these particular modes provide the most direct test of the solar interior that is available from solar oscillations in the 5-min band. We have verified by extensive calculations of the frequencies of other modes that model results for the higher l values are also consistent with the general trend of the data.

Although there have been suggestions that the longer-period gravity modes have been tentatively detected (Delasche and Scherrer, 1983), the interpretation of the measured frequencies is complicated by the combination of the complexity of the spectrum and the window function introduced by the diurnal observing pattern. As an indication of the sensitivity of the gravity modes to various model parameters, we include in Table XX the asymptotic gravity mode factor P_0 (see Christensen-Dalsgaard *et al.*, 1985, and references therein):

$$P_0 = 2\pi^2 \left[\int_0^{r_c} N \frac{dr}{r} \right]^{-1}, \tag{53}$$

where N is the buoyancy frequency and r_c is the radius at the base of the convection zone. Here $P_0/[l(l+1)]^{1/2}$ gives the approximately uniform period interval for the gravity modes.

For the modes in the 5-min band, a least-squares fit has been made using the form given in Eq. (40) for modes with $13 < n < 30$ and $n_0 = 18$. All the observational entries in Table XX have been derived from published or calculated frequencies in a uniform manner. In addition to the fitting coefficients, we give below each entry the derived standard error (square root of the variance) of the coefficient. This variance is partly a result of random variation about the fitting line (especially for the observations) and partly a result of the inadequacy of the fitting form. Although higher-order terms could be derived for the theoretical models, the observations do not contain enough information to permit a useful comparison with additional coefficients. Therefore we have limited the power series to the terms indicated in Eq. (40).

Table XX is divided into four sections. Entries 1–3 represent observations; entries 4–7 give properties of the sequence of standard solar models corresponding to rows

1, 2, 4 and 5 in Table XIV (Sec. V); entry 8 is a model developed to illustrate the complementarity of helioseismology and solar neutrino astronomy (see row 14 in Table XIV, the last column in Table XVIII, and Sec. IX.B); entries 9 and 10 were calculated to test the sensitivity of the p-mode oscillations to changes in the equation of state (see Sec. X.F.2 below); and the subsequent entries are for a series of models with inhomogene-

TABLE XX. Frequencies and frequency separations. For each entry, the numerical values for the coefficients are given in the top line and the variances are given in the second line. The units are μHz, except for the g-mode period P_0, which is given in minutes.

No. Case	P_0	ν_{00}	δ_{02}	$\Delta\nu_0$	$\Delta\nu_0 - \Delta\nu_2$	a_0	$a_0 - a_2$
1. Grec *et al.*(1983)		2630.457	9.445	134.433	−0.355	0.123	0.062
		0.430	0.462	0.129	0.145	0.025	0.026
2. Woodard(1984)		2629.751	9.871	134.653	−0.227	0.051	0.010
		0.422	0.476	0.330	0.373	0.053	0.028
3. Pallé *et al.*(1987)		2630.020	9.455	134.310	−0.101	0.112	−0.001
		0.200	0.252	0.064	0.088	0.009	0.011
4. Paper I	37.334	2615.728	10.515	134.326	−0.284	0.184	0.006
		0.150	0.228	0.048	0.082	0.007	0.010
5. New S	36.972	2616.341	10.430	134.303	−0.288	0.183	0.006
		0.147	0.222	0.047	0.080	0.007	0.010
6. All New	37.864	2619.264	10.438	134.442	−0.269	0.181	0.0004
		0.159	0.232	0.051	0.083	0.007	0.010
7. CNO Cor	37.661	2618.679	10.576	134.482	−0.284	0.182	0.004
		0.159	0.237	0.051	0.086	0.007	0.011
8. S34=0	37.750	2616.044	10.540	134.375	−0.266	0.186	0.007
		0.151	0.230	0.048	0.083	0.007	0.010
9. $P_{coul}=2\times P_{coul}$	37.046	2621.458	10.210	134.631	−0.333	0.195	0.011
		0.167	0.266	0.053	0.097	0.007	0.012
10. $P_{coul}=2\times P_{coul}$ for $T < 2\times 10^6$ °K	38.205	2617.484	10.371	134.532	−0.293	0.191	0.008
		0.182	0.278	0.058	0.100	0.008	0.012
11. Low Z1	40.328	2629.814	11.639	134.995	−0.461	0.196	0.023
		0.136	0.201	0.043	0.072	0.006	0.009
12. Low Z2	41.119	2613.678	12.028	134.576	−0.463	0.205	0.023
		0.151	0.240	0.048	0.087	0.007	0.011
13. Low Z3	40.559	2603.641	12.093	134.265	−0.431	0.202	0.020
		0.186	0.285	0.057	0.102	0.008	0.013
14. X down 0.025 for $M<0.05\ M_\odot$	36.902	2620.111	10.153	134.416	−0.301	0.181	0.005
		0.157	0.233	0.050	0.084	0.007	0.010
15. X down 0.025 for $M<0.10\ M_\odot$	37.162	2620.574	9.873	134.389	−0.329	0.184	0.008
		0.152	0.227	0.048	0.082	0.007	0.010
16. X down 0.025 for $M<0.20\ M_\odot$	36.042	2621.776	9.639	134.490	−0.282	0.186	0.013
		0.149	0.219	0.047	0.078	0.007	0.010
17. X down 0.025 for $M<0.40\ M_\odot$	37.298	2642.092	10.187	134.517	−0.229	0.181	−0.003
		0.131	0.196	0.042	0.071	0.006	0.009

ous initial chemical compositions (rows 11–17 in Table XX correspond to rows 6–12 in Table XIV). The entries in the first section give the fitting coefficients derived from the observations reported by Grec, Fossat, and Pomerantz (1983), Woodard (1984), and Pallé *et al.* (1987), respectively. We concentrate in the subsequent discussion on a comparison to the recent results of Pallé *et al.* (1987), which represent an improvement in precision over earlier observations.

The sequence of standard models in Table XX includes four models summarized in Table XIV, namely, paper I, NewS, AllNew, and CNO Cor. As described in Sec. X.D, these models are not identical to those used to derive the neutrino fluxes, since they have all been computed with CATMOS. The first solar model, designated as paper I, corresponds approximately to the computational procedure and parameters used in paper I.

We summarize in Fig. 15 the comparison between our best model, CNO Cor, and the most precise available frequencies, those of Pallé *et al.* (1987) in an echelle format diagram. We use the same format for this figure as has been adopted by many observer groups in order to facilitate comparison to observed results. This format diagram is similar to the way in which an echelle spectrograph displays a spectrum. With high-resolution data the full spectrum cannot be displayed in a single band, since that would either require a larger horizontal distance than is available or excessively narrow spectral bins. The problem is solved by cutting the spectrum into regularly spaced sections and displaying them one above the next. In the case of the solar oscillation spectrum this technique is especially effective, since the pattern of frequencies is regularly spaced. In fact, if the quadratic terms were absent and the spectral cutting interval were matched to the frequency spacing, we would find vertical lines on the echelle diagram. For the real spectrum the quadratic terms introduce curvature. The starting frequency for the regular sectioning of the spectrum is also arbitrary and can be selected in order to avoid interfering with the regularly spaced observed and calculated patterns formed by the different values of l. We have chosen the starting frequency, $\nu_{\rm start}$, and cutting interval, $\Delta\nu_{\rm cut}$, to be consistent with the figure given by Pallé *et al.* (1987). The echelle diagram then consists of a series of spectral sections beginning on the left with

$$\nu_{\rm cut}=k\,\Delta\nu_{\rm cut}+\nu_{\rm start}\ .$$

Here k is the integer rounded down from $(n+1+l/2)$. The abscissa for each section is $\nu_{\rm offset}=\nu-\nu_{\rm cut}$. In a true echelle spectral display, we would use the spectral energy density as the vertical axis. In fact, we simply mark the location of the identified spectral peaks on each horizontal section of this diagram and label the scale of the vertical axis with $\nu_{\rm cut}$. We have used $\Delta\nu_{\rm cut}=135.5$ μHz and $\nu_{\rm start}=28.5$ μHz. The X symbols represent individual measured frequencies and the □ symbols represent individual theoretical frequencies. The solid and dashed lines are the polynomial fits to the observed and theoretical frequencies, respectively.

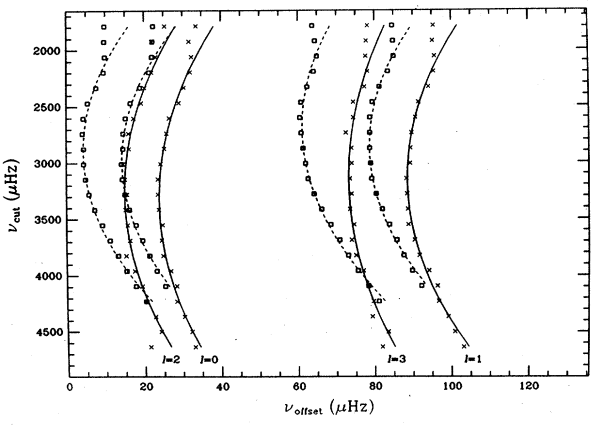

FIG. 15. Echelle diagram of the observed and theoretical frequencies of the solar oscillation spectrum. The high-resolution spectrum in the 5-min band has been cut into regularly spaced horizontal sections, which are displayed in successive strips that are displaced vertically from each other: ×, frequencies of observed power spectrum peaks from Pallé *et al.* (1987); □, theoretical frequencies for the CNO Cor model of this paper. The vertial axis gives the values of the cutting frequencies $\nu_{\rm cut}$, while the horizontal axis gives the offset frequency $\nu_{\rm offset}$.

The calculations represent well the quantitative features of the frequency spectrum. However, there are discrepancies between the calculated and the observed frequencies. For example, the small ($\sim$0.5%) but apparent discrepancy between the calculated and observed value of ν_{00} is not resolved by the various improvements in the physics. The general trend of the disagreements is evident both in the numerical values given in Table XX and in Fig. 15. The combined error in ν_{00} and in $\Delta\nu_0$ results in the mismatch in the lower-n frequencies. Ulrich and Rhodes (1983) showed that changes in the surface properties can alter ν_{00} and $\Delta\nu_0$ in such a way that the higher n frequency mismatch is improved but not the lower n frequency mismatch. The discrepancy in a_0 is not striking in Table XX but is evident in Fig. 15, where the curvature of the trend with n for all l clearly differs between the theory and observation. Perhaps the most significant discrepancy is the slightly larger than 3σ discrepancy between calculation and observation for the δ_{02} combination. Relative to the formal error, the discrepancy for ν_{00} is larger. However, ν_{00} is sensitive to the details of the model calculation, whereas the analysis of kernel functions in Sec. IX.B suggests that we should regard the δ_{02} problem as more revealing.

An examination of Table XX shows that the predictions of the asymptotic formula of Eq. (36), as represented by Eqs. (47) and (48), are not well met by either the observed or theoretical fits. The pattern of results seems to be different for the chemically inhomogeneous models, and we anticipate that the presence of such an inhomogeneity could well invalidate the asymptotic assumptions. Thus we concentrate on the comparison of the predic-

tions of Eqs. (47) and (48) to the observations of Pallé *et al.* (1987), which have small errors of measurement, and to models 4–7. The value of ε determined from Eqs. (42) to (44) is in the range of 0.6 to 1.3, so that $n_0+\varepsilon$ is about 18.6 to 19.3. Consequently Eq. (47) predicts a slope change of about -0.52 μHz, whereas the actual value is -0.1 for the observations and about -0.28 for the models. Since the error in the determination of this fitting parameter is only 0.08 μHz, the discrepancy is significant just at the 3σ level. The prediction from Eq. (48) that the curvature changes by 0.027 μHz is different from the actual results, which are between -0.001 and 0.006 μHz. However, the error in the determination of this paper is relatively larger, about 0.01 μHz, so that the discrepancy is slightly less than 3σ significant. The combined effect of these two discrepancies is that a strict fit of the asymptotic formula to both the theoretical and observational results would result in an artificial increase in the variance of the fitting parameters.

F. Models with nonstandard physics

In order to test the sensitivity of the fitting coefficients to the potential areas of uncertainty, we have computed several nonstandard solar models, which are listed in the third section of Table XX. All models in this subsection use the same parameters and physics as those for AllNew except where explicitly indicated otherwise. Some previous work (Ulrich and Rhodes, 1984; Korzennik and Ulrich, 1988) has shown that likely variations in the sound speed or the radiative opacity cannot explain the observed discrepancies.

1. Nuclear energy generation

Suppose we make a change in the rate of nuclear energy generation. Will this affect the computed oscillation frequencies? Certainly *not* if we just eliminate the ^{7}Be-p reaction (number 9) in Table I. As shown in Table XVIII (next to last column), this change would reduce the predicted rate for the ^{37}Cl experiment from 8 SNU to 2 SNU and would cause the predicted rates in the ^{2}H, ^{40}Ar, and ^{98}Mo experiments to be effectively zero. It would have a catastrophic effect on most future solar neutrino experiments, but would leave the overall nuclear energy generation essentially unaffected and would not change within believable accuracy the computed stellar structure variables.

We have made instead a hypothetical *drastic* change in the nuclear energy generation: we have set the cross section for the ^{3}He-^{4}He reaction (reaction 6 in Table I) equal to zero. This results in a model with no ^{8}B and ^{7}Be neutrino fluxes (see next to last row in Table XIV). The predicted solar neutrino capture rates are reduced by an order of magnitude for five of the seven experiments discussed in Sec. VIII (see last column in Table XVIII). The structure of the sun is also affected, since approximately 15% of the energy generated in the standard solar model involves this reaction.

The p-mode frequencies are insensitive to even this drastic change in nuclear energy generation. Let $\Delta\nu$ be the characteristic difference in frequencies caused by switching off the ^{3}He-^{4}He reaction (and all the higher-energy neutrino fluxes); then we find (see row 8 in Table XX) that

$$\frac{\Delta\nu}{\nu_{\text{standard}}} \lesssim 10^{-4} . \tag{54}$$

The g-mode frequencies exhibit a small sensitivity ($\sim$0.2%) to the hypothetical change in nuclear energy generation. The interior structure of the solar model is affected significantly by this change in nuclear energy generation. In particular, the central hydrogen abundance is increased by 10%, and the central ^{3}He abundance by 54%, relative to the standard solar model. The central pressure is increased by 3%. These fractional changes in central quantities are more than 2 orders of magnitude larger than the fractional changes in the p-mode oscillation frequencies [see Eq. (54)]. *This numerical experiment demonstrates the complementarity of the neutrino flux measurements and seismic analysis.*

2. Equation of state

Does the equation of state affect the computed oscillation frequencies? The thermodynamics of the solar medium is well described as an ideal gas with small corrections. The largest of the corrections is due to the Coulomb interaction, whose leading term is given by the Debye-Huckel formula. This term, as a fraction of the ideal gas pressure, depends on $(\rho/T^3)^{1/2}$, which in the convective envelope increases toward the surface and is only cut off by the onset of neutrality. An error in the treatment of this interaction could change the model structure in the outer regions of the sun. In order to test the sensitivity of the computed oscillation frequencies to this outer solar regime, we have artificially multiplied the Debye-Huckel correction by a factor of 2. The resulting frequencies are given in row 9 in Table XX: they are changed slightly from the standard model, but only by rather small fractions of the discrepancies.

We have carried out an additional test in which the factor-of-2 increment in the Coulomb term was restricted to regions in the convective zone and above that have $T<2.0\times10^6$ K. We explore in this way whether changes in the equation of state of solar surface alone can affect the computed frequencies. The resulting coefficients are given in row 10 in Table XX; the changes are again small. We conclude that the p-mode frequencies are insensitive to changes in the equation of state of the type we have considered.

G. Models with inhomogeneous initial composition

The calculated frequencies for the low-Z models discussed in Sec. X.A are in worse agreement with the ob-

served p-mode oscillation frequencies than are the values obtained with the standard solar model (see rows 11–13 in Table XX). The low-Z models could in principle "solve the solar neutrino problem" (see Table XIV, rows 6–8, and Table XVIII, columns 3–5), but they exacerbate the discrepancy for δ_{02}. For the low-Z models, the difference between observed and calculated values of δ_{02} is about 2 μHz, compared to about 1 μHz for the standard model. We conclude that the low-Z models are unlikely to be correct (see also Gough, 1981).

We have found one change in the physics that does affect the computed frequencies in the desired direction, namely, models with a primordial gradient in the helium abundance. We present these results in the spirit of an existence theorem which shows that the small (but significant) discrepancies between the computed and observed frequencies can be removed by changes in the physics that do not affect very much the calculated neutrino fluxes. The models we discuss here were introduced in Sec. IX.A, where we presented their neutrino fluxes and predicted event rates in solar neutrino experiments.

For specificity and simplicity, we have increased the abundance of helium by 0.025 in mass fraction (Y) for all regions of a variable core mass. In order to minimize the number of free parameters, we have assumed that the abundance follows a step function across the core boundary; a discontinuity of this type could result if the boundary represented the maximum extent of a convection zone. We required that the mean molecular weight always increase inward, since a zone with heavy matter above is unstable against doubly diffusive motions.

Rows 14–17 in Table XX give the frequency coefficients resulting from models with core masses of 0.05, 0.1, 0.2, and 0.4 $M_\odot$. The smallest core does not modify the frequencies enough to be interesting. The intermediate cases, however, do decrease the discrepancy in both ν_{00} and in δ_{02}. In effect, these models make the sun appear to be older than the known age of 4.6×10^9 yr. When the core becomes large, the constraint that the model match the solar luminosity and radius causes the frequencies to match those of the standard model. The rise of the frequency splitting for the $0.4M_\odot$ model (last line in Table XX) is a result of this effect.

According to Table XIV, the calculated ^{8}B neutrino flux is *increased* by of order 15% by the change in primordial helium abundance; the ^{7}Be flux is increased by of order 10%. We conclude that changes in the interior structure of the sun sufficient to account for the observed p-mode oscillation frequencies may change the predicted neutrino fluxes by amounts that are smaller than the uncertainties discussed in Sec. VI.

XI. SUMMARY AND CONCLUSIONS

We list here some of the principal results and conclusions of this article.

A. Parameter uncertainties

The most important parameter uncertainty for the solar neutrino problem is the value of the low-energy cross-section factor for the ^{7}Be+p reaction, a situation that has prevailed for about two decades (see the historical summary by Bahcall and Davis, 1982). The calculated counting rates for most of the proposed solar neutrino experiments discussed in Sec. VI are proportional, or approximately proportional, to the rate of this crucial reaction. The recognized uncertainty in the cross-section factor for the ^{7}Be+p reaction is about 22% (see Sec. II.A), our best estimate having decreased by 16% from the value we used in 1982 (paper I). With more than a decade and a half of careful work on this reaction (see Parker, 1986) as a basis for further refinements, it is important to perform additional laboratory experiments that are designed to fix even more firmly the absolute limits on the low-energy cross section.

The cross section for the ^{3}He+p reaction is important for calculating the number of high-energy neutrinos that may be observable in experiments that measure individual electron recoil energies. The crucial quantity that is required for this calculation is the capture cross section for thermal neutrons incident on ^{3}He (see Tegner and Bargholtz, 1983). The existing measurements are not sufficient for making a realistic 3σ error estimate (see Sec. II.A).

The fractional uncertainty in the heavy-element-to-hydrogen ratio is about 20%, which corresponds to the largest single uncertainty in the ^{37}Cl and a number of other experiments (see Table XVI).

A new systematic investigation of radiative opacities is urgently needed for the astrophysically relevant regimes. By comparing the new opacities with the Los Alamos opacities (which have provided the fundamental astronomical standard for more than two decades), one could make a more informed estimate of the true theoretical uncertainties. In the absence of a systematic reinvestigation, we have made several improvements in the radiative opacities that we use in our codes (see Sec. II.C and Appendix B). These include (1) an explicit calculation of the conversion of carbon and oxygen to nitrogen as a result of nuclear burning during the evolution of the sun; (2) a more accurate treatment of electron scattering; (3) more recent abundance determinations; and (4) a more precise numerical representation of the calculated opacities. Each of the improvements listed above increases the calculated ^{8}B neutrino flux, the largest change being the 28% increase caused by the new measured heavy-element-to-hydrogen ratio. Table XVI shows the uncertainties in event rates in different experiments that are caused by separate parameter uncertainties.

B. Neutrino spectra

The energy spectrum of neutrinos reaching us from the sun contains information both about the nuclear process-

es occurring in the solar interior and about the effects of weak interactions in changing the spectrum. If the solar neutrino problem is caused by something wrong with the standard solar model, then the shapes of the energy spectra from the individual sources listed in Sec. III should remain the same; only the number of neutrinos from one or more sources will have changed. On the other hand, most (but not all) currently popular explanations of the problem in terms of weak-interaction physics lead to significant changes in the shapes of the individual energy spectra from each of the sources.

Thus the shape of the measured energy spectrum will provide a crucial diagnostic of the solar interior and of weak-interaction physics. The ^{2}H, ^{40}Ar, and neutrino-electron scattering experiments will provide direct information on the spectrum of the ^{8}B neutrinos that reach the Earth.

Figure 2 shows the overall neutrino spectrum calculated with the aid of the standard solar model, "Best," that is discussed in Sec. V. Figures 3–5 illustrate the shapes of the individual energy spectra that are expected from the experimentally most accessible continuum sources: *p-p*, ^{8}B, and hep neutrinos. Because measurements of the spectra can provide fundamental tests of the solar models and weak-interaction physics, we also present in Tables IV–VI numerical representations of the normalized energy distributions of neutrinos produced by the *p-p*, ^{8}B, and hep sources.

Figure 8 shows where the *p-p*, ^{8}B, ^{7}Be, and hep neutrino fluxes originate in the sun. Fortunately, electron scattering, ^{2}H, and ^{40}Ar detectors can distinguish (see Sec. VIII) between the ^{8}B and the hep neutrinos, permitting one experiment to explore two different regions of the solar interior (one largely inside and one largely outside the volume where the energy production peaks; see Fig. 6).

C. Neutrino absorption cross sections

The rate at which events occur in a neutrino detector is proportional to the summed product of interaction cross sections times neutrino fluxes. Thus uncertainties in the detector cross sections are as important as, and sometimes more important than, the more publicized uncertainties in the predicted fluxes obtained with solar models. Unfortunately, this fact has sometimes been ignored and the anticipated results of solar neutrino experiments have been discussed without considering the errors in absorption cross sections. We have tried to remedy this situation by providing a full discussion in Sec. IV.B of the uncertainties involved in calculations of neutrino absorption cross sections. We discuss in Sec. IV.B.1 the general procedures for determining the uncertainties in the absorption cross sections and give in Sec. IV.B.2 the uncertainties that we have calculated for each source incident on each detector.

We have recalculated more accurate neutrino absorption cross sections for all of the targets for which experiments are currently being actively developed or are in progress. The main results are presented in Sec. IV.A and in Tables VII–IX. We have determined best estimates and uncertainties for the cross sections of neutrinos detectors made of targets with ^{2}H, ^{7}Li, ^{37}Cl, ^{40}Ar, ^{71}Ga, ^{81}Br, ^{98}Mo, and ^{115}In. For the last three detectors, the neutrino absorption cross sections are more uncertain, in our opinion, than the neutrino fluxes calculated from the standard solar models.

The cross sections averaged over the appropriate solar neutrino energy spectra are given in Tables VII and VIII. These values can be used for calculating the expected event rates for all nonstandard solar models, since changes in the solar physics affect the number of neutrinos of different types but not the shapes of the neutrino fluxes from each source.

We present in Table IX the cross sections as a function of incident neutrino energy in order that readers can make their own calculations of what is expected if weak-interaction effects cause the spectra to be different from the standard shapes shown in Figs. 2–5. The associated uncertainties can be inferred in most cases from the information given in Sec. IV.B, since the fractional uncertainties in the cross section for a given source are, to a satisfactory approximation in most instances, independent of the exact shape of the assumed spectrum. The cross sections given in Table IX are also useful in estimating the detectability of supernovae or other astronomical neutrino sources.

We discuss in Sec. IV.C the possibility of calibrating the ^{71}Ga, ^{81}Br, and ^{115}In detectors with the aid of an intense radioactive source of ^{51}Cr. The relevant absorption cross sections and their estimated theoretical uncertainties are displayed in Eqs. (5)–(7). For an ^{115}In detector, a laboratory calibration experiment would be very informative and is, in fact, necessary in order to reduce the uncertainties in the capture rate to a level that is comparable to the uncertainties in the neutrino fluxes calculated with the standard solar model. Laboratory calibration of the ^{71}Ga and ^{81}Br detectors will not reduce significantly the cross section uncertainties if the spectrum of incident neutrinos has the standard shape given in Fig. 2, but would be important if the high-energy neutrinos are significantly depleted.

A number of authors have discussed the possibility of calibrating the detector sensitivities of the ^{37}Cl and ^{71}Ga experiments with the aid of neutrinos from a stopped muon beam (see references in Sec. IV.D). We show in Sec. IV.D that calibrations with a muon beam can determine the overall performance of neutrino detectors to an accuracy of order 2, but unfortunately not to the desired accuracy of 10%. The main uncertainties are caused by forbidden corrections to allowed transitions and by forbidden transitions from the ground states of the target nuclei to various excited states in the daughter nuclei.

D. Standard model

Section V contains a description of the standard solar model. Figure 6 and Tables X and XI provide a numeri-

cal representation of the solar interior. Figure 6 shows where the energy generation originates in the sun and illustrates the distribution of temperature, total density, and electron density. Figure 7 shows the dependence of the most important mass fractions upon solar position. Table X gives as a function of solar radius (or enclosed mass) the physical variables that define the model and the most important isotopic abundances. Table XI lists the local production rates of nuclear energy and neutrino fluxes from different sources. These tables provide sufficient information so that one can perform accurate calculations of, for example, the effect of resonant neutrino absorption within the sun (the MSW effect).

Table XII lists the calculated solar luminosity, radius, and effective temperature as a function of time. The luminosity of the present-day solar model has increased by 41% relative to the zero-age model, and the effective temperature has increased by 3%.

The information given in this paper and in paper I is sufficient for testing a new stellar evolution code. We not only give our final results but also present explicitly the input parameters and the physical assumptions that we have used. The adopted nuclear reaction parameters are given in Sec. II.A and Table I (see also Sec. II.A of paper I), while the radiative opacities are presented in a convenient numerical form in Table III and are described in Sec. II.C and Appendix B.

The primordial mass fraction of helium abundance that is deduced for the standard model is $Y=0.271$. The principal reason that this value is larger than was obtained in paper I (where we found $Y=0.252$) is that the best estimate for the observed surface value of the heavy-element-to-hydrogen ratio has increased by 21% (see Sec. II.B).

E. Solar neutrino fluxes

The bottom line for our calculations of solar neutrino fluxes is given in Table XIII, where we list our best estimates and the total theoretical range for the flux of neutrinos from each of the nuclear fusion sources. The error estimates are discussed in Secs. VI and VII. The flux of *p-p* and pep neutrinos can be calculated accurately, with total theoretical uncertainties of 2% and 4%, respectively.[11] However, the important ^{7}Be and ^{8}B neutrino fluxes have much larger uncertainties, 14% and 34%, respectively. The standard model fluxes of CNO neutrinos are even more uncertain. The flux of hep neutrinos could be calculated accurately if we knew the rate of reaction 4 in Table I.

[11]It has often been claimed in the literature that the flux of *p-p* is practically "model independent." This is not correct. Without a theoretical solar model, the flux of *p-p* neutrinos could not be calculated to better than a factor of two (see discussion in Sec. V.C).

Table XIV lists the neutrino fluxes for a sequence of nonstandard and standard solar models. The standard models that we have constructed are described in Sec. V.C; the nonstandard models (which have inhomogeneous primordial compositions or *ad hoc* and presumably wrong nuclear physics) are discussed in Sec. IX.

The flux of ^{8}B neutrinos depends on the central temperature of the solar model, standard or nonstandard, as approximately T^{18}. This result is illustrated in Fig. 11. A measurement of the ^{8}B neutrino flux would determine the central temperature of the sun to an accuracy of order 2% if we knew that nothing happened to the neutrinos on the way to the Earth from the sun or if the total flux of high-energy neutrinos could be measured by neutral-current reactions, which are independent of neutrino flavor.

F. Solar neutrino experiments

According to our last count, the number of proposed solutions to the solar neutrino problem (nonstandard solar models or new weak-interaction physics) is about an order of magnitude larger than the number of funded solar neutrino experiments. Many of the proposed explanations lead to similar expectations for each of the experiments under consideration, especially when uncertainties in the calculations and in the neutrino measurements are included. The MSW effect by itself offers a wide range of possible parameter values. In general, there are six parameters to be determined: three masses and three mixing angles. (The above counting neglects *PC* violation.) If one assumes the simplest MSW hypothesis, that the electron neutrino mixes strong with only one other neutrino, then the particle physics goal for the foreseeable future will be to determine two parameters, the square of the neutrino mass difference and the mixing angle. Allowing for the full range of theoretical possibilities, we recognize that one must perform a large number of solar neutrino experiments both to test the theory of stellar evolution and to constrain fundamental weak-interaction theories.

The calculated "standard" event rates for different solar neutrino experiments are presented and discussed in Sec. VI. The results presented in equation form in Sec. VI assume both that the standard solar model is correct and that nothing happens to the neutrinos on the way to the Earth from the sun. In this case, the neutrino absorption cross sections given in Tables VII and VIII can be used to calculate the expected event rate. However, the observations from the ^{37}Cl experiment show that at least one of these conventional assumptions is incorrect. We give here, nevertheless, these maximally conventional results in order that there will be a unique prediction for each detector with which to compare the observational results. For nine nonstandard models, the event rates in different experiments are shown in Table XVIII. Some of these nonstandard models were discussed previously as possible solutions to the solar neutrino problem and some

were invented here to show the relation between solar neutrino experiments and helioseismology (see Sec. X).

For each detector, we show in Table XVI the individual uncertainties that derive from the most important input parameters, nuclear reaction cross sections, primordial composition, opacity, and neutrino interaction cross sections.

The capture rates predicted by the standard solar model are shown in Table XVII for each of the experiments considered here. The contributions of individual neutrino sources, as well as the total calculated event rate, are shown separately.

The predicted capture rate for the ^{37}Cl experiment is $7.9(1\pm0.33)$ SNU, of which 6.1 SNU are from ^{8}B neutrinos. The observed value of 2 SNU is outside the range allowed by the recognized uncertainties. This discrepancy is known as the "solar neutrino problem."

Figure 10 shows, as a function of the date of publication, all of the predicted capture rates and their quoted errors (when given in the published paper) for each of the papers in this long series. Several different input parameters make comparably large contributions to the present-day total uncertainty; it therefore seems unlikely that the effective 3σ uncertainty will be reduced much below 2 SNU in the foreseeable future, except by an accurate experimental determination of the ^{8}B neutrino flux. A comparison of the calculated event rate with the observed rate (Davis, 1978; Rowley, Cleveland, and Davis, 1985) shows that the flux of ^{8}B neutrinos at Earth is between zero and one-half the calculated standard value [see Eq. (23)].

The calculated standard capture rate for the ^{71}Ga experiment is 132^{+20}_{-17} SNU. Neutrinos from the basic *p-p* reaction contribute about 54%, or 71 SNU; the other main contributors are ^{7}Be neutrinos, 26%, and ^{8}B neutrinos, 11%. The dominant uncertainty (see Table XVI) is caused by transitions to excited states whose matrix elements must be inferred from (p,n) measurements. The calibration of a ^{71}Ga detector with a ^{51}Cr source, or a stopped muon beam, cannot remove the uncertainty due to transitions to highly excited states. The size of the uncertainty in the calculated capture rate depends upon what one assumes about the solar model and the weak-interaction processes that may affect the incident neutrino spectrum. The so-called "No ^{8}B" model provides a special case with a particularly small uncertainty, 10%, in the predicted rate.

The ^{98}Mo detector is sensitive to ^{8}B and hep neutrinos averaged over the past few million years. The calculated capture rate is $17.4^{+18.5}_{-11}$ SNU. Lack of knowledge of the neutrino absorption cross sections dominates the uncertainty estimate; the uncertainty from all other sources is only 6 SNU.

The standard prediction for the ^{7}Li detector is $51.8(1\pm0.31)$ SNU, of which 43% (23 SNU) are from ^{8}B neutrinos and 25% (13 SNU) from ^{15}O neutrinos. This experiment provides one of the best opportunities for detecting the CNO neutrinos. For the nonstandard "No ^{8}B" model, 53% of the total calculated 29 SNU are contributed by CNO neutrinos.

The predicted capture rate for a ^{81}Br detector is 27.8^{+17}_{-11} SNU, of which 55% are from ^{8}B neutrinos and 31% from ^{7}Be neutrinos. The (p,n) measurements reported by Krofcheck *et al.* (1987) show that this detector is most sensitive to ^{8}B neutrinos, if the standard solar model is correct, instead of to ^{7}Be neutrinos, as was previously believed. Most of the uncertainty (all but 7 SNU) in the standard model prediction is from the neutrino absorption cross sections. If the "No ^{8}B" model is correct, then most (69%) of the capture rate is from ^{7}Be neutrinos. In fact, for this case the calculated rate is 12.5^{+5}_{-4} SNU, of which 8.6 SNU are from ^{7}Be neutrinos.

The predicted capture rate for a ^{205}Tl detector is very uncertain because of difficulties in estimating the neutrino absorption cross sections (see Sec. VI.A.7). We estimate a nominal value of 263 SNU, of which 173 SNU come from *p-p* neutrinos and about 80 SNU come from ^{7}Be and ^{8}B neutrinos. Within the recognized uncertainties in the cross sections, one cannot establish with a high confidence level whether or not the *p-p* neutrinos are more important than the ^{8}B plus ^{7}Be neutrinos, since different nuclear transitions are most important for the two groups of (lower- and higher-energy) neutrinos.

We consider four experiments in which individual recoil electrons are detected. They are neutrino-electron scattering and neutrino absorption by ^{2}H, ^{40}Ar, and ^{115}In. All four of these experiments can be used to provide direct information about the energy spectrum of incident solar neutrinos.

Neutrino-electron scattering as a technique for studying solar neutrinos has been discussed extensively by Bahcall (1987). This paper gives the predicted energy and angular dependence of the recoil electrons, as well as the total cross sections, for all of the important solar neutrino sources. The results are presented for both ν_e and ν_μ. A number of experiments have been proposed that will detect solar neutrinos via neutrino-electron scattering; they are described briefly in Sec. VI.B.

The Kamiokande II natural-water detector (see references in Sec. VII.B) is the first electron scattering experiment to yield a definite result. Hirata *et al.* (1987b) give an upper limit at the 90% confidence level for the flux of ^{8}B neutrinos of $\phi(^{8}\mathrm{B}) \leq 3.2\times10^{6}$ cm^{-1}s^{-1}. This upper limit is about 55% of the value calculated with the best standard solar model and is inconsistent, at the 90% confidence level, with the range of values allowed by the recognized uncertainties in the calculation of the flux. The Kamiokande II result confirms experimentally the existence of a solar neutrino problem, but has not yet yielded a limit on the flux of ^{8}B neutrinos that is more stringent than is provided by the ^{37}Cl experiment [cf. Eq. (23)]. If the MSW effect is the correct explanation of the solar neutrino problem, then the Kamiokande II experiment should detect a definite solar signal at a flux level that is 14% or more of the value predicted by the standard model.

The standard predicted capture rate for an ^{2}H detector with a threshold energy of 5 MeV is $6.23(1\pm0.38)$ SNU, of which all but 0.02 SNU come from ^{8}B neutrinos. Almost all of the estimated uncertainty derives from the uncertainty in the ^{8}B neutrino flux. An absolute measurement to high statistical accuracy of the capture rate with this detector would determine the incident flux of electron-flavor ^{8}B neutrinos to an accuracy of order $\pm10\%$ (see Sec. IV.B). For the 1-kt detector proposed by Aardsma *et al.* (1987), the absorption rate should be 1.2×10^4 events per yr if the standard model is correct and nothing happens to the neutrinos after they are produced in the solar core. The corresponding number of neutrino-electron scattering events in the detector is 1.0×10^3 per kt per yr, i.e., about 9% of the absorption rate. If the MSW effect converts essentially all of the higher-energy electron neutrinos into neutrinos of a different flavor, then the expected rate for neutrino-electron scattering with a 5-MeV threshold is reduced to 1.5×10^2 scattering events per kt per yr. This rate can be considered as a plausible lower limit provided that the standard solar model is not disastrously incorrect and that neutrinos do not decay on the way to the Earth from the sun. The proposed deuterium detector can also observe neutrons from the neutral-current disintegration of the deuteron. The ratio of the number events caused by the charged current (absorption) to the number of events caused by the neutral current (disintegration) is a sensitive indicator of weak-interaction processes, such as the MSW effect.

A ^{11}B detector would provide several simultaneous experiments with ^{8}B solar neutrinos, neutral-current excitations to three excited nuclear states in ^{11}B, charged-current transitions to four nuclear levels in the mirror nucleus ^{11}C, and neutrino-electron scattering. The ratios of corresponding neutral-current and charged-current transitions would indicate the relation between the spectrum of electron-flavor neutrinos to the spectrum of all neutrinos (which contribute to the neutral-current excitations).

For a liquid-argon detector, the total number of absorption events per yr is 8×10^2 per kt of detector, provided the standard solar model is correct and nothing happens to the neutrinos on the way to the Earth from the sun. The recoil electrons will be accompanied by prompt and characteristic γ-ray deexcitation of the isobaric-analog state that is excited by the neutrino capture, which will provide an efficient way of measuring the spectrum of incident ^{8}B neutrinos of electron flavor. The predicted number of neutrino-electron scattering events is larger than the predicted number of absorption events, by 11% for a threshold recoil energy of 5 MeV and by a factor of 13.5 for a recoil threshold of 8 MeV. If the MSW effect converts all of the ^{8}B neutrinos to a different flavor, then the expected event rate is reduced by a factor of 6.6 to about 140 scattering events per kt per yr. This value may be regarded as a plausible lower limit for the expected event rate provided that the standard solar model is not disastrously wrong and that neutrinos do not decay on the way to the Earth from the sun.

The predicted standard capture rate for an ^{115}In detector is 639^{+639}_{-320} SNU, of which 73% (468 SNU) are from the basic proton-proton reaction. No other target we have discussed has such a high percentage contribution from the *p-p* reaction. There is also a large signal expected from ^{7}Be neutrinos, 116 SNU (or 18%). The ^{7}Be signal is above most of the background in this experiment. All of the usual astrophysical and nuclear reaction uncertainties are relatively small in this experiment (see Table XVI); they amount for the standard model to only 26 SNU. The total uncertainty in the predictions is presently dominated by the uncertainty in the neutrino absorption cross sections. Fortunately, a calibration experiment with ^{51}Cr could provide a direct determination of the absorption cross sections of greatest importance [see Eq. (7) of Sec. IV.C and the related discussion].

G. Nonstandard models

We have calculated a set of nonstandard solar models that were constructed with the same numerical precision as the standard solar models. We use these nonstandard models to illustrate what can be learned about stellar evolution from different solar neutrino experiments and to establish the relation between helioseismology and solar neutrinos.

The neutrino fluxes from the different models are given in Table XIV, and the event rates that the models predict for different solar neutrino experiments are shown in Table XVIII.

We construct models with artificial chemical inhomogeneities: "low-Z" models in which the heavy-element abundance is lower in the interior than on the surface and "high-Y" models in which the primordial helium abundance is assumed to be larger in the interior regions than on the surface. The low-Z models reduce the calculated capture rate in the ^{37}Cl experiment to about 1.5 SNU, approximately consistent with the observed rate. The high-Y models increase the calculated capture rate by between 0.1 and 1 SNU, giving a predicted ^{37}Cl rate of between 8.3 to 9.2 SNU. The low-Z models are inconsistent (see below) with the existing helioseismological data; the high-Y models yield better agreement (see below) with the measured *p*-mode oscillation frequencies than does the standard solar model. We also consider *ad hoc* models in which the ^{3}He + ^{4}He reaction (number 6 in Table I) is set equal to zero and a model in which the rare ^{8}B-producing reaction (number 9 in Table I) does not occur. These models, if correct, predict undetectably low counting rates for most of the proposed solar neutrino experiments, but do not change significantly the calculated *p*-mode oscillation frequencies (see below and Sec. X).

Models in which some of the energy transport in the solar interior is carried by weakly interacting massive particles (WIMP's) reduce, compared to the standard

model, the expected event rate by a factor of between 2 and 4 for experiments sensitive mainly to ^{8}B neutrinos (cf. the second and the last columns in Table XVIII). WIMP's have rather minor effects on the expected counting rate for experiments with detectors such as ^{71}Ga or ^{115}In that are sensitive to p-p neutrinos.

H. hep neutrinos

The extremely rare but very informative hep neutrinos can be detected by their unique energy signature. The hep neutrinos have the highest end-point energy (18.773 MeV) of any of the significant solar neutrino sources. Moreover, the hep neutrinos are produced in a different region of the sun from the other high-energy neutrinos that come from ^{8}B decay (see Sec. V.C, Fig. 8 and Table XI); the hep neutrinos are produced over a much more extended region and are much less sensitive to temperature than are the ^{8}B neutrinos.

The expected event rates are small, but nevertheless potentially observable, if the standard model is correct and solar neutrinos do not change their flavor on the way to the Earth. In the ^{2}H experiment, hep neutrinos will dominate the capture rate for electron recoil energies above 13.5 MeV. For the 1-kt detector discussed by Aardsma *et al.* (1987), one expects 11 events per yr in this energy range from hep neutrinos and only 1.5 from ^{8}B neutrinos. In a liquid-argon detector, hep neutrinos will dominate the capture rate for electron recoil energies above 9 MeV. Per kt per yr of liquid argon, one expects 3.4 events above 9 MeV from hep neutrinos and only 0.8 events from ^{8}B neutrinos. For a several kt detector, the event rate in liquid argon should be observable. The expected event rate in the fiducial volume of 0.7 m^3 of the Kamiokande II natural-water experiment (Beier, 1986; Suzuki, 1986; Hirata *et al.*, 1987) is too small to be detectable in the region where hep neutrinos are more numerous than ^{8}B neutrinos. One expects only 0.09 events per yr above 14 MeV from hep neutrinos.

hep neutrinos may be observable in the deuterium and liquid-argon experiments even if the standard solar model predicts too large a flux for the temperature-sensitive ^{8}B neutrinos. From the point of view of stellar evolution, the flux of hep neutrinos is much more reliably determined than is the flux of ^{8}B neutrinos. For the standard solar model, about 50 absorption and scattering events per yr would be expected from hep in the proposed 1-kt ^{2}H detector and about 21 absorption events in the planned 3-kt liquid-argon detector, all with recoil electron kinetic energies above 5 MeV.

If one assumes the correctness of nonstandard solar models in which ^{3}He is mixed into the core on a time scale shorter than or comparable to the ^{3}He nuclear burning time, then higher event rates from hep neutrinos might be expected for all of the above-mentioned experiments. Thus the ^{2}H, ^{40}Ar, and perhaps even the Kamiokande II natural-water detector, in all of which the energies of individual electrons are measured, provide a direct way of testing the nonstandard mixing models for the solar interior (for a discussion of these solar models see Bahcall, Bahcall, and Ulrich, 1968; Ezer and Cameron, 1968; Shaviv and Salpeter, 1968).

I. Helioseismology

We discuss helioseismology in Sec. X. We review in Sec. X.A the state of the art of helioseismology and focus upon the information that is derivable about the solar interior from observations of p-mode eigenfrequencies. We suggest a specific polynomial representation of both the observations and the calculations [see Eq. (40]; the characteristic parameters of the polynomial are only weakly dependent upon the choice of mode frequencies. We argue in Secs. X.B and X.C that the difference between the fiducial frequencies referring to the $l=0$ and the $l=2$ modes, which we denote by δ_{02} [see Eq. (41)], is relatively independent of uncertainties regarding the surface properties of the sun and therefore offers the best opportunity for determining characteristics of the solar interior by measuring p-mode oscillation frequencies. Unfortunately, we are not able to establish a quantitative upper limit on the contribution of complicated surface physics (convection, magnetic fields, inhomogeneities, and surface activity) to δ_{02}, although we do present arguments that suggest that the surface uncertainties largely cancel out in forming the frequency difference that δ_{02} represents.

Our calculations of oscillation frequencies are independent of some of the usual uncertainties associated with using asymptotic integral expressions. We calculate the eigenfrequencies directly from the solar models using three different solar analysis codes that are described in Sec. X.D and Appendix C. The reader can obtain a feeling for the contents and structures of the codes from the descriptions.

We compare, in Sec. X.E and Table XX, the calculated oscillation frequencies with observations. Figure 15 is a pictorial representation of the agreement between calculation and observation.

The calculations using the standard solar model represent well the quantitative features of the solar p-mode frequency spectrum. However, there are small ($\sim 0.5\%$) discrepancies between observation and calculation. The most significant discrepancy in our opinion is the difference between the calculated and observed values of δ_{02}, which we estimate to be at approximately the 3σ level of significance. The observed value for δ_{02} is between 8.9 and 9.9 μHz (Pallé *et al.*, 1987), depending upon the number of radial nodes in the oscillation mode. The value calculated with the standard solar model is 10.6 μHz (cf. Table XX and the uncertainties quoted therein).

We have demonstrated the complementarity of solar neutrino experiments and helioseismology by calculating the oscillation frequencies for a solar model in which we have made a drastic change in the nuclear energy genera-

tion cycle, namely, setting the cross section for the $^3He + {}^4He$ reaction equal to zero. This results in a model with no ^8B and no ^7Be neutrino fluxes (see the next to last row in Table XIV). This model, if correct, would have catastrophic implications for planned solar neutrino experiments (see the last column in Table XVIII); there would be effectively no measurable event rate in the ^2H, ^{11}B, ^{40}Ar, and ^{98}Mo experiments, and much reduced rates in ^{71}Ga and ^{81}Br experiments. *Quite remarkably, this drastic change in the nuclear energy generation, and the associated change in the interior solar structure, produces only a negligibly small change in the p-mode oscillation frequencies [see Fig. 6, Eq. (54), and row 8 in Table XX].* The *g*-mode oscillation frequencies are changed by only a small amount, $\sim 0.2\%$.

On the other hand, we show in Sec. X.G that a small gradient in the primordial helium abundance can modify the calculated oscillation frequencies significantly and in the correct sense to improve the agreement with observations (see rows 14–17 in Table XX). The calculated ^8B neutrino flux is increased by about 15% by the specified *ad hoc* assumption regarding the composition gradient. We conclude that changes in the interior structure of the sun sufficient to account for the observed *p*-mode oscillation frequencies may change the predicted neutrino fluxes by amounts that are smaller than the currently estimated uncertainties in calculating the neutrino fluxes. We speculate that the explanation of some of the most significant discrepancies between observation and calculation of *p*-mode oscillation frequencies may require a composition gradient that is slightly different from what is assumed in the standard solar model.

The low-*Z* models, which have often been considered as a possible solution to the solar neutrino problem, result in a worse disagreement between the observed and calculated values of δ_{02} than for the standard solar model. The discrepancy is of order 2 μHz for the low-*Z* models and of order 1 μHz for the standard model, out of a total observed value of about 9 μHz (see Table XX).

J. Our bottom line

The discrepancy between the predicted and the observed event rates in the ^{37}Cl and the Kamiokande II solar neutrino experiments cannot be explained by a "likely" fluctuation in input parameters with the best estimates and uncertainties given in this paper. Whatever is the correct solution to the solar neutrino problem, we think it is unlikely to be a "trivial" error. If the cause of the discrepancy is that the neutrino fluxes from the standard solar model have been calculated incorrectly, then the identification of this error will probably have other important consequences for the theory of stellar evolution and therefore many branches of astronomy. If new weak-interaction physics is the correct explanation, then the many scientists who have helped to probe and define the solar neutrino problem will have been extraordinarily fortunate in finding something fundamental about microscopic physics while attempting to test a basic macroscopic theory, stellar evolution.

ACKNOWLEDGMENTS

This research was supported by the National Science Foundation Grant No. PHY-8217352 and by NASA Grant No. NAGW472 at UCLA. We have benefited from valuable comments, suggestions, criticisms, and private communications from many of our colleagues during the two long years in which this manuscript was being prepared. For their generous help, often requiring considerable personal effort, we are extremely grateful. We thank explicitly C. Alcock, E. Beier, H. Bethe, A. E. Boesgaard, E. Carlton, M. Cassé, A. Cox, A. Dar, R. Davis Jr., W. A. Fowler, C. Goodman, D. O. Gough, W. Hampel, W. Haxton, W. Huebner, P. Hut, D. Krofcheck, A. McDonald, R. Noyes, B. Paczynski, P. Parker, R. S. Raghavan, E. E. Salpeter, D. Schramm, D. Spergel, E. Sugarbaker, and L. Wolfenstein. We are grateful to D. Saxe for expert help in running the Monte Carlo simulations on the IAS microvaxes and to M. Best for a skilled job of T_EX setting and correcting.

APPENDIX A: NUCLEAR ENERGY GENERATION

We describe in this appendix how we compute the rate, ε, at which thermal energy is generated by nuclear reactions. The basic relation is

$$\varepsilon \equiv \Sigma_r Q_{\mathrm{eff},r} R_r \ , \tag{A1}$$

where the individual nuclear reaction rates are represented by R_r. We computed new values for $Q_{\mathrm{eff},r}$, the thermal energy communicated to the star by nuclear reaction *r*.

Table XXI lists the values of Q_{eff} that we used (and also indicates how we grouped nuclear reactions when calculating the energy generation). The tabulated values include—in addition to the nuclear mass differences—corrections for the neutrino energy losses, determined by averaging the neutrino energy over the relevant neutrino emission spectrum. The *Q* value for the *p-p* reaction takes account of the fact that in about 0.25% of the conversions of two protons to deuterium an electron is captured from the initial state (pep reaction), which results in the loss of about 1.442 MeV of neutrino energy not including corrections described below (instead of 0.2649 MeV from the usual *p-p* reaction). For the ^7Be electron-capture reaction, we did the thermal average over the electron-capture rate and also took account of the γ-ray energy released following transitions to the first excited state of ^7Li. For the ^8B β decay, we used the recently redetermined neutrino spectrum (Bahcall and Holstein, 1986). We also included corrections for the thermal motion of the reacting particles, which changes the maximum neutrino energies. For the *p-p* and pep reactions, we evaluated the most probable center-of-mass interac-

TABLE XXI. Effective Q values for nuclear reactions. The values listed are corrected for neutrino energy loss and represent the average thermal energy communicated to the star per reaction.

Reactions	Q_{eff} (MeV)	Notes
$^1\text{H}(p, e^+\nu_e)^2\text{H}$ $^2\text{H}(p, \gamma)^3\text{He}$	6.664	Includes thermal energy loss via p-p neutrinos; also pep reaction.
$^3\text{He}(^3\text{He}, 2p)^4\text{He}$	12.860	
$^3\text{He}(\alpha, \gamma)^7\text{Be}$	1.586	
$^7\text{Be}(e^-\nu_e)^7\text{Li}(p, \alpha)^4\text{He}$	17.394	Includes branching to excited state of ^{7}Li and correction for thermal energy loss in the electron capture.
$^7\text{Be}(p, \gamma)^8\text{B}(e^+\nu_e)^8\text{Be}^*$ $^8\text{Be}* \rightarrow 2\alpha$	11.499	Used experimental α spectrum to compute neutrino energy loss.
$^{12}\text{C}(p, \gamma)^{13}\text{N}(e^+\nu_e)^{13}\text{C}$ $^{13}\text{C}(p, \gamma)^{14}\text{N}$	11.008	0.707 MeV neutrino energy loss
$^{14}\text{N}(p, \gamma)^{15}\text{O}(e^+\nu_e)^{15}\text{N}$	9.054	0.997 neutrino energy loss
$^{15}\text{N}(p, \alpha)^{12}\text{C}$	4.966	
$^{15}\text{N}(p, \gamma)^{16}\text{O}$	12.128	
$^{16}\text{O}(p, \gamma)^{17}\text{F}(e^+\nu_e)^{17}\text{O}$ $^{17}\text{O}(p, \alpha)^{14}\text{N}$	3.553	0.999 MeV energy loss

tion energies, and for the pep and ^{7}Be electron-capture reactions we added the average electron thermal energy carried away by the neutrinos. These corrections cause additional neutrino energy losses Δq, which when averaged over the neutrino spectra are

$$\Delta q(p\text{-}p) \simeq 3.6 T_{15}^{2/3} \text{ keV} , \quad \text{(A2)}$$

$$\Delta q(^7\text{Be}+e^-) \simeq 2.6 T_{15} \text{ keV} , \quad \text{(A3)}$$

and

$$\Delta q(\text{pep}) \simeq 3.6 T_{15}^{2/3} \text{ keV} + 2.6 T_{15} \text{ keV} , \quad \text{(A4)}$$

where T_{15} is the temperature in units of 15×10^6 K.

For simplicity, we approximated the small corrections represented in Eqs. (A2)–(A4) by their values at $T_{15} \equiv 1.0$. The average thermal corrections are negligibly small [$\sim (v_{\text{thermal}}/c)^2 q \sim 10^{-6} q$] for the β decays of ^{8}B, ^{13}N, and ^{17}O, which have only one particle in the initial state.

The average energy loss from the CNO neutrino emitters is, respectively, 0.707 MeV (^{13}N), 0.997 MeV (^{15}O), and 0.999 MeV (^{17}F).

APPENDIX B: CNO OPACITY CORRECTION

We present in this appendix the fractional changes in the radiative opacity that result from the conversion of carbon and oxygen to nitrogen as a result of nuclear burning in the CNO cycle. This effect has been discussed in Sec. II.C.

Table XXII presents the fractional changes, $\Delta\kappa/\kappa \equiv (\kappa - \kappa^{\text{Table III}})/\kappa$, in the radiative opacity as a function of T, ρ/T_6^3, and X. These corrections were derived using the Ross-Aller abundances of ^{12}C and ^{16}O as fiducial values: $X_{12}^{\text{RA}} = 0.003\,900$ and $X_{16}^{\text{RA}} = 0.008\,620$. The opacities given in Table III were calculated for slightly different initial ^{12}C and ^{16}O mass fractions: $X_{12}^{\text{Table III}} = 0.004\,13$ and $X_{16}^{\text{Table III}} = 0.009\,15$.

The corrections to the radiative opacity used in calcu-

TABLE XXII. Opacity correction due to conversion of carbon and oxygen to nitrogen.

	Carbon				Oxygen			
	X=0.35		0.75		0.35		0.75	
ρ/T_6^3	0.0350	0.0410	0.0350	0.0410	0.0350	0.0410	0.0350	0.0410
T6								
1.0	−0.06593	−0.06592	−0.05671	−0.05671	−0.52291	−0.52290	−0.54133	−0.53211
2.0	−0.11428	−0.10011	−0.12274	−0.11082	−0.14746	−0.10580	−0.15587	−0.11195
3.0	−0.08554	−0.06673	−0.09326	−0.08184	−0.04770	0.00138	−0.05069	−0.00630
4.0	−0.05467	−0.03145	−0.05853	−0.04887	−0.01615	0.03810	−0.01505	0.02618
5.0	−0.03041	−0.00211	−0.03001	−0.02176	−0.00862	0.05236	−0.00409	0.03473
6.0	−0.01319	0.02086	−0.00875	−0.00133	−0.01082	0.05885	−0.00319	0.03470
7.0	−0.00203	0.03830	0.00602	0.01318	−0.01699	0.06303	−0.00651	0.03187
8.0	0.00415	0.05111	0.01537	0.02273	−0.02459	0.06707	−0.01146	0.02865
9.0	0.00624	0.06012	0.02023	0.02821	−0.03242	0.07195	−0.01675	0.02611
10.0	0.00099	0.06926	0.01945	0.02963	−0.04665	0.08537	−0.02627	0.02470
11.0	0.00499	0.06600	0.02138	0.03032	−0.03987	0.07802	−0.02178	0.02456
12.0	−0.00528	0.07033	0.01497	0.02658	−0.05264	0.09400	−0.03000	0.02568
13.0	−0.01346	0.06955	0.00833	0.02160	−0.05781	0.10379	−0.03300	0.02807
14.0	−0.02324	0.06720	−0.00016	0.01494	−0.06215	0.11471	−0.03527	0.03165
15.0	−0.03435	0.06349	−0.01017	0.00686	−0.06567	0.12660	−0.03675	0.03625
16.0	−0.04665	0.05864	−0.02156	−0.00240	−0.06848	0.13944	−0.03762	0.04189

lating the solar model called "CNO Cor" in the text and in the main tables were obtained by interpolating in Table XXII. We used the values of T, ρ/T_6^3, and X at each point in the model and then evaluated the correction to the opacity from the expression

$$\frac{\Delta\kappa}{\kappa}=\frac{\Delta\kappa_C}{\kappa}[(X_{12}^{\text{Table III}}-X_{12})/X_{12}^{RA}]+\frac{\Delta\kappa_O}{\kappa}[(X_{16}^{\text{Table III}}-X_{16})/X_{16}^{RA}]\,.$$

APPENDIX C: HISTORY AND DESCRIPTION OF THE CODES

The solar interior structure and oscillation frequencies are calculated with a set of three codes: SINEV, CATMOS, and KWAVES. The history and characteristics of these codes is of interest to anyone who wishes to compare them with other codes in use today. Although the physics of the nuclear reactions is well documented in this series of papers (see the references in the caption to Fig. 10), some other aspects of the interior calculations are less well summarized, and in fact the description of the physics of the three codes is spread over a variety of publications. Some of the most pertinent characteristics of SUNEV and CATMOS are briefly reviewed in Sec. X.C.

The three codes will be made publicly available through the Global Oscillation Network Group (GONG) project sponsored by the National Solar Observatory (NSO) in Tucson, Arizona. Indeed the KWAVES program is currently available along with the current standard solar mode (Best) on the computing facilities at the NSO. In support of this project and to make available adequate information on the computational procedures, this appendix gives a history and description of three codes.

The sequence of computations begins with the determination of the nuclear stratification and gravitational energy generation using SUNEV. The structure of the outer layers starting with the innermost parts of the coro-

na and extending inward to about 1% of the solar radius is calculated with CATMOS. Finally, this complete structure is analyzed with KWAVES. Most of the calculations are currently being carried out using the VAX/750 operated by the Department of Astronomy at UCLA or a MicroVAX operated by the Institute for Advanced Study. The CPU time required for SUNEV is about 15 min in order to obtain a fully converged solar model starting from a guess that is close to the correct l/H and Y (within 0.01 and 0.004, respectively). Typically, we compute five to seven such fully converged models in order to match the solar luminosity and radius to one part in 10^5. CATMOS takes about 25 min and KWAVES about 15 s per mode. Since some of the applications require about 2000 modes to be analyzed per model, the KWAVES part of the code sequence can be the most time consuming.

The SUNEV code is in many respects a second-generation solar structure code. We intended in 1970 to combine the best features of two parent codes—a code called ASTRA, which was written by Rakavy, Shaviv, and Zinamon (1967) and modified by Shaviv for this collaboration, and a code called STEVE, which was written by Henyey, Forbes, and Gould (1964) and Bodenheimer, Forbes, Gould, and Henyey (1965). The modification of the ASTRA code by Shaviv consisted of replacing the numerical integration scheme described by Rakavy, Shaviv, and Zinamon by a simple fitting procedure, which uses fourth-order Runge-Kutta trial integrations from the center and the surface. The basic architecture of the Shaviv modified ASTRA was adopted, and the development of SUNEV began with this code. The code was gradually rewritten to include new physics and to improve performance on the computation of solar models. At present, none of the original code from ASTRA remains in SUNEV. The features remaining from the Shaviv version of ASTRA are the definition of the physical variables and dimensional scaling, the use of a fitting method for finding the solar models, and the use of the entropy instead of the internal energy and density to compute the gravitational and thermal energy-generating contributions. The features taken over from STEVE are the strategy for computing the nuclear abundances as a function of time (see Bodenheimer *et al.*, 1965, Appendix C) and the treatment of partial electron degeneracy (see Bodenheimer *et al.*, 1965, Appendix A). The backward time differencing method adopted from STEVE for the study of the nuclear evolution allows the consistent treatment of the approach to steady-state abundance over a wide range of reaction rates and time steps. Our approach to this problem has been described in Appendix B of paper I.

There is a problem with the fitting method, which is well known and has led to its abandonment for the study of stellar models that have evolved off the main sequence. This problem is the difficulty of carrying trial integrations over regions in the star for which the thermal diffusion time (see Henyey and L'Ecuyer, 1966) is long compared to the time step. Under those conditions a trial solution will diverge exponentially from the correct solution and lead to nonphysical conditions such as negative temperature. This problem places a fundamental limitation on the smallness of the time steps. For most solar evolution applications, this limitation is not serious. However, there are some applications for which it is desirable to use very small time steps. In order to accommodate such applications, we developed a modified fitting method in which multiple interior fitting points are used. The information from the inner boundary condition can be carried forward across an integration zone, and the number of trial integrations remains three for all zones. There are two inefficiencies in using multiple fitting points: the need to doubly compute the properties of each fitting point and the need to carry out a modest computation to use the inner boundary condition information. The limitation on the time step becomes the requirement that the time step exceed the longest diffusion time across any zone. As many as 45 fitting points out of a total of 130 mass zones have been successfully used in applications such as those reported on by Ulrich and Burger (1976). There was no noticeable reduction in the speed of the computation as a result of the additional fitting points. The only significant difficulties are the need to produce a first guess for the properties at each fitting point and the fact that the method is inherently serial rather than parallel, so that modern array processors cannot be effectively used. For all but the first model of any evolutionary sequence, the properties of the previous model can be used. Since relatively short sequences of models are used for the studies of the solar evolution, multiple fitting points are rarely useful for computing solar models. The absence of parallelism is not a serious restriction for solar models, since this part of the sequence is the least computation intensive. The multiple fitting point option is available in SUNEV for those applications which require short time steps.

A feature of SUNEV that simplifies the code and produces stable and reproducible results is the absence of any rezoning algorithm. The distribution of mass points is specified by the user and remains unchanged during an integration sequence. This procedure yields stable numerical derivatives by eliminating the possibility of small changes induced in the model by variable mass zoning in different models. There is a potential hazard, since it is possible for a user to carry out an integration with inappropriate zoning. The time step sequence is also under direct user control. Care is required in setting up the SUNEV models.

The principal application of SUNEV has been to compute neutrino fluxes. During the computation of the neutrino fluxes it is important to calculate both the luminosity of the model and the neutrino flux in a consistent manner. We have found over the course of our investigations of the solar neutrino problem that a large fraction of any expected change in the neutrino spectrum because of a different specification of the physics of the model is

compensated by the need to match the solar luminosity. The same consideration applies to the numerical specification of the model. We therefore use two methods to calculate the model luminosity. During the relaxation of the fitting method, the luminosity is calculated along with the other principal variables of stellar structure from the Runge-Kutta formalism. After the match at the fitting point has been achieved, the luminosity and the neutrino fluxes are calculated from a trapezoidal rule. The precision of this second calculation is lower than that of the Runge-Kutta integration, but the precision is the same as that for the neutrino fluxes, which are also calculated from a trapezoidal rule. The match to the observed solar luminosity is required of the trapezoidal rule result rather than the Runge-Kutta result. Typically these two luminosities differ by $0.0005L_{\odot}$. Using the partial derivatives given in Table XV, we see that this difference would not have caused a significant error in any of our derived neutrino fluxes.

The second code in the sequence is CATMOS. This software began with the code described by Henyey, Vardya, and Bodenheimer (1965). The code continues to use the opacities from Vardya (1964) even though the more modern results from, for example, the Los Alamos Opacity Library would include more contributors to the opacity and a better treatment of the line opacity. The reason that we have kept the older opacities is that they use the electron pressure rather than the density as the second independent variable. The H^- opacity is the dominant continuum source in the solar photospheric regions and depends primarily on the electron pressure rather than the density. Consequently, by determining the opacity from the electron pressure, we achieve more consistent results than would be possible with the density. Minor variations in the detailed distribution of metals like Na, which are important at low temperatures, will be automatically included in the opacity this way; they would not be included if the density were used. Except for the changes noted below, the equation of state is that of Vardya (1965). Modifications were made in this code to permit the optional computation of models with nonlocal convection. This option has been used on rare occasions and has not been invoked for any of the models reported on in this paper. Because of this option, the basic convection equations were rewritten in a form that is superficially different from that used by Henyey, Vardya, and Bodenheimer but that in fact reduces to the standard result for the local mixing-length theory. The treatment of the full solar model by an algorithm originally designed to compute atmospheres and the improvement of the models for computation of the oscillation frequencies has necessitated several modifications, which are listed below.

The detailed thermal stratification (see Ulrich and Rhodes, 1977, 1983) as given by Vernazza, Avrett, and Loeser (1981) is used to compute the structure of layers above the photosphere and extending into the low corona. CATMOS is structured so that the thermal stratification of these layers can be changed by altering a separate input data set, which gives temperature and turbulent velocity as a function of optical depth. The T-τ format is required by the basic depth integration algorithm of CATMOS and can make matching the published chromosphere and coronal structures awkward, since the latter usually give temperature as a function of altitude. Typically some trial and error searching is necessary to obtain a satisfactory T-τ relation.

The equation of state for hydrogen and helium is that of Vardya (1965), except for the modification of the partition function described by Ulrich (1982) and the inclusion of the detailed ionization equilibrium for the CNO elements as given in the same reference. The effects of the Debye-Huckel approximation to the Coulomb interactions were first incorporated in this code in the work reported on by Lubow and Ulrich (1979).

The integration is carried to the center of the solar model by using the abundances from SUNEV and by incorporating into the CATMOS code the energy and neutrino generation formalism from SUNEV. The abundances and gravitational energy generation are interpolated using the mass variable from SUNEV and a 6-point Lagrangian formula. The points for this interpolation are chosen so that the mass of interest is between the third and fourth points unless a boundary of the model is too close or a chemical discontinuity would be spanned by the 6 points. This procedure was first used in the present paper. Linear interpolation was used in the preceding papers reporting on solar oscillation frequences by Ulrich and co-authors.

CATMOS treats the model as if it were defined by four variables that come in two pairs—the luminosity and radius are one pair and the helium abundance and the mixing length are another pair. CATMOS satisfies the inner boundary conditions by iterating the values of one pair of variables while holding the other pair constant. Thus one has a choice of computing the model to match a specified star, like the sun, or of computing the model as if it were part of a cluster of presumably known composition.

Although not important for solar models, CATMOS includes a treatment of molecular opacity according to the formalism described by Scalo and Ulrich (1975). These additional opacity sources can be important for models of cooler stars. A minimal molecular equilibrium network is used to calculate explicitly the abundances of the key species.

The zoning in CATMOS is governed by the increment in the temperature from one point to the next. The spacing can be adjusted to include additional points in regions of interest. The algorithm attempts to keep the spacing in the logarithm of the pressure uniform. As the integration approaches the center of the model, the algorithm attempts to keep the spacing in radius uniform. Since the integration is going in the unstable direction towards a singularity, it is possible to follow an unphysical solution which corresponds to the existence of a point mass at the

center of the sun. If the integration pursues this spurious solution too far, the numerical derivatives become badly defined and convergence does not occur. This difficulty is prevented by terminating the integration when a specified temperature is reached, which is typically slightly above the central temperature from SUNEV. Additional details about the application of the inner boundary conditions are given in Ulrich and Rhodes (1983).

The center of the sun is a singular point and requires special care in order to avoid introducing spurious solutions. We use an analytic representation of the regular solution in order to obtain the values of the variables at the innermost point of the model. The regular solution to the structure equation is characterized by the approach of the thermodynamic intensive variables T, P, and ρ to a constant value, with deviations being proportional to r^2. At the innermost point, r_1 say, the expansion of the properties of the model is a series in $\varepsilon=(P_c-P_1)/P_c$. The value of ε in terms of the properties of the model at r_1 is given by $\varepsilon=(2\pi/3)(G\rho_1^2 r_1^2/P_1)$. The value of ε in SUNEV is typically 0.001 and in CATMOS is typically 0.005. We retain only the leading term in the series expansion that represents change in the intensive variable near the solar center; we thus make an error of this magnitude in the difference between the central variables and the value we adopt at the first point. This error is negligible for the calculation of the structure of models computed by either code. Christensen-Dalsgaard, Dilke, and Gough (1974) have retained the next higher term in the expansion when it is applied to the calculation of the eigenmodes. They choose their inner point slightly further out than we do for SUNEV, about where we do for CATMOS. We prefer not to use higher-order terms in ε, since if two are needed, then others may be required also. Instead, when we compute the eigenfrequencies from the CATMOS model, we insert an analytic representation of the regions interior to the innermost point of CATMOS and extend the mode in to where $\varepsilon<5\times10^{-5}$. At this point, the treatment of the inner boundary condition does not influence our solution to any significant accuracy. [Christensen-Dalsgaard *et al.* (1974) could continue to have effects at the 10^{-3} level; they indeed describe a numerical experiment that is in accordance with this expectation. More recent calculations by Christensen-Dalsgaard and Gough achieve greater precision.]

The final code in the sequence is KWAVES. This code originated in 1968 as a response to the observations reported by Frazier (1968a, 1968b), which indicated that the 5-min oscillations were not being caused by the solar granulation, but rather were being temporarily disrupted by the arrival of individual granules and then reestablished themselves in phase with their previous wave train after the granule had passed. The general working hypothesis at that time was that these oscillations were a purely atmospheric phenomenon; they were described extensively as gravity-modified acoustic waves in a plane-parallel atmosphere. Particularly complete treatments of this problem are to be found in the work of Souffrin (1966) and Stein (1968). Because of this background, the initial formulation of the code was a result of an attempt to include the temperature gradient in the analysis. It is important to recognize this origin because the more popular formulation today begins from the point of view of nonradial oscillations of stars and is based on definitions and variables typically used in this literature (see, for example, Ando and Osaki, 1975). The initial application by Ulrich (1970) of the code (then called WAVES) to the solar atmosphere showed for the first time that trapping of the acoustic waves below the solar surface could lead to resonances at well defined frequencies which depend on the horizontal wave number. Prior to that work, the frequencies of the 5-min oscillations had been assumed random within a broad band. The subsequent observational confirmation of Ulrich's prediction by Deubner (1975) and Rhodes, Ulrich, and Simon (1977) represents the beginning of the use of solar oscillations as a probe of solar internal structure. The observations by Claverie *et al.* (1979) and by Grec, Fossat, and Pomerantz (1980) demonstrated the potential precision of the data available for the analysis of the solar interior and the possibility of obtaining information about the innermost parts of the sun. The potential of the helioseismic method evident from these observations stimulated some of the improvements in the three codes that are described in this appendix.

The definition of the numerical algorithm for KWAVES is given in Ulrich (1970). Important refinements beyond that algorithm were developed in Ulrich and Rhodes (1977), where the plane-parallel assumption was relaxed, and in Ulrich and Rhodes (1983), where the gravitational potential perturbation was included, the chemical gradients were properly treated, and the integration was carried to the solar center. The radiative interaction as described by Ulrich (1970) was used up to 1983, but is no longer included since it is now more primitive than alternate available formulations such as that by Christensen-Dalsgaard and Frandsen (1983). The additional computing time associated with carrying out the nonadiabatic calculation makes the use of a primitive formulation an undesirable use of resources. Based on the pioneering work by Gough (1984a), the WAVES program has been extended to yield the kernel functions that are needed for the analysis of the solar interior using inverse theory. This additional capability is reflected in the renaming of the code KWAVES.

In developing all the codes, we have struggled to minimize the number of programming errors. This is a tedious and difficult task in complicated codes, particularly ones, like ours, in which separate parts are constructed over many years. We have found one technique to be particularly useful: we document the history of the calculated numbers (such as neutrino fluxes or oscillation frequencies) and make sure that we understand and can demonstrate the causes for any changes. This tracking

technique has been used for both SUNEV and CATMOS; the recorded history goes back to 1970, when both codes were shorter and simpler.

The historical method of finding errors has on occasion revealed subtle bugs that may otherwise have escaped detection. The reader may find one example especially interesting, since the bug resulted in better agreement with the observations than did the corrected code. In 1978, Ulrich and Rhodes extended the atmospheric structure to include the transition region and the lower corona. This extension improved the agreement between the calculations and observations of the high l modes; however, the change was larger than anticipated. After a protracted investigation, the bulk of the change turned out to be due to an erroneous determination of the value of l. If we had adopted the model with the extended upper atmosphere without tracking the changes in detail, we would probably have interpreted the better agreement with observation as a confirmation of the improved theory. In fact, the improvement was spurious and reflected a programming error.

The moral of the above story is not "better is worse." We simply want to share with the reader a procedure for checking codes that we have found useful.

REFERENCES

Aardsma, G., *et al.*, 1987, Phys. Lett. B **194**, 321.

Adelberger, E. G., and W. C. Haxton, 1987, Phys. Rev. C **36**, 879.

Aglietta, M., *et al.*, 1986, Nuovo Cimento C **9**, 588.

Alexander, T. K., G. C. Ball, W. N. Lennard, H. Geissel, and H. B. Mak, 1984, Nucl. Phys. **A427**, 526.

Alfimenkov, V. P., S. B. Borzakov, G. G. Bunatyan, J. Wierzbicki, L. B. Pikelner, and E. I. Sharapov, 1980, Sov. J. Nucl. Phys. **31**, 10.

Aller, L. H., 1986, in *Spectroscopy of Astrophysical Plasmas,* edited by A. Dalgarno and D. Layzer (Cambridge University Press, Cambridge, England), p. 89.

Ando, H., and Y. Osaki, 1975, Publ. Astron. Soc. Jpn. **27**, 581.

Arisaka, K., *et al.*, 1985, J. Phys. Soc. Jpn. **54**, 3213.

Backus, G. E., and J. E. Gilbert, 1967, Geophys. J. R. Astron. Soc. **13**, 247.

Badino, G., *et al.*, 1984, Nuovo Cimento C **7**, 573.

Baglin, A., P. J. Morel, and E. Schatzman, 1985, Astron. Astrophys. **149**, 309.

Bahcall, J. N., 1964, Phys. Rev. Lett. **12**, 300.

Bahcall, J. N., 1966, Phys. Rev. Lett. **17**, 398.

Bahcall, J. N., 1969a, in *Proceedings of the International Conference on Neutrino Physics and Astrophysics* (F. I. Acad. Sci. USSR, Moscow), Vol. 2, p. 133.

Bahcall, J. N., 1969b, Phys. Rev. Lett. **23**, 251

Bahcall, J. N., 1977, Astrophys. J. Lett. **216**, 115.

Bahcall, J. N., 1978, Rev. Mod. Phys. **50**, 881.

Bahcall, J. N., 1981, Phys. Rev. C **24**, 2216.

Bahcall, J. N., 1986, in *Solar Neutrinos: Theory,* Weak and Electromagnetic Interactions in Nuclei, Proceedings of the International Symposium, Heidelberg, edited by H. V. Klapdor (Springer, Berlin), p. 705.

Bahcall, J. N., 1987, Rev. Mod. Phys. **59**, 505.

Bahcall, J. N., N. A. Bahcall, W. A. Fowler, and G. Shaviv, 1986, Phys. Lett. B **26**, 359.

Bahcall, J. N., N. A. Bahcall, and G. Shaviv, 1968, Phys. Rev. Lett. **20**, 1209.

Bahcall, J. N., N. A. Bahcall, and R. K. Ulrich, 1968, Astrophys. Lett. **2**, 91.

Bahcall, J. N., N. A. Bahcall, and R. K. Ulrich, 1969, Astrophys. J. **156**, 559.

Bahcall, J. N., M. Baldo-Ceolin, D. B. Cline, and C. Rubbia, 1986, Phys. Lett. B **178**, 324.

Bahcall, J. N., N. Cabibbo, and A. Yahil, 1972, Phys. Rev. Lett. **28**, 316.

Bahcall, J. N., B. T. Cleveland, R. Davis, Jr., I. Dostrovsky, J. C. Evans, Jr., W. Frati, G. Friedlander, K. Lande, J. K. Rowley, W. Stoenner, and J. Weneser, 1978, Phys. Rev. Lett. **40**, 1351.

Bahcall, J. N., B. T. Cleveland, R. Davis, Jr., and J. K. Rowley, 1985, Astrophys. J. **292**, L79.

Bahcall, J. N., and R. Davis, 1976, Science **191**, 264.

Bahcall, J. N., and R. Davis, 1982, in *Essays in Nuclear Astrophysics,* edited by C. A. Barnes, D. D. Clayton, and S. Schramm (Cambridge University Press, Cambridge, England), p. 243.

Bahcall, J. N., G. B. Field, and W. H. Press, 1987, Astrophys. J. **320**, L69.

Bahcall, J. N., and S. C. Frautschi, 1969, Phys. Lett. B **29**, 263.

Bahcall, J. N., W. A. Fowler, I. Iben, and R. L. Sears, 1963, Astrophys. J. **137**, 344.

Bahcall, J. N., J. Gelb, and S. P. Rosen, 1987, Phys. Rev. D **35**, 2976.

Bahcall, J. N., and B. R. Holstein, 1986, Phys. Rev. C **33**, 2121.

Bahcall, J. N., W. F. Huebner, S. H. Lubow, N. H. Magee, Jr., A. L. Merts, M. F. Argo, P. D. Parker, B. Rozsnyai, and R. K. Ulrich, 1980, Phys. Rev. Lett. **45**, 945.

Bahcall, J. N., W. F. Huebner, W. H. Lubow, P. D. Parker, and R. K. Ulrich, 1982, Rev. Mod. Phys. **54**, 767 (paper I).

Bahcall, J. N., W. F. Huebner, N. H. Magee, A. L. Merts, and R. K. Ulrich, 1973, Astrophys. J. **184**, 1.

Bahcall, J. N., K. Kubodera, and S. Nozawa, 1988, Phys. Rev. D (in press).

Bahcall, J. N., and R. M. May, 1969, Astrophys. J. **155**, 501.

Bahcall, J. N., and C. P. Moeller, 1969, Astrophys. J. **155**, 511.

Bahcall, J. N., S. T. Petcov, S. Toshev, and J. W. F. Valle, 1986, Phys. Lett. B **181**, 369.

Bahcall, J. N., and R. L. Sears, 1972, Ann. Rev. Astron. Astrophys. **10**, 25.

Bahcall, J. N., and G. Shaviv, 1968, Astrophys. J. **115**, 113.

Bahcall, J. N., and R. K. Ulrich, 1970, Astrophys. J. **160**, L57.

Bahcall, J. N., and R. K. Ulrich, 1971, Astrophys. J. **170**, 593.

Bakich, A. M., and L. S. Peak, 1985, in *Solar Neutrinos and Neutrino Astronomy,* AIP Conference Proceedings No. 126, edited by M. L. Cherry, W. A. Fowler, and K. Lande (AIP, New York), p. 238.

Baltz, A. J., and J. Weneser, 1987, Phys. Rev. D **35**, 528.

Barabanov, I. R., *et al.*, 1985, in *Solar Neutrinos and Neutrino Astronomy,* AIP Conference Proceedings No. 126, edited by M. L. Cherry, W. A. Fowler, and K. Lande (AIP, New York), p. 175.

Barker, F. C., and R. H. Spear, 1986, Astrophys. J. **307**, 847.

Beier, E. W., 1986, in *Proceedings of Seventh Workshop on Grand Unification, ICOBAN '86,* Toyama, Japan (Japanese Press, Tokyo), p. 79.

Bethe, H. A., 1986, Phys. Rev. Lett. **56**, 1305.

Bodenheimer, P., 1964, Astrophys. J. **142**, 451.

Bodenheimer, P., J. E. Forbes, N. L. Gould, and L. G. Henyey,

1965, Astrophys. J. **141**, 1019.
Boercker, D. B., 1987, Astrophys. J. **316**, L95.
Boesgaard, A. M., 1976, Publ. Astron. Soc. Pac. **88**, 353.
Boesgaard, A. M., K. G. Budge, and E. E. Burck, 1988, Astrophys. J. **325**, 749.
Boesgaard, A. M., K. G. Budge, and M. E. Ramsay, 1988, Astrophys. J. (in press).
Bogdan, T. J., and E. G. Zweibel, 1985, Astrophys. J. **298**, 867.
Bollinger, L. M., R. J. Specht, and G. E. Thomas, 1973, Bull. Am. Phys. Soc. **18**, 591.
Booth, N. E., 1987, Appl. Phys. Lett. **50**, 293.
Booth, N. E., G. L. Salmon, and D. A. Hukin, 1985, in *Solar Neutrinos and Neutrino Astronomy,* AIP Conference Proceedings No. 126, edited by M. L. Cherry, W. A. Fowler, and K. Lande (AIP, New York), p. 216.
Bopp, P., D. Dubbers, L. Hornig, E. Klemt, J. Last, and H. Schultze, 1986, Phys. Rev. Lett. **9**, 919.
Bowles, T., B. Cleveland, and H. Robertson, 1986 (private communication).
Boyd, R. N., R. E. Turner, B. Sur, L. Rybarcyk, and C. Joseph, 1985, in *Solar Neutrinos and Neutrino Astronomy,* AIP Conference Proceedings No. 126, edited by M. L. Cherry, W. A. Fowler, and K. Lande (AIP, New York), p. 145.
Braun, E., and I. Talmi, 1986, in *Solar Neutrinos: Theory,* Proceedings of the International Symposium, Weak and Electromagnetic Interactions in Nuclei, Heidelberg, edited by H. V. Klapdor (Springer, Berlin), p. 47.
Cabrera, B., L. M. Krauss, and F. Wilczek, 1985, Phys. Rev. Lett. **55**, 25.
Cabrera, B., L. M. Krauss, and F. Wilczek, 1985, Phys. Rev. Lett. **57**, 1801.
Cahen, S., M. Cassé, and C. Doom, 1986, in *'86 Massive Neutrinos in Astrophysics and Particle Physics,* Proceedings of the Sixth Moriond Workshop, edited by O. Fackler and J. Tran Thanh Van (Editions Frontières, Gif-sur-Yvette), p. 83.
Carlson, E. D., 1986, Phys. Rev. D **34**, 1454.
Cassé, M., 1986 (private communication).
Cassé, M., S. Cahen, and C. Doom, 1986, in *Neutrinos and the Present Day Universe, Colloque de la Societé Francaise de Physique,* edited by T. Montmerle and M. Spiro (CEA, CEN Saclay), p. 49.
Champagne, A. E., G. E. Dodge, R. T. Kouzes, M. M. Lowry, A. B. McDonald, and M. W. Roberson, 1987, Bull. Amer. Phys. Soc. **32**, 1437.
Chen, H. H., 1985, Phys. Rev. Lett. **55**, 1534.
Christensen-Dalsgaard, J., 1982, Mon. Not. Roy. Astron. Soc. **199**, 735.
Christensen-Dalsgaard, J., and S. Frandsen, 1983, Solar Phys. **82**, 165.
Christensen-Dalsgaard, J., F. W. W. Dilke, and D. Gough, 1974, Mon. Not. Roy Astron. Soc. **169**, 429.
Christensen-Dalsgaard, J., D. Gough, and J. Toomre, 1985, Science **229**, 923.
Claverie, A., G. R. Isaak, C. P. McLeod, H. B. van der Raay, and T. Roca Cortes, 1979, Nature **282**, 591.
Claverie, A., G. R. Isaak, C. P. McLeod, H. B. van der Raay, and T. Roca Cortes, 1981, Nature **293**, 443.
Cline, D. L., 1985, in *Solar Neutrinos and Neutrino Astronomy,* AIP Conference Proceedings No. 126, edited by M. L. Cherry, W. A. Fowler, and K. Lande (AIP, New York), p. 295.
Cline, D. L., and C. Rubbia, 1987 (private communication).
Cowan, G. A., and W. C. Haxton, 1982, Science **216**, 51.
Cox, A. N., and J. N. Stewart, 1970, Astrophys. J. Suppl. **19**, 261.
Cribier, M., J. Rich, M. Spiro, D. Vignaud, W. Hampel, and B. T. Cleveland, 1987, Phys. Lett. B **188**, 168.
D'Antona, F., and I. Mazzitelli, 1984, Astron. Astrophys. **138**, 431.
Däppen, W., R. L. Gilliland, and J. Christensen-Dalsgaard, 1986, Nature **321**, 229.
Dar, A., and A. Mann, 1987, Nature **235**, 790.
Davids, C. N., T. F. Wang, I. Ahmad, R. Holzmann, and R. V. F. Janssens, 1987, Phys. Rev. C **35**, 1114.
Davis, R., Jr., 1964, Phys. Rev. Lett. **12**, 303.
Davis, R., Jr., 1978, in "Proceedings of Informal Conference on Status and Future of Solar Neutrino Research," edited by G. Friedlander (Brookhaven National Laboratory Report No. 50879), Vol. 1, p. 1.
Davis, R., Jr., 1986, in *Proceedings of the Seventh Workshop on Grand Unification, ICOBAN '86,* Toyoma, Japan (Japanese Press, Tokyo) p. 237.
Davis, R., Jr., E. C. Fowler, S. L. Meyer, and J. C. Evans, Jr., 1973, LAMP Report No. 53.
de Bellefon, A., P. Espigat, and G. Waysand, 1985, in *Solar Neutrinos and Neutrino Astronomy,* AIP Conference Proceedings No. 126, edited by M. L. Cherry, W. A. Fowler, and K. Lande (AIP, New York), p. 227.
Delasche, P., and P. H. Scherrer, 1983, Nature **306**, 651.
Deubner, F. L., 1975, Astron. Astrophys. **44**, 371.
Deubner, F. L., 1984, Ann. Rev. Astron. Astrophys. **22**, 593.
Deubner, F. L., and D. O. Gough, 1984, Ann. Rev. Astron. Astrophys. **22**, 593.
Diesendorf, M. O., 1970, Nature **227**, 266.
Diesendorf, M. O., and B. W. Ninham, 1969, Astrophys. J. **156**, 1069.
Duncan, D. K., 1981, Astrophys. J. **248**, 651.
Ebeling, W., and R. Sandig, 1973, Ann. Phys. (Leipzig) **28**, 289.
Eggleton, P. P., J. Faulkner, and B. P. Flannery, 1973, Astron. Astrophys. **23**, 325.
Ellis, S. D., and J. N. Bahcall, 1968, Nucl. Phys. **A114**, 636.
Evans, J. C., Jr., R. Davis, Jr., S. L. Meyer, E. C. Folwer, and J. Cunnane, 1975, Brookhaven National Laboratory Informal Report No. 1980.
Ezer, D., and A. G. W. Cameron, 1968, Astrophys. Lett. **1**, 177.
Faulkner, J., and R. L. Gilliland, 1985, Astrophys. J. **299**, 994.
Faulkner, J., D. O. Gough, and M. N. Vahia, 1986, Nature **321**, 226.
Filippone, B. W., 1982 (private communcation)
Filippone, B. W., A. J. Elwyn, C. N. Davids, and D. D. Koetke, 1983, Phys. Rev. **28**, 2222.
Filippone, B. W., and D. N. Schramm, 1982, Astrophys. J. **253**, 393.
Fowler, W. A., 1984, Rev. Mod. Phys. **56**, 149.
Fowler, W. A., 1987 (private communcation).
Fowler, W. A., G. R. Caughlan, and B. A. Zimmerman, 1975, Ann. Rev. Astron. Astrophys. **13**, 69.
Frazier, E. N., 1968a, Astrophys. J. **152**, 557.
Frazier, E. N., 1968b, Z. Astrophys. **68**, 345.
Freedman, M. S., 1978, in "Proceedings of Informal Conference on Status and Future of Solar Neutrino Research," edited by G. Friedlander (Brookhaven National Laboratory), Report No. 50879, Vol. 1, p. 313.
Freedman, M. S., 1986 (private communication).
Freedman, M. S., *et al.*, 1985, Science **193**, 1117.
Gavrin, V. N., A. V. Kopylov, and A. V. Streltsov, 1985, in *Solar Neutrinos and Neutrino Astronomy,* AIP Conference Proceedings No. 126, edited by M. L. Cherry, W. A. Fowler, and K. Lande (AIP, New York), p. 185.

Gelmini, G. B., L. J. Hall, and M. J. Lin, 1987, Nucl. Phys. **B281**, 726.
Gilliland, R. L., 1982, Astrophys. J. **253**, 399.
Gilliland, R. L., J. Faulkner, W. H. Press, and D. N. Spergel, 1986, Astrophys. J. **306**, 703.
Goodman, C. D., 1985, in *Solar Neutrinos and Neutrino Astronomy,* AIP Conference No. 126, edited by M. L. Cherry, W. A. Fowler, and K. Lande (AIP, New York), p. 109.
Gough, D. O., 1977, in *The Energy Balance and Hydrodynamics of the Solar Chromosphere and Corona,* edited by R. M. Bonnet and P. Delache (de Bussex, Clermont-Ferrand), p. 3.
Gough, D. O., 1981, Astron. Astrophys. **104**, 173.
Gough, D. O., 1982, Nature **298**, 350.
Gough, D. O., 1984a, Mem. Soc. Astron. Ital. **55**, 13.
Gough, D. O., 1984b, in *Solar Seismology from Space: a Conference at Snowmass, Colorado,* edited by R. K. Ulrich, J. Harvey, E. J. Rhodes, Jr., and J. Toomre (Jet Propulsion Laboratory, Pasadena; JPL Publication 84-84), p. 49.
Gould, A., 1987, Astrophys. J. **321**, 560.
Grec, G., E. Fossat, and M. Pomerantz , 1980, Nature **288**, 541.
Grec, G., E. Fossat, and M. A. Pomerantz, 1983, Solar Phys. **82**, 55.
Grevesse, N., 1984, Phys. Scr. **T8**, 49.
Gribov, V., and B. Pontecorvo, 1969, Phys. Lett. B **28**, 495.
Griest, K., and D. Seckel, 1987, Nucl. Phys. B **283**, 681.
Griffiths, G. M., M. Lal, and C. D. Scarfe, 1963, Can. J. Phys. **41**, 724.
Hampel, W., 1985, in *Solar Neutrinos and Neutrino Astronomy* AIP Conference Proceedings No. 126, edited by M. L. Cherry, W. A. Fowler, and K. Lande (AIP, New York), p. 162.
Hampel, W., and L. P. Remsberg, 1985, Phys. Rev. C **31**, 666.
Hampel, W., and R. Schlotz, 1984, in *Proceedings of the 7th International Conference on Atomic Masses and Fundamental Constants (AMCO-7),* Darmstadt-Seeheim, edited by O. Klepper (Technische Hochschule, Darmstadt), p. 89.
Haxton, W., 1986, Comments Nucl. Part. Phys. **16**, 95.
Haxton, W., 1987 (private communication).
Henning, W., *et al.*, 1985, in *Solar Neutrinos and Neutrino Astronomy,* AIP Conference Proceedings No. 126, edited by M. L. Cherry, W. A. Fowler, and K. Lande (AIP, New York), p. 203.
Henning, H. M., and P. H. Scherrer, 1986, in *Seismology of the Sun and the Distant Stars,* edited by D. O. Gough, NATO ASI Series C (Reidel, Dordrecht), Vol. 169, p. 55.
Henyey, L. G., J. E. Forbes, and N. L. Gould, 1964, Astrophys. J. **139**, 306.
Henyey, L. G., and J. L. L'Ecuyer, 1966, Astrophys. J. **148**, 549.
Henyey, L. G., M. S. Vardya, and P. Bodenheimer, 1965, Astrophys. J. **142**, 841.
Hirata, K., *et al.*, 1987a, Phys. Rev. Lett. **58**, 1490.
Hirata, K., *et al.*, 1987b, University of Tokyo ICEPP Report No. UT-87-04.
Hiroi, S., H. Sakuma, T. Yanagida, and M. Yoshimura, 1987, report.
Hiroi, S., H. Sakuma, T. Yanagida, and M. Yoshimura, 1987, unpublished.
t Hooft, G., 1971, Phys. Lett. B **37**, 195.
Huebner, W. F., 1986, in *Physics of the Sun,* edited by P. A. Sturrock, T. E. Holzer, D. M. Mihalas, and R. K. Ulrich (Reidel, Boston), Vol. 1, p. 33.
Hurst, G. S., C. H. Chen, S. D. Kramer, B. T. Cleveland, R. Davis, Jr., R. K. Rowley, Fletcher Gabbard, and F. J. Schima, 1984, Phys. Rev. Lett. **53**, 1116.
Hurst, G. S., C. H. Chen, S. D. Kramer, and S. L. Allman, 1985, in *Solar Neutrinos and Neutrino Astronomy,* AIP Conference Proceedings No. 126, edited by M. L. Cherry, W. A. Fowler, and K. Lande (AIP, New York), p. 152.
Itoh, N., and Y. Kohyama, 1981, Astrophys. J. **246**, 989.
Kajino, T., H. Toki, and S. M. Austin, 1987, Astrophys. J. **319**, 531.
Kirsten, T., 1986, in *'86 Massive Neutrinos in Astrophysics and in Particle Physica,* edited by O. Fackler and J. Tran Thanh Van (Editions Frontières, Gif-sur-Yvette), p. 119.
Korzennik, S. G., and R. K. Ulrich, 1988 (in preparation).
Kouzes, R. T. M. M. Lowry, and C. L. Bennett, Phys. Rev. C **25**, 1076.
Krauss, A., H. W. Becker, H. P. Trautvetter, and A. Rolfs, 1987, Nucl. Phys. **A467**, 273.
Krauss, L. M., K. Freese, D. N. Spergel, and W. H. Press, 1985, Astrophys. J. **299**, 1001.
Krofcheck, D., 1987, Ph.D. thesis (Ohio State University), and private communication.
Krofcheck, D., *et al.*, 1985, Phys. Rev. Lett. **55**, 1051.
Krofcheck, D., *et al.*, 1987, unpublished.
Kuo, T. K., and J. Pantaleone, 1987, Phys. Rev. D **35**, 3432.
Kuzmin, V. A., 1966, Sov. Phys—JETP **22**, 175.
Kuzmin, V. A., and G. T. Zatsepin, 1966, in *Proceedings of the International Conference on Cosmic Rays,* London (Institute of Physics, London), Vol. 2, p. 1023.
Langacker, P., 1986, in *Solar Neutrinos: Theory,* proceedings of the International Symposium on Weak and Electromagnetic Interactions in Nuclei (Heidelberg), edited by H. V. Klapdor (Springer, Berlin), p. 879.
Lanou, R. E., H. J. Maris, and G. M. Seidel, 1987, Phys. Rev. Lett. **58**, 2498.
Lebreton, Y., and A. Maeder, 1987, Astron. Astrophys. **175**, 99.
Leibacher, J. W., R. W. Noyes, J. Toomre, and R. K. Ulrich, 1985, Sci. Am. **253**, 48.
Leibacher, J.W., and R. F. Stein, 1971, Astrophys. Lett. **7**, 191.
Leighton, R. B., R. W. Noyes, and G. W. Simon, 1962, Astrophys. J. **135**, 474.
Lowry, M. M., and T. T. Kouzes, 1985, Phys. Rev. C **31**, 1052.
Lowry, M. M., R. T. Kouzes, F. Loeser, A. B. McDonald, and R. A. Naumann, 1987, Phys. Rev. C **35**, 1950.
Lubow, S. H., and R. K. Ulrich, 1979, in "Proceedings of Informal Conference on Status and Future of Solar Neutrino Research," edited by G. Friedlander (Brookhaven National Laboratory), Report No. 50879, p. 157.
Mann, A. K., 1986, unpublished.
Marthoff, C. J., 1987, Science **237**, 507.
Mikheyev, S. P., and A. Yu. Smirnov, 1986, Nuovo Cimento C **9**, 17.
Muller, E. A., E. Peytremann, and R. de La Reza, Solar Phys. **41**, 53.
Newman, M. J., 1986, in *Physics of the Sun,* edited by P. A. Sturrock, T. E. Holzer, D. M. Mihalas, and R. K. Ulrich (Reidel, Boston), Vol. III, p. 33.
Nichiporuk, W., and C. B. Moore, 1974, Geochim. Cosmochim, Acta **38**, 1691.
Nozawa, S., 1987, unpublished.
Nozawa, S., Y. Kohyama, T. Kaneta, and K. Kubodera, 1986, J. Phys. Soc. Jpn. **55**, 2636.
Okun, L. B., 1986, Sov. J. Nucl. Phys. **44**, 546.
Osborne, J. L., C. A. Barnes, R. W. Kavanagh, R. M. Kremer, G. J. Mathews, J. L. Zyskind, P. D. Parker, and A. J. Howard, 1982, Phys. Rev. Lett. **48**, 1664.
Osborne, J. L., C. A. Barnes, R. W. Kavanagh, R. M. Kremer,

G. J. Mathews, J. L. Zyskind, P. D. Parker, and A. J. Howard, 1984, Nucl. Phys. A **419**, 115.
Pallé, P. L., J. C. Perez, C. Regulo, T. Roca Cortes, G. R. Isaak, C. P. McLeod, and H. B. van der Raay, 1987, Astron. Astrophys. **170**, 114.
Parker, P. D., 1986, in *Physics of the Sun,* edited by P. A. Sturrock (Reidel, New York), Vol. I. p. 15.
Parker, R. L., 1977, Annu. Rev. Earth Planet. Sci. **5**, 35.
Popper, D. M., and R. K. Ulrich, 1986, Astrophys. J. Lett. **307**, L61.
Press, W. H., and D. N. Spergel, 1985, Astrophys J. **296**, 679.
Raby, S. B., and G. West, 1987, Nucl. Phys. B (in press).
Raghavan, R. S., 1976, Phys. Rev. Lett. **37**, 259.
Raghavan, R. S., 1978, in "Proceedings of Informal Conference on Status and Future of Solar Neutrino Research," edited by G. Friedlander (Brookhaven National Laboratory), Report No. 50879, Vol. 2, p. 1.
Raghaven, R. S., 1986, Phys. Rev. D **34**, 2088.
Raghavan, R. S., 1987 (private communication).
Raghavan, R. S., S. Pakvasa, and B. A. Brown, 1986, Phys. Rev. Lett. **57**, 1801.
Rakavy, G., G. Shaviv, and A. Zinamon, 1967, Astrophys. J. **150**, 131.
Rapaport, J., *et al.*, 1985, Phys. Rev. Lett. **54**, 2325.
Reeves, H., and J.-P. Meyer, 1978, Astrophys. J. **226**, 613.
Reines, F., and W. R. Kropp, 1964, Phys. Rev. Lett. **12**, 457.
Rhodes, E. J., Jr., R. K. Ulrich, and G. W. Simon, 1977, Astrophys. J. **218**, 901.
Robertson, R. G. H., P. Dyer, T. J. Bowles, R. E. Brown, N. Jarmie, C. J. Maggiore, and S. M. Austin, 1983, Phys. Rev. C **27**, 11.
Rolfs, C., and R. W. Kavanagh, 1986, Nucl. Phys. **A455**, 179.
Rood, R. T., 1978, in "Proceedings of Informal Conference on Status and Future of Solar Neutrino Research," edited by G. Friedlander (Brookhaven National Laboratory), Report No. 50879, Vol. 1, p. 175.
Ross, J. E., and L. H. Aller, 1976, Science **191**, 1223.
Rowley, J. K., 1978, in "Proceedings of Informal Conference on Status and Future of Solar Neutrino Research," edited by G. Friedlander (Brookhaven National Laboratory), Report No. 50879, Vol. 1. p. 265.
Rowley, J. K., B. T. Cleveland, and R. Davis, Jr., 1985, in *Solar Neutrinos and Neutrino Astronomy,* AIP Conference Proceedings No. 126, edited by M. L. Cherry, W. A. Fowler, and K. Lande (AIP, New York), p. 1.
Roxburgh, I. W., 1985a, in *Solar Neutrinos and Neutrino Astronomy,* AIP Conference Proceedings No. 126, edited by M. L. Cherry, W. A. Fowler, and K. Lande (AIP, New York), p. 88.
Roxburgh, I. W., 1985b, Solar Phys. **100**, 21.
Sarantakos, S., A. Sirlin, and W. J. Marciano, 1983, Nucl. Phys. **B217**, 84.
Scalo, J. M., and R. K. Ulrich, 1975, Astrophys. J. **200**, 682.
Schatzman, E., 1969, Astron. Astrophys. **3**, 339.
Schatzman, E., 1985, in *Solar Neutrinos and Neutrino Astronomy,* AIP Conference Proceedings No. 126, edited by M. L. Cherry, W. A. Fowler, and K. Lande (AIP New York), p. 69.
Schatzman, E., and A. Maeder, 1981, Astron. Astrophys. **96**, 1.
Scherrer, P. H., J. M. Wilcox, J. Christensen-Dalsgaard, and D. O. Gough, 1983, Solar Phys. **82**, 75.
Scott, R. D., 1976, Nature **264**, 729.
Sears, R. L., 1964, Astrophys. J. **140**, 477.
Shaviv, G., and E. E. Salpeter, 1968, Phys. Rev. Lett. **21**, 1602.
Sinclair, D., *et al.*, 1986, Nuovo Cimento C **9**, 308.
Souffrin, P., 1966, Ann. Astrophys. **29**, 55.
Spergel, D. N., and W. H. Press, 1985, Astrophys. J. **294**, 663.
Stein, R. F., 1968, Astrophys. J. **154**, 297.
Suffert, M., and R. Berthollet, 1979, Nucl. Phys. **A318**, 54.
Suzuki, A., 1986, in *Proceedings of the Twelfth International Conference on Neutrino Physics and Astrophysics,* edited by T. Kitagaki (World Scientific, Singapore), p. 306; University of Tokyo Report No. UT-ICEPP-86-07, unpublished.
Taddeucci, N. T., *et al.*, 1987, Nucl. Phys. (in press).
Tassoul, M., 1980, Astrophys. J. Suppl. **43**, 469.
Tegner, P. E., and C. Bargholtz, 1983, Astrophys. J. **272**, 311.
Toomre, J., 1986, in *Seismology of the Sun and Distant Stars,* edited by D. O. Gough (Reidel, Boston).
Totsuka, Y., 1987, "Talk given at Workshop on Elementary Particle Picture of the Universe, KEK, February," ICEPP Report No. UT-87-02.
Ulrich, R. K., 1970, Astrophys. J. **162**, 993.
Ulrich, R. K., 1982, Astrophys. J. **258**, 404.
Ulrich, R. K., 1986, Astrophys. J. Lett. **306**, L37.
Ulrich, R. K., and H. L. Burger, 1976, Astrophys. J. **206**, 509.
Ulrich, R. K., and E. J. Rhodes, Jr., 1977, Astrophys. J. **218**, 521.
Ulrich, R. K., and E. J. Rhodes, Jr., 1983, Astrophys. J. **265**, 551.
Ulrich, R. K., and E. J. Rhodes, Jr., 1984, in *Solar Seismology from Space: a Conference at Snowmass, Colorado,* edited by R. K. Ulrich, J. Harvey, E. J. Rhodes, Jr., and J. Toomre (Jet Propulsion Laboratory, Pasadena; JPL Publication 84-84), p. 371.
Ulrich, R. K., E. J. Rhodes, Jr., S. Tomczyk, P. J. Dumont, and W. M. Brunish, 1983, in *Science Underground* (AIP Conference Proceedings No. 96, edited by M. M. Nieto, W. C. Haxton, C. M. Hoffman, E. W. Kolb, V. D. Sandberg, and J. W. Toevs (AIP, New York), p. 66.
Vandakurov, Yu. V., 1967, Astron. Zh. **44**, 786.
Vardya, M. S., 1964, Astrophys. J. Suppl. **8**, 277.
Vardya, M. S., 1965, Mon. Not. R. Astron. Soc. **129**, 205.
Vernazza, J. E., E. H. Avrett, and R. Loeser, 1981, Astrophys. J. Suppl. **45**, 635.
Volk, H., H. Kräwinkel, R. Santo, and L. Walleck, 1983, Z. Phys. A **310**, 91.
Voloshin, M. B., and M. I. Vysotskii, 1986, Sov. J. Nucl. Phys. **44**, 544.
Voloshin, M. B., M. I. Vysotskii, and L. B. Okun, 1986, Sov. J. Nucl. Phys. **44**, 440.
Warburton, E. K., 1986, Phys. Rev. C **33**, 303.
Weinberg, S., 1987, Int. J. Mod. Phys. A **2**, 301.
Werntz, C., and J. G. Brennan, 1973, Phys. Rev. D **8**, 1545.
Wilkinson, D. H., and F. E. Adelburger, 1971, Phys. Rev. Lett. **26**, 1127.
Wolfenstein, L., 1978, Phys. Rev. D **17**, 2369.
Wolfsberg, K., G. A. Cowan, E. A. Bryant, K. S. Daniels, S. W. Downey, W. C. Haxton, V. G. Niesen, N. S. Nogar, C. M. Miller, and D. J. Rokop, 1985, in *Solar Neutrinos and Neutrino Astronomy,* AIP Conference Proceedings No. 126, edited by M. L. Cherry, W. A. Fowler, and K. Lande (AIP, New York), p. 196.
Woodard, M., 1984, in *Solar Seismology from Space: a Conference at Snowmass, Colorado,* edited by R. K. Ulrich, J. Harvey, E. J. Rhodes, Jr., and J. Toomre (Jet Propulsion Laboratory, Pasadena; JPL Publication 84-84), p. 195.